61

ADDENDUM
to CIGRE Document N° 20 (1974) :

INTERFERENCES PRODUCED BY CORONA EFFECT OF ELECTRIC SYSTEMS

(Description of Phenomena and Pratical Guide for Calculation)

CIGRE Working Grop 36.01
EMC Aspects of Corona,
Electric and Magnetic Fields

December 1966

Document prepared by Working Group 36.01 (EMC Aspects of Corona, Electric and Magnetic Fields) presently composed of :

R. Conti, Italy	L. Jermendy, Hungary	D.C. Renew, Great Britain
D. Cristescu, Romania	U. Jonsson, Sweden	F. Soto, Spain
F. Deschamps, France	J. Petterson, Denmark	S. Visacro, Brazil
J. Gartland, Ireland	P. Pirotte, Belgium (convenor)	P.S. Wong, Canada
F. Hirsch, Germany (secretary)	A. Porrino, Italy	

This project was on the scope of the Working Group for more than 5 years already. Prof. W. Janischewskyj, University of Toronto, Canada, was the leader of the Task Force responsible for the preparation of this Addendum.
Fortunately former members, corresponding members and members of the study committee participated with most useful contributions. We wish to express our gratitude therefore to :

J. Arciscewski, Poland	C. Gary, France	T. Sasano, Japan
A. Britten, South Africa	W. Janischewskyj, Canada	A.T. Wilson, Australia
V.L. Chartier, USA	I. Kabrhel, Czech Republic	L. Timashova, Russia
R. Cortina, Italy	P.S. Maruvada, Canada	L. Zaffanella, USA

Recognizing not only his endeavours as to the editorial difficulties of the final draft, we are grateful for the help of G. Lourtie, University of Liège and his assistance concerning the revision of the brochure.

Foreword

As far as we know, the corona phenomena and its consequences are a very complicated problem. Since decades, the engineers are concerned with this question and the actual solutions are more or less adequate.

Partial electrical discharges in air at the atmospheric pressure around overhead line conductors and under all the possible weather conditions are a real complex exercise. To face with this problem, involving numerous parameters, the engineers work on short section experimental lines or on cages. In any case, it is necessary to perform long term measurements, corona being related with the weather conditions (rain, fog, snow, ...).

The principal parameter which governs the corona consequences is the voltage gradient on the conductor. All actual measurements are related to an idealized smooth conductor which is used for calculation. The influence of actual surface conditions is expressed by empirical factors. So, only this voltage gradient on the surface of an idealized smooth conductor can be applied to the formulae presented in this booklet.

In brief, we observe discrete sites where corona occurs. The number of sites is changing along the sag and each site does not produce the same corona level.

The modeling of such a situation is highly complicated and makes experiments necessary.

Moreover, the results obtained by measurements on experimental test stations need a great care to be compared because the main differences appear in the experimental set up itself and the weather conditions are neither easy to define nor to compare.

This Addendum refers to the actual knowledge of phenomena and practical experiences from test facilities and lines in operation.

The phenomena following stochastic laws are characterized by statistical terms, which must be taken into consideration when limits have to be verified. A profound data base is available for radio interference, much less practical experiences for audible noise and even less for corona loss and television interference.

As far as possible, the same symbols are used throughout all chapters. Thus some nominations are different from the original references.

The model of an AC line is used to demonstrate the calculation algorithms only. These results must be taken as "possible tendency" values more than accurate ones.

Table of contents

Chapter 1

Background to Addendum

1.1 Introduction

As a result of the extensive technical activity on corona effects throughout the world during the 1960s and 1970s, the CIGRE Working Group 36.01 "Interferences" prepared and issued in 1974 a Guide on "Interferences Produced by Corona Effect of Electric Systems" [1.1]. This Guide will be referred to throughout this brochure as the Guide. The Guide has served designers for decades in evaluating the influence of corona discharges as part of their assessments of the technical performance and economic competitiveness of AC transmission lines. The contents of the Guide is reproduced in Appendix 1.

During the last two decades, several changes have occurred that critically affect this particular aspect of transmission line design; operating voltages of AC transmission lines have exceeded the 1000 kV level, and the use of HVDC transmission at voltages up to ± 600 kV has become much more widespread.

The study of corona phenomena has also progressed, expanding our understanding especially in the area of rain corona and of microgap discharges. The associated nanosecond range of rise times has necessitated the consideration of electromagnetic disturbances, not only in the radio frequency range, but also in the television range of frequencies. Consequently, interference studies have expanded beyond the 30 MHz limit of the original Guide. Finally, over the 20 years that the Guide has been in existence, additional operating experience has been gained.

1.2 Reasons for the Addendum

Once the need to provide further information was established by WG 36.01 at the beginning of the 1990s, resolution was necessary as to how to implement the change. A separate Task Force was established and, as its first act, it considered two avenues of approach. One was to completely re-edit the Guide and to re-issue it. The other was to continue using the existing document in its present form and to prepare a supplementary document in which only the topics requiring updating would be treated. Following an exhaustive debate, it was decided that an ADDENDUM to the 1974 Guide on „Interferences Produced by Corona Effect of Electric Systems" should be prepared and published.

A detailed review was made of the progress achieved since the issue of the original document, in the areas of transmission line design and operation. It was observed that during the 1970s and 1980s, considerable research effort was devoted towards studies of AC power transmission at voltages in the range of 1000 kV and above [1.2].

As part of the Hydro Quebec James Bay Development, IREQ conducted, during the years 1972 to 1976, experiments and theoretical studies that resulted in a completed design of an 1100 kV transmission line. Project UHV at Pittsfield, Massachusetts considered, from 1974 to 1980, AC transmission voltages above the, then existing, 765 kV. During the years 1975 to 1982, BPA ran its 1200 kV Project near Lyons, Oregon and ENEL ran its 1000 kV Project at Suvereto, Italy. All these studies produced valuable information on various aspects of line design, including those relevant to this ADDENDUM. Pertinent studies in the former USSR were conducted at that time at Leningrad, Moscow and Novosibirsk. Similar studies in Japan concentrated on the development of a double-circuit 1000 kV line at the Akagi UHV Testing Laboratory.

All these investigations have resulted in viable designs for AC transmission at voltages in the range from 1000 to 1500 kV. While the West has not found the economic justification for construction of an operating line in this voltage range, the former USSR constructed, in 1985, its 1200 kV line from Siberia to the Orals. A double circuit 1100 kV line was constructed in 1994 in Japan and is presently being operated at 500 kV.

In approximately the same span of time, HVDC experienced rapid growth as a result of developments in solid state conversion technology at high voltages. Station design changes were the first consequence of this development, however the impact of solid state power conversion did not stop there. The possibility of using higher voltages at HVDC had its impact upon overhead line design as well. Numerous experimental stations have provided design data for HVDC systems at voltages up

to ± 600 kV. The availability of this data has also been an impetus for the preparation of this ADDENDUM.

Another very important factor that changed from the time the original Guide was published, is the economic situation throughout the world. The changes in economic outlook affected the relative costs of line components, of materials used in line construction and the cost of land. These factors impact the cost-benefit analysis and the distribution between fixed and variable costs. They therefore change not only the price, but also the parameters of the optimal design. Indeed the change in cost may be responsible for the shift from one Governing Design Criterion to another. The challenge to increase the power transmission capacity of an existing line (upgrading) justify the actual studies on conventional and unconventional compact lines.

1.3 Governing Design Criteria

When a multi-parameter design is considered, such as the design of a power line, several design criteria must be taken into account at the same time. The separation of phases, for instance, or the location of the overhead conductor, will not only determine the lightning performance of the line, but simultaneously it will change the surface voltage gradient of the phase conductors. Thus it will influence the corona performance of the line with all the consequences that this brings. There will be several criteria by which the corona performance itself is assessed including energy loss, electromagnetic interference and audible noise. Each criterion is usually associated with a limit or target level.

When target level of a particular criterion is reached, a further change in the key parameter, such as the reduction of phase separation, is not permitted, although other criteria would still allow that reduction. For such a situation, this particular criterion is said to "govern" the design [1.3].

The design of power lines is, in principle, dominated by efforts to minimize the costs of energy transmission. Once the voltage level has been chosen, the geometric dimensions are determined from minimum distances between phases and to ground measuring to assure safe and reliable service conditions. The optimal cross section of conductors for lines below the 200 kV level is normally possible with single conductors which rarely produce corona discharges. Above rated voltages of 300 kV however bundle configurations are necessary to control disturbing corona effects. Radio interference as the governing criterion is superseded, usually above the 500 kV level, by audible noise. In many cases the first issue of a line design with respect to the actual governing criterion covers the acceptable limits for other corona criteria. However, they must at least be checked and in addition criteria such as the level of electric and magnetic fields at the ground should be evaluated.

It is important to remind ourselves that the original Guide as well as this ADDENDUM do not cover all possible aspects of power line design. They concentrate on the performance that is related to electrical partial discharges that are the consequence of the operating voltage and possible environmental influences, such as precipitation, pollution, temperature, etc. A properly designed power line must satisfy all these aspects, and comply with all other design requirements, electrical, mechanical, thermal, visual, and so on [1.4].

1.4 Technical Advances

Experimental studies and research conducted during the 1970s and 1980s throughout the world, ascertained the technical feasibility of power transmission at voltages beyond the 750 kV range [1.2]. In the process, relatively few "exotic" problems were experienced, although engineering challenges encountered in the one million volt range contributed to development of new technical solutions. Construction of transmission lines in the UHV range is now a question of economics not of technical feasibility [1.5]. Indeed, the former USSR, where free-market forces have never played a role, has constructed in 1985 and put into operation, a long distance line at 1200 kV [1.6]. Technical advances, attained since the issue of the 1974 Guide, have their impact and for that reason must be considered as the important background for this ADDENDUM.

1.4.1 Large Bundles

The first impression of the UHV line design is their use of bundles with a large number of subconductors and with bundle diameters that are not small in comparison to phase spacing and the height of phases above ground. Table 1.1, taken from [1.2] clearly indicates this trend.

Test Location	Subconductor Diameter (cm)	Number of Subconductors	Typical Subconductor Spacing (cm)
Romania	2.53	5	40
South Africa	2.86	6	28-80
Italy	3.15	8	20-60
Japan	3.42	8	40
Russia	2.41	8, 12	40-100
Japan	3.84	8, 10	40
Italy	2.69	10	45
USA	3.52	12, 16	24-63

Table 1.1

The consequence of the combination of the large number of subconductors and large diameter of the bundle is the fact that the voltage gradient surrounding each conductor is quite different. In particular, the maximum value of the voltage gradient on the surface of each subconductor varies over a much larger range for UHV lines than it does on EHV designs [1.7]. It is one of technical details that will be considered in this ADDENDUM.

1.4.2 Insulators and Fittings

Within the review of UHV designs the possibility exists of unconventional solutions especially at points of transmission line support. V-string configuration of insulators is very common in order to restrict the movement of phases and to maintain clearances that are much more critical for UHV designs. A catenary of insulators strung between two guyed supports, as shown in Figure 1.1, is a refined solution developed for the 1100 kV design [1.2].

Large size of bundles makes it difficult, although not impossible, to control the electric field at suspension clamps using traditional shields made up of shaped tubes. The use of the conductor bundle itself instead constitutes an elegant way of handling the situation.

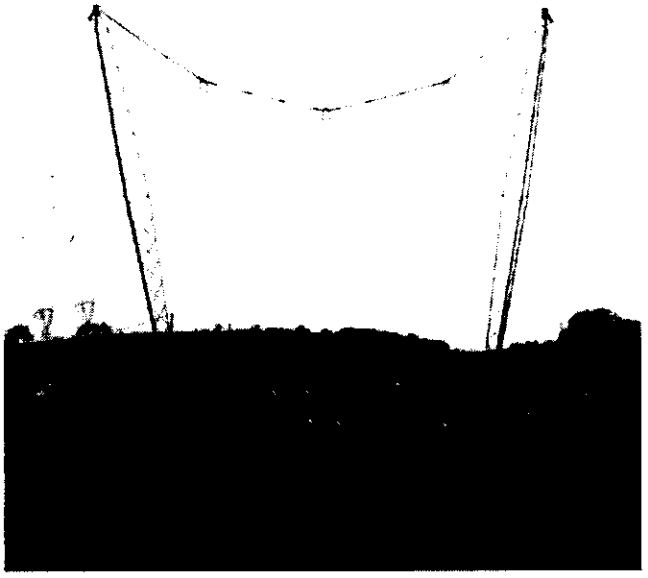

Figure 1.1

1.4.3 Audible Noise

At UHV levels, audible noise is expected to be the governing criterion for line design as far as corona performance is concerned. Because of the large number of subconductors in the bundle, designs in the 1 MV range will have many more potential corona discharge points along a given length of line than those in the EHV range, where a substantially smaller number of subconductors is needed. The increased number of corona sources per unit length of the line will not change the electromagnetic interference level of the line much since it is related directly to the energy radiated from individual discharges and only indirectly to their number. In contrast audible noise constitutes direct addition of acoustic pressures emanating from each discharge point. As a result, the audible noise of a UHV line which has an acceptable RI performance may exceed acceptable levels, while the audible noise of the EHV line with the same RI rating could be perfectly acceptable. This fact is reflected in the ADDENDUM.

1.4.4 HVDC Transmission

The 1980s have seen a very significant progress especially in the area of solid-state power conversion [1.8]. This progress has made it possible to consider not only ± 600 kV but also ± 800 kV and maybe even higher voltages as viable for HVDC transmission.

From the standpoint of their operation, the design of HVDC facilities must include consideration not only of energy losses, audible noise and electromagnetic interference caused by conductor corona but also that of electromagnetic noise caused by HVDC converter stations. Filtering at the terminals of these facilities is an important means of preventing leakage of this noise onto HVDC transmission lines.

In view of this state of affairs, a separate section on HVDC lines is included in this ADDENDUM.

1.5 Scope of the Addendum

As a consequence of the advanced developments described above, it was found necessary to include in the ADDENDUM information on topics which were not covered in sufficient detail in the original GUIDE and to give a comprehensive update of some items of the primary publication with respect to some 20 years experience. The chapter headings used in the ADDENDUM provide an easy key to this expansion.

The original GUIDE dealt primarily with corona caused electromagnetic noise in the frequency range below 30 MHz. It concentrated on Radio Interference within the AM broadcast band. In the ADDENDUM other topics related to corona discharges on power lines are addressed: electromagnetic noise above 30 MHz, corona loss, audible noise, oxidant production, DC lines, substations, and design considerations are the new topics in the ADDENDUM. A new aspect in the ADDENDUM is the treatment of bundles with a large number of subconductors, as used in transmission line designs of the 1 MV class.

Appendix 1 Contents of the 1974 Guide

References

[1.1] "Interferences Produced by Corona Effect of Electric Systems; Description of Phenomena, Practical Guide for Calculation", Brochure No. 20, WG 36.01, CIGRE, Paris 1974.

[1.2] "Electric Power Transmission at Voltages of 1000 kV AC or ± 600 kV DC and above", WG 38.04 & TF 38.04.04, Electra, No. 122, January 1989, pp. 41-75.

[1.3] W. Janischewskyj, J.S. Rogers, "Economic Design and Governing Criteria; Well-head Generation and Long-distance Transmission", Proceedings of the Fifth Power System Computation Conference, Cambridge, England, 1975.

[1.4] "Electric Power Transmission and the Environment : Fields, Noise and Interference", Brochure No. 74, WG 36.01, CIGRE, Paris, 1993.

[1.5] R. Elsliger, G. Lamontagne, J.C. Roy, "Transmission of 16000 MW over a Distance of 1200 km from James Bay to Hydro-Quebec's Load Centres", CIGRE 1974 Session, paper 32-07, 12 pages, Paris, France.

[1.6] I.M. Bortnik et al., "1200 kV Transmission Line in the USSR - The First Results of Operation", CIGRE 1988 Session, paper 38-09, 6 pages, Paris, France.

[1.7] M.G. Comber, L.E. Zaffanella, F.S. Young, "Three Phase UHV AC Transmission Lines Research at EPRI's Project UHV", CIGRE 1978 Session, paper 31-10, 13 pages, Paris, France.

[1.8] L. Carlsson, "Recent Developments in HVDC Converter Station Design", IEEE Transactions on Power Apparatus and Systems, Vol. PAS-103, No. 8, August 1984, pp. 2166-2172.

[1.9] D. Cristescu, M. Ungureanu, P. Postolache, "Nouveaux résultats concernant l'effet couronne en tension alternative. Corrélations, pertes, perturbations radioélectriques, bruit acoustique", CIGRE 1984 Session, paper 36-06, Paris, France.

Chapter 2

Basics of Phenomena and Calculation Comments

2.1 Basic Physics

If the energy of free electrons or ions accelerated in an electric field near an electrode is sufficient to produce ionised avalanches, a discharge process is initiated. It ends either in a sparkover, as the top of the avalanche meets the opposite electrode, or diminishes as the avalanche penetrates into areas where the field is too weak for ionisation. Both discharge forms can appear under service conditions of high voltage installations.

2.2 Corona Discharge

Fundamental physical processes of power line corona have been thoroughly treated in the original Guide [1.1]. Initiation of ionization, development of an avalanche, differences in pulsative forms of positive and negative discharges are fully dealt with.

Corona on conductors or fittings of actual transmission lines usually occurs at randomly distributed irregularities of the surface of electrodes. They produce local enhancements of the electric field. The electric field above which corona discharge arises, here and after called the critical corona onset gradient g_c, depends on the voltage, the conductor radius, the conductor surface condition, the ambient atmospheric conditions and the bundle spacing.

The basic equation for the critical corona onset gradient was derived from visual observation tests by Peek [2.1] for bifilar and for coaxial conductors. A slightly developed version of Peek's empirical equation is given here. It differs from the original equation for AC using the correction for ambient air conditions and the variable m to allow for the conductor surface irregularity.

$$g_c = g_0 \cdot \delta \cdot m \cdot \left(1 + \frac{K}{\sqrt{\delta \cdot r}}\right)$$

where g_c = critical corona onset gradient (kV/cm)

g_o = corona onset gradient (normal ambient conditions: 25 °C, 76 cm Hg) (kV/cm)

r = radius of a tube with the same outer diameter as the actual stranded conductor (cm)

1)

25 °C 76 cm Hg		g_0 (kV/cm) peak value	K ($\sqrt{cm}$)	References
AC	bifilar configuration	30	0.301	[2.1]
AC	coaxial configuration	31	0.308	[2.1], [1.1]
DC-	coaxial configuration	31	0.308	[2.2]
DC+	coaxial configuration	33.7	0.241	[2.2]

2) m : conductor surface irregularity factor

For orientation purpose only, the following values are often proposed :

m = 1	smooth and polished surface
m = 0.6 to 0.8	actual dry weather service condition
m = 0.3 to 0.6	raindrops, snowflakes, extreme pollution
m = 0.25	heavy rain

3) δ : relative air density (RAD)

$$\delta = K_d \frac{p}{273 + t}$$

p = pressure of the ambient air (cm Hg or Pa)

t = temperature of the ambient air (°C)

	K_d
normal conditions (25 °C, 76 cm Hg)	
°C and cm Hg	3.921
°C and Pa	0.00294
IEC normal conditions (20 °C, 76 cm Hg)	
°C and cm Hg	3.855
°C and Pa	0.00289

In Peek's formula, derived for a narrow range of RAD above 1, g_c is almost proportional to RAD. Other investigators suggest for a wider range of RAD g_c is proportional to $\delta^{2/3}$ or $\delta^{1/2}$.

All these expressions result from experiments with rather thin wires, not comparable to actual line conductors.

The influence of RAD on corona onset gradient has to be taken into account when constructing a line at high altitudes. From radio interference and audible noise measurements at different heights q (m) above sea level, the value should be increased by q/300 dB. This empirical term seems to be valid up to more than 3000 m. When the conductor surface gradient is between 13 kV/cm and 17,5 kV/cm it is also valid for corona loss (discussion of [2.3] by C. Gary).

However, the dominant influence on g_c is the surface irregularities factor m. Stable detectable corona activities, producing radio interference, audible noise or loss, can be found on well-aged conductors. Their actual corona onset gradient was investigated empirically for well defined conditions on test lines or cages. The cages, generally coaxial, allow a grater flexibility than the short test lines. They maintain the similar equipotential field pattern around the bundle than in normal operation. Confirmation of these values by statistical measurements of corona effects are difficult to evaluate.

Usually the statistical distribution of values of all corona effects can be split into subdivisions:

Fair weather values, characterized by dry conductor surface, after subdivision with respect to seasonal variants usually match a normal Gaussian distribution fairly well.

Rain values of all corona effects are dependent on rain intensity. The long term probability distribution of rain values is composed of individual rain intensity subdivisions, which overlap more or less.

Thus different rain values are reported:

50%-values of all rain values or wet conductor values, sometimes defined as „light rain or average rain".

„Heavy rain" or average stable foul weather values, either as 95 % value of all rain values, or the 50 % of the maximum rain rate values.

From artificial rain experiments in cages all corona effects show some saturation under rather high rain intensities which rarely occur in nature and are, never, uniformly distributed along the lines in operation.

These values are easily reproducible in cages and therefore very well suited to compare the corona behavior of different conductor configurations.

Most investigations on corona effects in cages or on test line sections had been made without load currents. On an actual line the heating of conductors by load currents has a definite effect on foul weather corona activity [2.4]. It discourages condensation of dew or fog, mitigates the effect of frost and accelerates drying of the surface after rain. Less understood remains the influence of conductor heating during fair weather. Probably the relative air density, being inversely proportional to temperature, is lowered near the heated surface of the conductor, thus encouraging corona activity.

The effects of load currents might help to explain the different form of the probability distributions of radio interference or audible noise from test lines and actual lines under service conditions and unloaded test lines. With heated conductors, the subdivisions „dry conductor" and „foul weather" are more clearly defined.

2.3 Microgap Discharge

Familiarity with the basic physical processes of line corona is needed as the background for adequate treatment of microgap discharges. Studies in this area conducted over the last 20 years have provided new information [2.5].

Microgap discharges are the consequences of a complete breakdown of air insulation between the electrodes of a very small gap. On a power line, microgaps are formed in situations where two parts of a metallic hardware, such as a bolt and nut or a metallic staple holding a groundwire to a wooden pole, become electrically separated.

Such situations arise more often on lower voltage lines than on those operating at high and extra high voltages [2.6]. Voltage between electrodes of such a gap may be induced either by the action of the electric field caused by power conductors, or by leakage along the surfaces of insulators and portions of the wood pole. In the first case we are dealing with capacitive coupling, in the second with conductive coupling of the microgap. Once critical voltage between microgap electrodes is reached, sparkover will result. The discharge starts in the portion of the air volume with excessive electric field and leads in a very short time to the complete breakdown of the whole gap. Through the resultant arc, charges are exchanged between the two electrodes until their potentials are equalized. At the moment the discharge process stops and the air begins to regain its dielectric strength, charging of microgap electrodes restarts, and the buildup to the next discharge event is initiated.

Classical laboratory studies of breakdown in microgap geometries were commenced about 20 years ago [2.7]. Physical processes in the gap were observed first separately for the positive point-to plane geometry [2.8], and then for the same geometry with negative active point [2.9]. These studies were fundamental in describing the details of the breakdown process. The process starts with the increase of the applied voltage until the onset level is reached and ionization is initiated, followed by the formation of avalanches, the corona phase, the development of streamer and leader forms and the final establishment of the arc.

For both polarities three phases of breakdown development are recognized:

(i) the initial process,

(ii) the intermediate process and

(iii) the final process.

The first phase is characterized by the evolution of streamers, the second relates to leader formation and the last phase is associated with the development of the arc. As the capacitance of the microgap becomes charged, a critical level of electric field strength is reached somewhere in the interelectrode space. At that instant, in similarity with initiation of corona processes, avalanche ionization begins and thus the first phase of the breakdown (initial process) commences. This phase is characterized by presence of ionizing process and a sequence of primary, secondary, and sometimes tertiary streamers. Ionizing processes may propagate from both electrodes and they lead to the second phase (intermediate process), the creation of ionized leaders. During these first two phases of the breakdown considerable amount of space charge is generated. Existence of space charge in various parts of the gap influences significantly the ionization process, including the velocity with which the discharge develops. Once the whole interelectrode space becomes fully ionized and conducting plasma is formed, the third phase of the breakdown (final process) is reached and the arc is established.

Detailed investigations of electromagnetic noise at television frequencies were conducted by several power utilities. Observations collected in the space surrounding EHV lines indicated that normally in

fair weather there was little noise at frequencies above 30 MHz. Only during rainy periods those noise levels near EHV lines became occasionally high enough to be of concern [2.10].

Measurements in the vicinity of distribution lines, indicated excessive field levels at television frequencies during fair weather [2.11]. With developed techniques, location and elimination of noise sources became possible [2.12]. Nevertheless, with the aim in mind of avoiding costly maintenance, attempts were made to introduce appropriate changes during the design stage of distribution lines [2.13].

Details of intensive laboratory studies above 30 MHz can be found in the literature [2.5]. Primarily, questions of television interference were dealt with [2.14]; special investigations were related to HVDC problems [2.15, 2.16]. Microgaps of different electrode shapes and spacings were studied [2.17].

2.3.1 Waveshapes and Frequency Spectra

As is well known from the Fourier Transform

$$I(f) = \int_0^\infty i(t)\, e^{-2\pi ft}\, dt \qquad (2.1)$$

the level of energy radiated within a band of the frequency spectrum depends on the waveshape of each individual current pulse and on the time between their successive occurrences.

Consequently, for the study of detrimental effects caused by these discharges, characteristics of individual pulses as well as their repetition rates are relevant.

Figure 2.1 represents a typical discharge current pulse. Similarly to characterization of pulsative corona, the waveform of this current pulse can be described by the following parameters :

I_{cr} (amplitude) -	the maximum value of current wave, (A or mA)
T_r (rise time) -	the time between the 10 % and 90 % value of the amplitude measured on the front of the wave, (ns)
T_f (fall time) -	the time between 90 % and 10 % value of the amplitude measured on the tail of the wave, (ns)
T_d (pulse duration) -	the time from initiation to completion of the current wave, (ns).

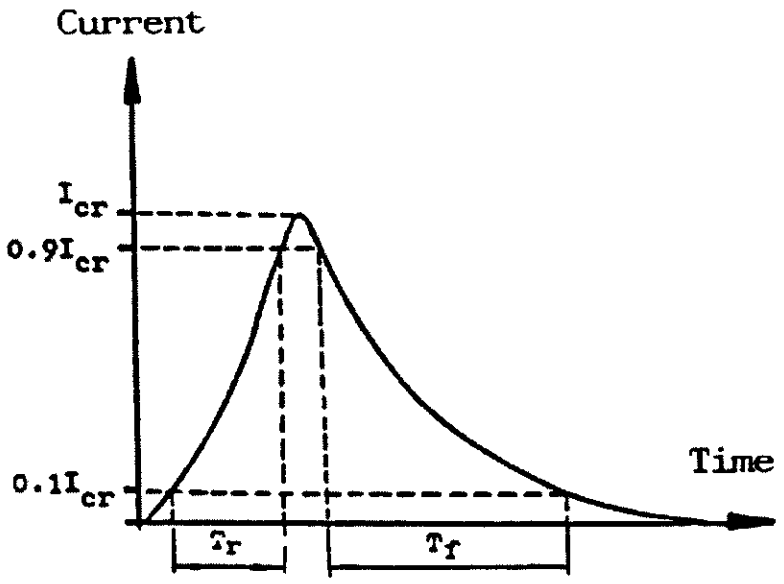

Figure 2.1

Typical discharge current pulse

The influence of a train of pulses is taken into account by the parameter called „pulse repetition rate" (PRR) measured in pulses per second. Table 2.1 presents typical values of the above parameters for microgap discharges and compares them with identical parameters of positive and negative corona.

Type of pulse	I_{cr}, mA	T_r, ns	T_f, ns	T_d, ns	PRR, pulses/s
Microgap discharge	1,000	1	2	5	up to 2,000
Positive corona	50	10	100	200	up to 10,000
Negative corona	2	3	80	100	up to 100,000

Table 2.1

Typical characteristics of corona and microgap discharges

The comparison shows that microgap discharges have a much larger amplitude than either the positive or negative pulsative corona, and a much steeper front and tail of the wave. However, the repetition rate of microgap discharges is much smaller than that of corona discharges.

It was the systematic study of undisturbed discharge waveforms that became the focal point of investigations [2.5]. Sample waveshapes of positive and negative discharges, at onset voltage, for several gap spacings, are shown in Figure 2.2. Corresponding measured frequency spectra are displayed in Figure 2.3. Inspection of waveshape diagrams (Figure 2.2) reveals an increase of pulse amplitude and of pulse duration with the increase of gap spacing. These changes in the waveform are reflected in the frequency spectrum (Figure 2.3) by a corresponding increase in its energy level and a decrease in its bandwidth.

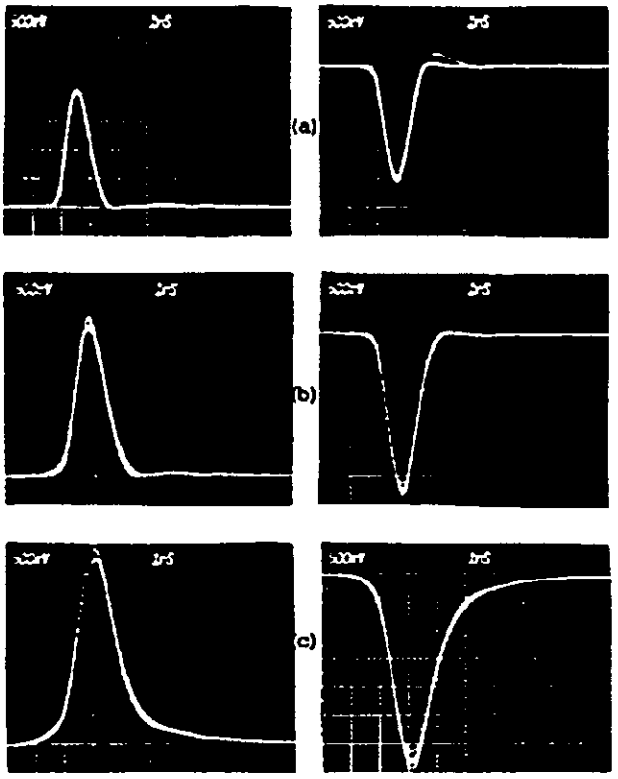

Figure 2.2

Examples of the effect of gap size upon current waveforms of microgap discharges
gap size : (a) 0.1 mm (b) 0.2 mm (c) 0.5 mm
Scale : 1 ns and 500 mV

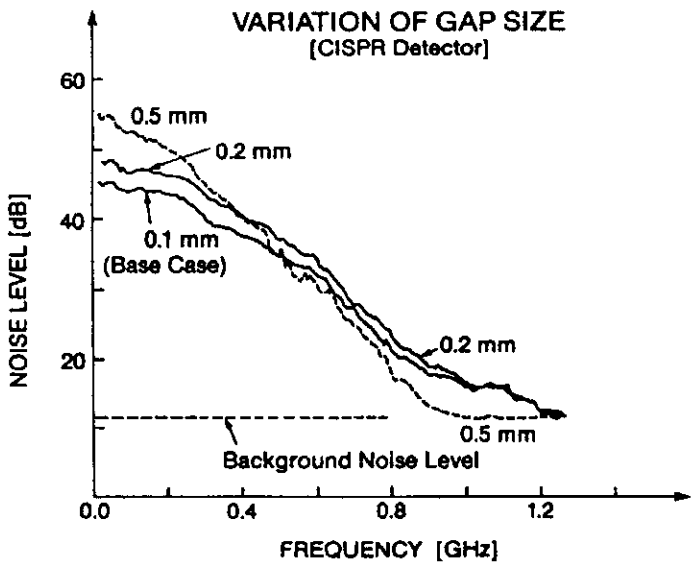

Figure 2.3

Frequency Spectra for various gap sizes

2.3.2 Pulse Repetition Rate

For any given setting of the microgap geometry, observed waveshapes of discharges were identical, within expected statistical limits [2.18]. The size of the coupling capacitor or of the coupling resistor did not influence the discharge process or the waveshape, but determined the repetition rate of current pulses. This fact is clearly seen from the shape of frequency spectra shown in Figure 2.4. The shape of frequency spectra remains practically unchanged, indicating essentially no change in the form of the discharge current waveshape, whereas the peak values of the impulses are related to the charging resistances or capacitances.

These observations are consistent with the physics of electrical discharges. The discharge process is governed by the geometrical details of the gap, but the repetition rate of pulses is influenced by other factors. The time between individual breakdowns of a microgap depends upon the time needed to charge the capacitance of the gap to the level at which onset voltage will be reached. Under normal circumstances pulse duration is negligible in comparison to the charging time, thus charging time is the most important factor in influencing the repetition rate of discharge pulses.

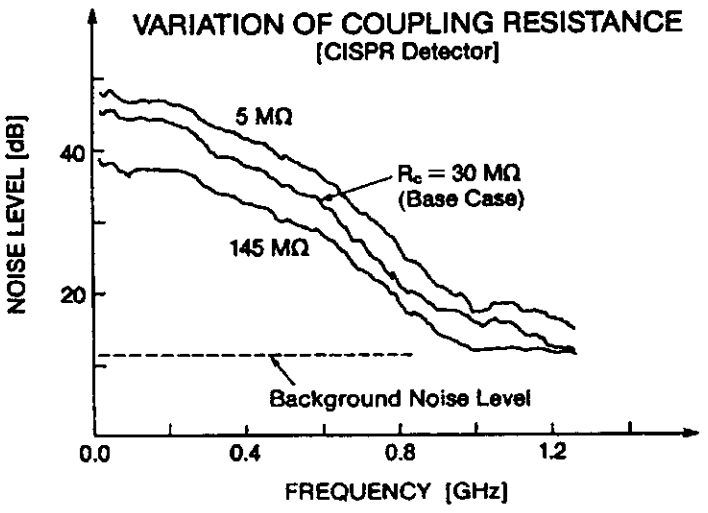

Figure 2.4

Effect of coupling resistance upon noise level of microgap discharges

2.3.3 Effects of Gap Spacing

Distance between electrodes of a gap determines the value of voltage at which the discharge is initiated. Figure 2.5 indicates that the relation between onset voltage and gap size is non-linear [2.19]. Furthermore, it is different for positive and negative discharges. For gaps of small size, where the field between electrodes is reasonably uniform, there is no difference in the onset values of the two polarities. However, for larger spacings, when field intensity between the two electrodes becomes nonuniform, negative onset voltage is lower than that for the case of positive polarity.

The somewhat increased positive onset voltage is responsible for a slightly increased amplitude of the positive current pulse in comparison with that of negative discharges in case of larger size gaps. Figure 2.6 shows not only the mean values of current amplitudes for discharges of both polarities, but also the observed range. Considerable variation in current amplitude is seen as the result of statistical processes responsible for initiation of discharges [2.18]. The larger the gap, the larger is the observed variation in current amplitude, since in a more nonuniform interelectrode field, conditions appropriate for initial ionization exist only in a smaller percentage of the gap volume.

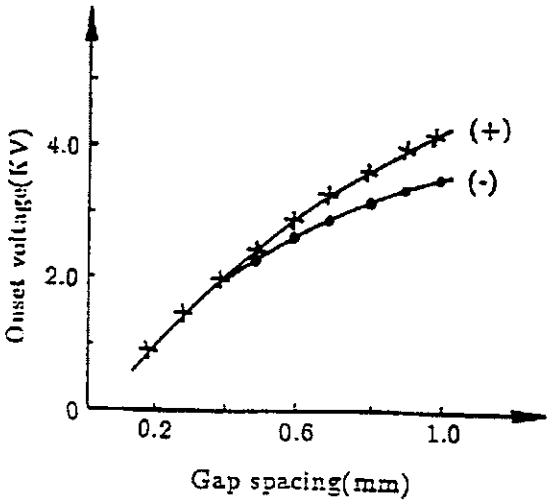

Figure 2.5

Effect of gap size upon positive and negative onset voltage

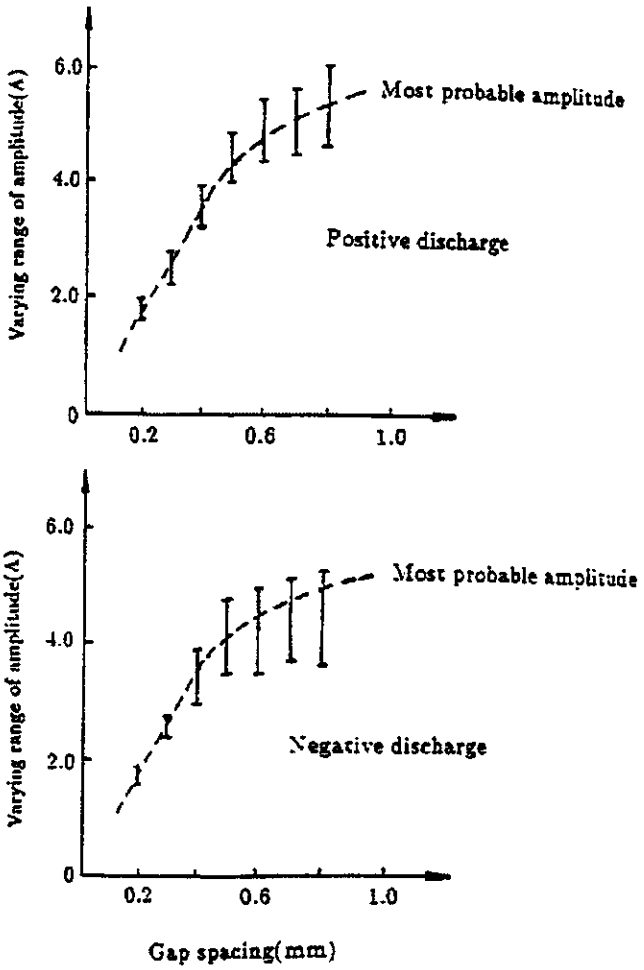

Figure 2.6

Effect of gap size upon amplitude of discharge current at onset voltage

2.3.4 Rain Corona

The detrimental influence of inclement weather upon electromagnetic noise in general, and upon television interference in particular, has been long recognized [2.6]. However, the mechanism of noise generation was not fully appreciated originally. At first it was believed that the presence of water droplets or ice formation on conductors was responsible for an earlier onset of critical voltage and, therefore, for the general elevation of the noise level. It was later recognized that in addition to the general rise a change in the shape of the frequency spectrum takes place [2.20]. Studies of water droplets on energized conductors and of their effects conducted in the laboratory revealed increased elevation of the radiated energy in the range of higher frequencies, including those inherent in operation of television stations [2.21]. Figure 2.7 gives a comparison of the frequency spectrum for a dry conductor with that for a wetted conductor, both subjected to the same operating voltage. The figure shows an overall increase in the energy level of the wetted conductor and the change in the shape of its frequency spectrum.

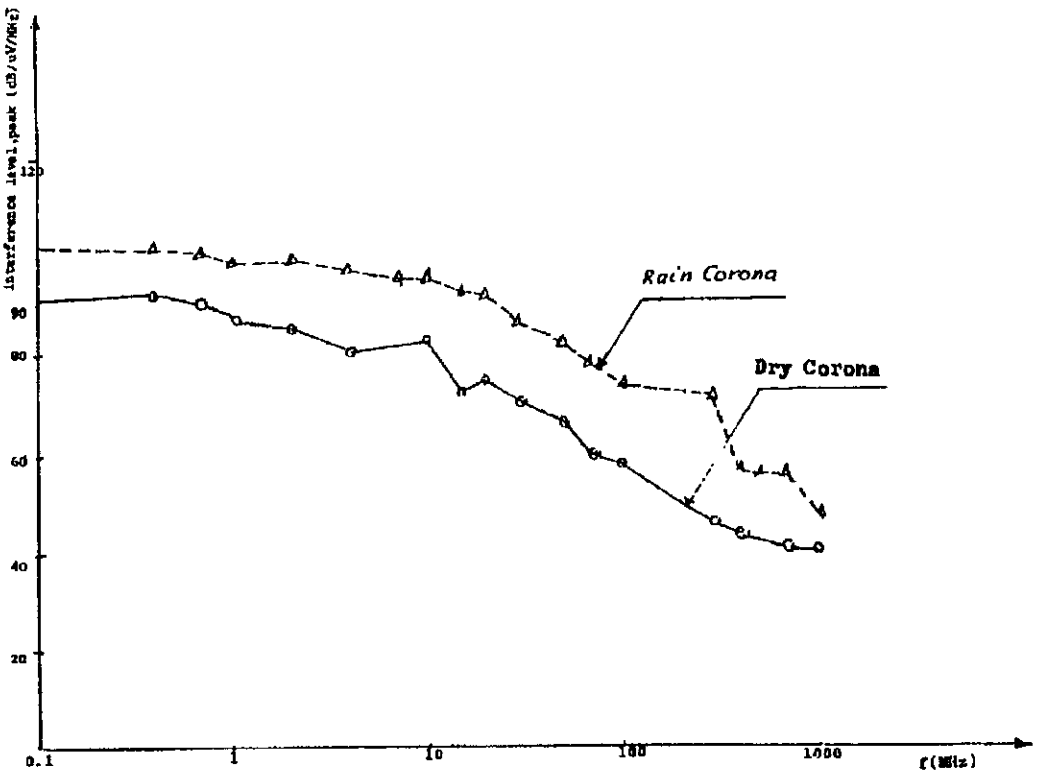

Figure 2.7

Comparison of frequency spectra from a dry and a wetted conductor

The mechanism responsible for the increase in the energy level and the change in the shape of the frequency spectrum was observed by very fast photography. When a wetted corona point on a conductor under voltage was photographed at 400 or 800 frames per second, it became possible to see first the change in the shape of the adhering water droplet and then its subdivision into many subdroplets [2.22]. As the subdroplets descended by the force of gravity and of electric field they became charged, and small discharges were occasionally observed in the space close to the conductor. These discharges, occurring between the subdroplets and the conductor as well as between subdroplets themselves, resemble somewhat microgap discharges described in preceding subsections. Consequently, their radiated electromagnetic energy contains components responsible for an increased energy level and for a change in the shape of the frequency spectrum. In view of these findings, rain corona should be considered as a combination of genuine corona discharges mixed with microgap discharges.

2.4 Insulator Noise

Contaminated insulators are also seen to produce electromagnetic noise when discharges start occurring between adjacent patches of contamination on their surfaces. The surface of the insulator enhances the growth of the discharge and thereby reduces the time required for its development [2.22]. Since the capacitance of contaminated patches is small, the radiated noise spectrum is very wide and includes television frequencies. Consequently this source of electromagnetic noise must be included as well when radiation from power lines in the frequency range above 30 MHz is considered.

2.5 Comments on Conductor Surface Gradient Computation

The considered example (three-phase line in flat configuration) presents the following characteristics :

Voltage between phases	U = 1050 kV
Number of subconductors	n = 8
Subconductor diameter	d = 3 cm
Spacing between subconductors	s = 45 cm
Radius of the circumference carrying the 8 subconductors	R = 58.8 cm
Height above ground $h_{average} = h_{minimum} + \frac{1}{3}$ sag $h_{average} = h_{anchoring} - \frac{2}{3}$ sag	$h_1 = h_2 = h_3 = 20$ m
Interphase spacing	S = 15 m
Earth resistivity	$\rho = 100\ \Omega$ m

2.5.1 Approached Method as in the Previous Guide

The conductor surface gradient can be computed by the method of the CIGRE Guide [1.1] with the following hypotheses :
- perfectly cylindrical subconductors
- conductors parallel to a perfectly plane ground
- uniform earth ground resistivity

1) to calculate the surface gradient of conductors in a bundle, the total charge Q of the bundle is first determined by introducing its equivalent radius, r_e, into the expressions for the potential coefficients.

$$r_e = R\sqrt[n]{\frac{n\,r}{R}} \qquad \Rightarrow \qquad r_e = 58.8\sqrt[8]{\frac{8 \cdot 1.5}{58.8}} = 48.2 \text{ cm}$$

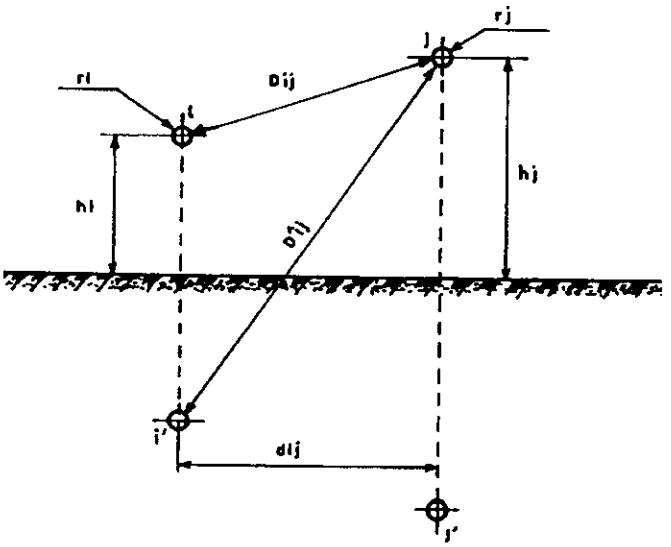

Figure 2.8

Potential coefficients calculation

2) using the notations of Figure 2.8, let :

$$D'_{ij} = \sqrt{d_{ij}^2 + (h_i + h_j)^2} \qquad D_{ij} = \sqrt{d_{ij}^2 + (h_i - h_j)^2}$$

3) matrix of potential coefficient $[\lambda]$

$$\lambda_{ii} = \frac{1}{2\pi\varepsilon_0} \cdot \ln\frac{2h_i}{r_i}$$

$$\lambda_{ij} = \lambda_{ji} = \frac{1}{2\pi\varepsilon_0} \cdot \ln\frac{D'_{ij}}{D_{ij}}$$

$$[\lambda] = \frac{1}{2\pi\varepsilon_0}\begin{pmatrix} 4.419 & 1.047 & 0.511 \\ 1.047 & 4.419 & 1.047 \\ 0.511 & 1.047 & 4.419 \end{pmatrix}$$

4) the capacitance matrix

$$[C] = [\lambda]^{-1} = 2\pi\varepsilon_0\begin{pmatrix} 0.241 & -0.0534 & -0.0152 \\ -0.0534 & 0.252 & -0.0534 \\ -0.0152 & -0.0534 & 0.241 \end{pmatrix}$$

5) the charges matrix

$$[Q] = [C][V]$$

$$\text{with } [V] = \begin{bmatrix} V_1 \\ V_2 \\ V_3 \end{bmatrix} = V\begin{bmatrix} 1 + j\,0 \\ -\frac{1}{2} + j\frac{\sqrt{3}}{2} \\ -\frac{1}{2} - j\frac{\sqrt{3}}{2} \end{bmatrix}$$

$$[Q] = 2\pi\varepsilon_0\begin{pmatrix} 0.241 & -0.0534 & -0.0152 \\ -0.0534 & 0.252 & -0.0534 \\ -0.0152 & -0.0534 & 0.241 \end{pmatrix}\begin{pmatrix} 1 + j\,0 \\ -\frac{1}{2} + j\frac{\sqrt{3}}{2} \\ -\frac{1}{2} - j\frac{\sqrt{3}}{2} \end{pmatrix} 606.2\ 10^3$$

$$[Q] = 2\pi\varepsilon_0\begin{pmatrix} 166705 - j\,20089.5 \\ -92324.3 + j\,160036.8 \\ -65954.6 - j\,154581 \end{pmatrix}$$

$$Q_1 = \left|[Q]_1\right| = 2\pi\varepsilon_0\ 167911 \quad \text{in C}$$

$$Q_2 = \left|[Q]_2\right| = 2\pi\varepsilon_0\ 184758 \quad \text{in C}$$

$$Q_3 = \left|[Q]_3\right| = 2\pi\varepsilon_0\ 168063 \quad \text{in C}$$

6) the mean gradient of a conductor is then given by :

$$g_a = \frac{1}{n} \frac{Q}{2 \pi \varepsilon_0 r}$$

since it is assumed that the total charge of the bundle is equally distributed on the n subconductors.

$g_{a1} = g_{a3} = 14.0$ kV/cm

$g_{a2} = 15.4$ kV/cm

7) the maximum gradient of the subconductors is defined by :

$$g = g_a \left[1 + \frac{(n - 1) r}{R} \right]$$

$g_1 = g_3 = 16.5$ kV/cm

$g_2 = 18.2$ kV/cm

2.5.2 Numerical Method

Using a computing code based on FE (Finite Elements) or BE (Boundary Elements), for example by BE [2.23] and [2.24], the following results for the conductor surface gradient are obtained (figure 2.9 and table 2.2).

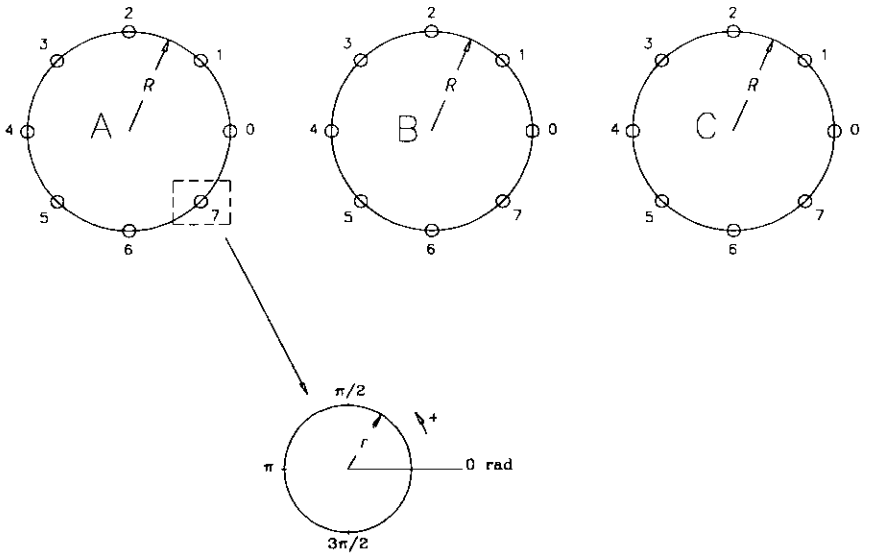

(a) geometry of the three-phase line in flat configuration used for the computed example by BE code

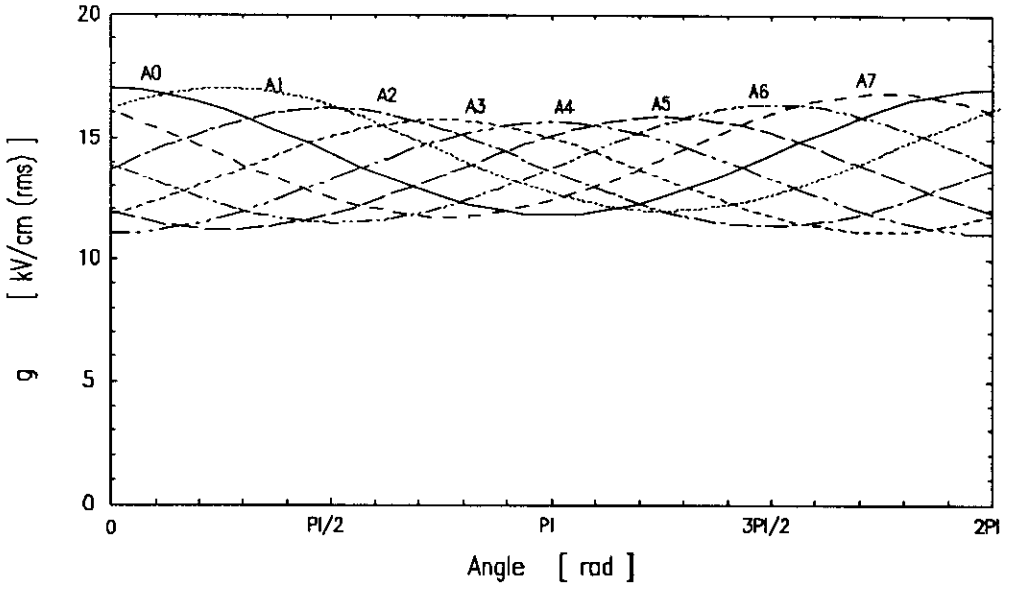

(b) variations of the conductor surface gradient around each subconductors of the lateral phases

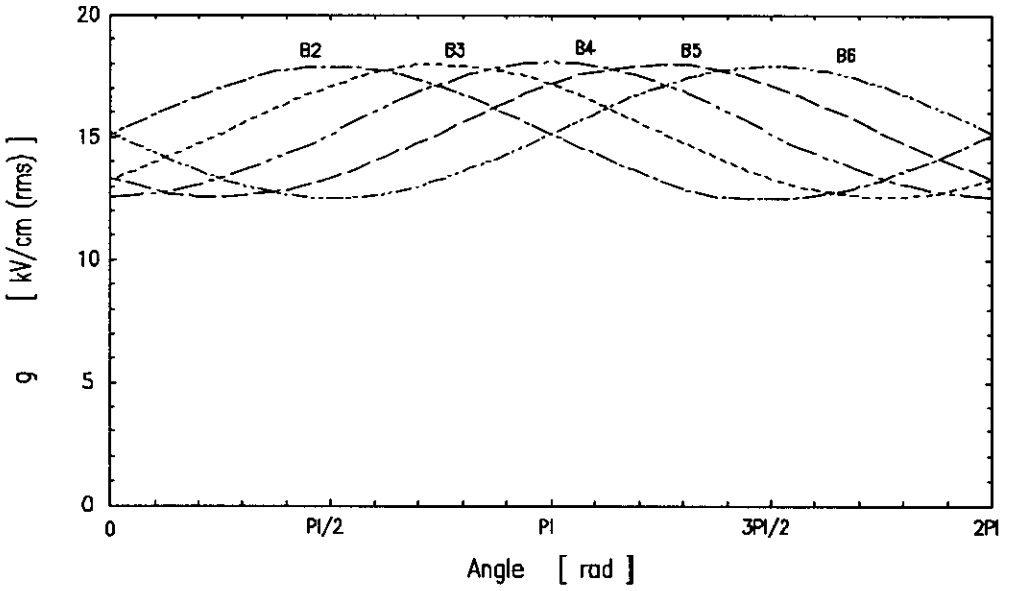

(c) variations of the conductor surface gradient around the subconductors of the central phase

Figure 2.9 *(a), (b), (c)*

Computation of the conductor surface gradient by BE code, [2.23] and [2.24]

Conductor	g_{max} kV/cm (rms)	g_{min} kV/cm (rms)
A0 - C4	16.99	11.78
A1 - C3	16.70	11.66
A2 - C2	16.20	11.33
A3 - C1	15.77	11.08
A4 - C0	15.68	11.01
A5 C7	15.90	11.15
A6 - C6	16.38	11.43
A7 - C5	16.82	11.66
Average of g_{max}	16.30	
Method [1.1]	16.5	

Conductor	g_{max} kV/cm (rms)	g_{min} kV/cm (rms)
B0	18.09	12.59
B1	17.96	12.56
B2	17.87	12.51
B3	17.96	12.56
B4	18.09	12.59
B5	17.98	12.57
B6	17.91	12.51
B7	17.98	12.57
Average of g_{max}	17.98	
Method [1.1]	18.2	

Table 2.2

Computation of the conductor surface gradient by BE [2.23], [2.24], and by approached method [1.1]

Despite the fact that the computed configuration is relatively far from the previous one (i. e. 4 subconductors), the difference between the precise (BE code, [2.23], [2.24]) and approached [1.1] computed values for the effective value of the average of the maximum conductor surface gradient are less than 1.5 %.

2.5.3 Computation of the Radius of the Equivalent Zero Potential Cylinder

R_z is determined to obtain the same capacitance in a concentric cylindrical arrangement as on the real line.

- $R_z = r_e \cdot e^{2\pi\varepsilon_0/C_c}$

  with C_c = total capacitance per length of the conductor within the line configuration (F/m)

- $C_c = \dfrac{2\pi\varepsilon_0}{\ln\left(\dfrac{R_z}{r_e}\right)}$ $\qquad g_a = \dfrac{1}{n}\dfrac{Q}{2\pi\varepsilon_0 r}$ $\qquad Q = C_c \cdot V$

$$\Rightarrow \quad C_c = \frac{g_a\, 2\pi\varepsilon_0\, r\, n}{V} \quad \Rightarrow \quad \ln\left(\frac{R_z}{r_e}\right) = \frac{V}{g_a\, r\, n} \quad \Rightarrow \quad R_z = r_e\, e^{\frac{V}{g_a r n}}$$

In the case of the example, for the central phase : $R_z = 48.2\, e^{\frac{606.2}{15.4\ 1.5\ 8}} = 1281$ cm

2.5.4 Computation of the Critical Corona Onset Gradient

$$g_c = g_0 \cdot \delta \cdot m \cdot \left(1 + \frac{K}{\sqrt{\delta \cdot r}}\right)$$

where $g_0 = 31$ kV/cm, K= 0.308 $\sqrt{\text{cm}}$, $\delta = 1$ and r = 1.5 cm

$$\Rightarrow \quad g_c = m \cdot 38.8 \text{ kV/cm} \quad \text{or} \quad g_c = m \cdot 27.4 \text{ kV/cm (rms)}$$

Glossary chapter 2

C_c	total capacitance per length of the conductor	F/m
d	subconductor diameter	cm
g	effective value of the average of the maximum gradients of the individual subconductors	kV/cm (rms)
g_0	corona onset gradient	kV/cm
g_a	average gradient of subconductors	kV/cm
g_c	critical corona onset gradient (visual)	kV/cm
I_{cr}	maximum value of current wave	A or mA
K	constant factor	$\sqrt{cm}$
K_d	constant factor	°C/cm(Hg) or °C/Pa
ln	$\ln \equiv \log_e$, e = 2.7182	
log	$\log \equiv \log_{10}$	
m	conductor surface irregularity factor	
n	number of subconductors	
p	pressure of the ambient air	cm Hg or Pa
q	altitude above sea level	m
Q	charge	C
r	radius of the subconductors	cm
R	bundle radius	cm
r_e	equivalent radius of the bundle	cm
R_z	radius of the equivalent zero potential cylinder	cm
s	spacing between subconductors	cm
S	interphase spacing	m
t	temperature of the ambient air	°C
T_d	pulse duration (time from initiation to completion of the current wave)	ns
T_f	fall time (time between the 90 % and 10 % value of the amplitude measured on the tail of the wave)	ns
T_r	rise time (time between the 10 % and 90 % value of the amplitude measured on the front of the wave)	ns
U	voltage between phases	V or kV
V	voltage between phase and ground	V or kV
δ	relative air density (RAD)	

[C]	capacitance matrix	
[Q]	matrix of charges	
[λ]	matrix of potential coefficient	
λ_{ii}	potential coefficient	C^{-1}
λ_{ij}	potential coefficient	C^{-1}
ρ	earth resistivity	Ω m

References

[1.1] "Interferences Produced by Corona Effect of Electric Systems; Description of Phenomena, Practical Guide for Calculation", Brochure No. 20, WG 36.01, CIGRE, Paris 1974.

[2.1] F. W. Peek, "Dielectric Phenomena in High Voltage Engineering", 2nd American edition, Ackermann, Librairie Delagrave, Paris, 1924.

[2.2] J.B. Whitehead, "High Voltage Corona", International Critical Tables, McGraw Hill, 1929.

[2.3] V.L. Chartier, L.Y. Lee, L.D. Dickson, K.E. Martin, "Effect of High Altitude on High Voltage AC Transmission Line Corona Phenomena", IEEE Transactions, Vol. PWRD-2, No. 1, Jan. 1987, pp. 225-237.

[2.4] V. L.. Chartier, "Effect of Load Current on Conductor Corona", Report to CIGRE SC36 Lausanne, October 1993.

[2.5] W. Janischewskyj, "Study of Gap Type TV Interference in the Field and in the Laboratory", NSERC Project CRD-8416, Final Report, May 1986.

[2.6] F. W. Warburton, T. W. Liao & N. A. Hoglund, "Power Line Radiations and Interference above 15 MHz", IEEE Transactions on Power Apparatus and Systems, Vol. PAS-88, No. 10, October 1969, pp. 1492 - 1501.

[2.7] T. Suzuki, "Breakdown Phenomena in Point-to-plane Gaps", IEEE Transactions on Industry Applications, Vol. IA-12, No. 1, January/February 1976.

[2.8] T. Suzuki, "Transition from Primary Streamer to Arc in Positive Point-to-plane Corona", Journal of Applied Physics, Vol. 42, No. 10, September 1971, pp. 3766 - 3777.

[2.9] T. Suzuki, "Transition from Primary Streamer to Arc in Negative Point-to-plane Corona", Journal of Applied Physics, Vol. 44, No. 10, October 1973, pp. 4534 - 4544.

[2.10] G. K. Hatanaka, "Field Measurements of VHF Noise from an Operating 500 kV Power Line", IEEE Transactions on Power Apparatus and Systems, Vol. PAS-100, No. 2, pp. 863 - 872.

[2.11] W. Janischewskyj, J. Reichman, "Active Television Interference from Power Lines", Paper No. 19, CEA E &O Meeting, Montreal, Quebec, March 25 - 28, 1985.

[2.12] M. O. Loftness, "Instrumentation and Techniques for the Location of TVI Sources on Power Lines", IEEE Tutorial Course on "The Location, Correction and Prevention of RI and TVI Sources from Overhead Power Lines", IEEE 76CH1163-5-PWR, pp. 40 - 54, 1976.

[2.13] J. Reichman, D. B. Craig, "Development of TVI-Reduced Design of Distribution Lines", Canadian Electrical Association, Report No. 77 - 45, 1982.

[2.14] W. Janischewskyj, A. Arainy, "Microgap Discharges as Sources of Television Interference", IEEE International Electrical, Electronics Conference, Toronto, Canada, September 1983, pp. 638 - 641

[2.15] W. Janischewskyj, N. Miguchi, K. Arai, "Characteristics of Electromagnetic Noise from a Conically Shaped Electrode", International Symposium on Electromagnetic Compatibility, Tokyo, Japan, October 16 -18, 1984.

[2.16] K. Arai, W. Janischewskyj, "Short-Gap Discharge as Source of Television Interference", Japan-US Seminar on Detection and Control of Electric Field and Space Charge in Electrical Environmental Problems, Fukuoka, Japan, Oct. 15 - 18, 1984.

[2.17] K. Arai, W. Janischewskyj, N. Miguchi, "Micro-gap Phenomena and Television Interference", IEEE Transactions on Power Apparatus and Systems, Vol. PAS-104, No. 1, January 1985, pp. 221 - 232.

[2.18] W. Janischewskyj & A. A. Al-Arainy, "Statistical Characteristics of Microgap Discharge", US-Japan Seminar on EMI in High Advanced Social System, August 1988, Honolulu, USA.

[2.19] S. Ying, "Study of Microgap Discharges and Television Interference", PhD thesis, University of Toronto, Canada, 1995.

[2.20] W. Janischewskyj, A. Arainy, "Corona Characteristics of Simulated Rain", Paper No. A79 496-1, IEEE/PES Summer Meeting Vancouver, B. C., July 15 - 20, 1979.

[2.21] A. A. Arainy, "The Effect of Rain on Electromagnetic Characteristics of Corona", MASc Thesis, University of Toronto, Canada, 1977.

[2.22] S. Y. Li, K. D. Srivastava, G. D. Theophilus, "Nanosecond Streak Photography of Discharges on Spacer Surfaces in Gases", IEEE Transactions on Dielectrics and Electrical Insulation, Vol. 2, No. 1, February 1995, pp. 114 - 120.

[2.23] F. Delincé, P. Dular, A. Genon, H. Hedia, W. Legros, A. Nicolet, "A subdomain method for FEM-BEM coupling in electromagnetism", Boundary Element Technology VI, C.A. Brebbia ed., Elsevier, 1991, pp. 77-88.

[2.24] P. Dular, A. Genon, W. Legros, J. Mauhin, A. Nicolet, M. Umé, "Comparison of pure and coupled BEM method for the study of a thin plate induction oven", Boundary Elements XIII, C.A. Brebbia & G.S. Gipson ed., Elsevier, 1991, pp. 375-384.

[2.25] P. Pirotte, "Contribution a l'étude des conséquences de l'effet de couronne sur les lignes aériennes à THT continue", Université de Liège, 1972.

Chapter 3

Electromagnetic Interference

3.1 Generation of Electromagnetic Interference (EMI) from Power Systems

Electromagnetic Interference (EMI) is any effect on the reception of a wanted radio or TV signal due to any unwanted disturbance within the radio frequency spectrum. For the purposes of this treatment the frequency is divided into two parts so that Radio Interference (RI) relates to frequencies up to 30 MHz. Television Interference (TVI) relates to frequencies higher than 30 MHz and affects the frequencies used for television broadcasting. EMI is, in general, concerned only with amplitude modulation (AM) radio reception and AM radio and television video signals. Other modulation systems (frequency modulation used for radio broadcasting and for television audio signals) are generally much less affected by disturbances.

Some natural phenomena including lightning discharges and sun-spot activities and several man-made devices (electrical appliances, engine ignition systems, electronic equipment, etc.) may also produce electromagnetic interference.

Transmission lines may also be responsible for EMI resulting from certain phenomena occurring on the various components of the line. The main interference sources are corona on conductors and fittings, discharges on insulators, and sparks at bad contacts (microgap discharges).

3.2 Characteristics of EMI Interference

Electric discharge phenomena produce various effects (power loss, high frequency electromagnetic fields, acoustic and luminous emission, ions and ozone generation). In particular, the electric pulses produced by the local ionizations, whose characteristics (shape, amplitude and repetition rate) vary for the different phenomena, give rise to the high frequency disturbing fields. Depending on these characteristics, the disturbing electromagnetic fields generated are characterized by different frequency spectra, different type of propagation [1] (guided or radiated) and different statistical variations as a function of ambient conditions.

3.2.1 Corona Disturbances

Corona disturbances are characterized by frequency spectra that generally extend up to only a few MHz, thus not interfering with TV frequencies. An example of the frequency spectrum for a 420 kV line at 15 m from the lateral conductor is given in Figure 3.1. Only in the particular case of a transmission line operating with high conductor-surface electric fields combined with unfavourable atmospheric conditions (heavy snow or rain), interferences with low amplitude TV signals, in the 40-60 MHz band, have been experienced. While between 1 MHz and 30 MHz, the amplitude of the spectrum is inversely proportional to the square of the frequency, in the TV broadcasting frequency it is only inversely proportional to the frequency.

---

[1] It is usual to express the electromagnetic field in terms of electric field E measured in dB above 1 μV/m (E in dB = 20 log (E/E_o); E_o=1 μV/m). The RI spectrum is generally given in relative values, the reference point being taken at a frequency of 0.5 MHz. This frequency is adopted by CISPR as reference frequency for the measurements.

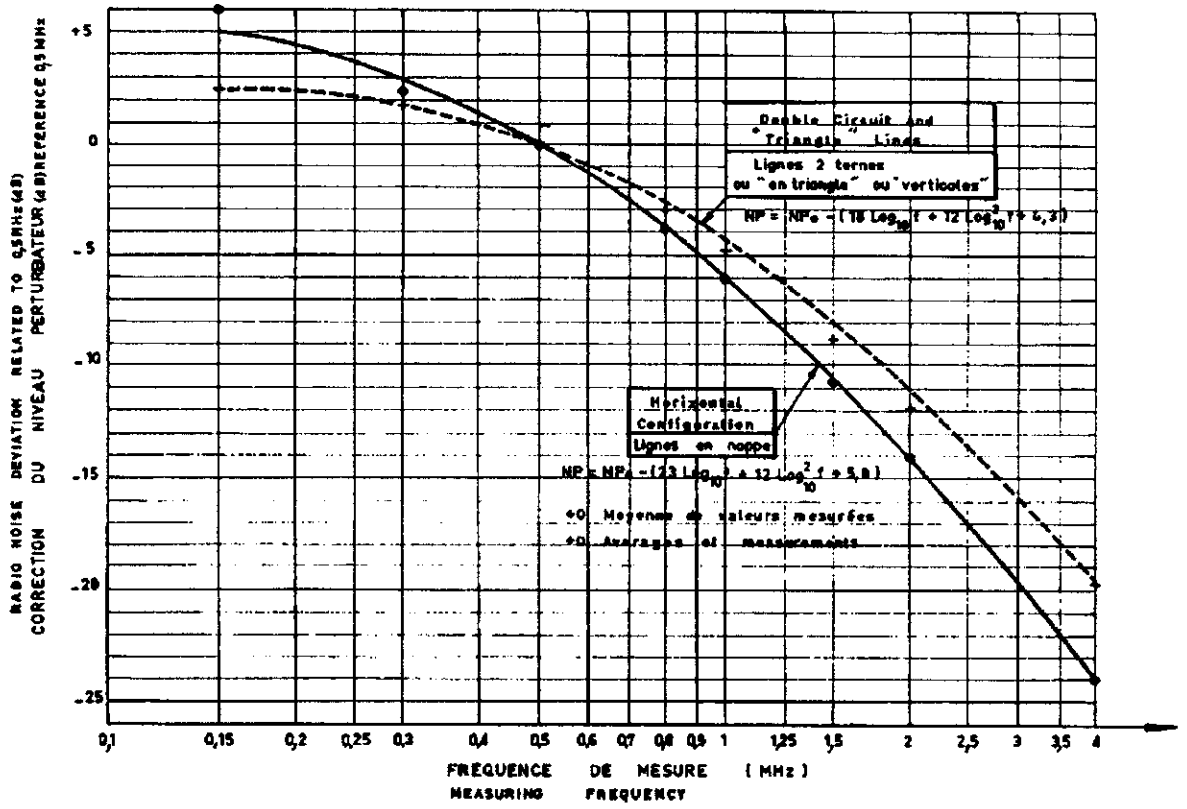

Figure 3.1

Example of frequency spectrum of the radio noise field generated by corona on a 420 kV line. NP is the deviation with respect to the reference level at 0.5 MHz, [1.1]

Because of the relatively low frequencies involved, the propagation of the disturbance is mainly guided along the line. For the most common line lengths, when they are exposed to uniform weather, the generation of disturbance is constant along their whole length and the electromagnetic field is laterally attenuated according to a profile that depends on the line configuration and on the ground characteristics (resistivity and shape). A few lateral profiles of the electromagnetic field at 0.5 MHz are given in Figure 3.2. They are expressed in dB relative to the value at a lateral distance of 15 m from the point directly under the outer phase conductor.

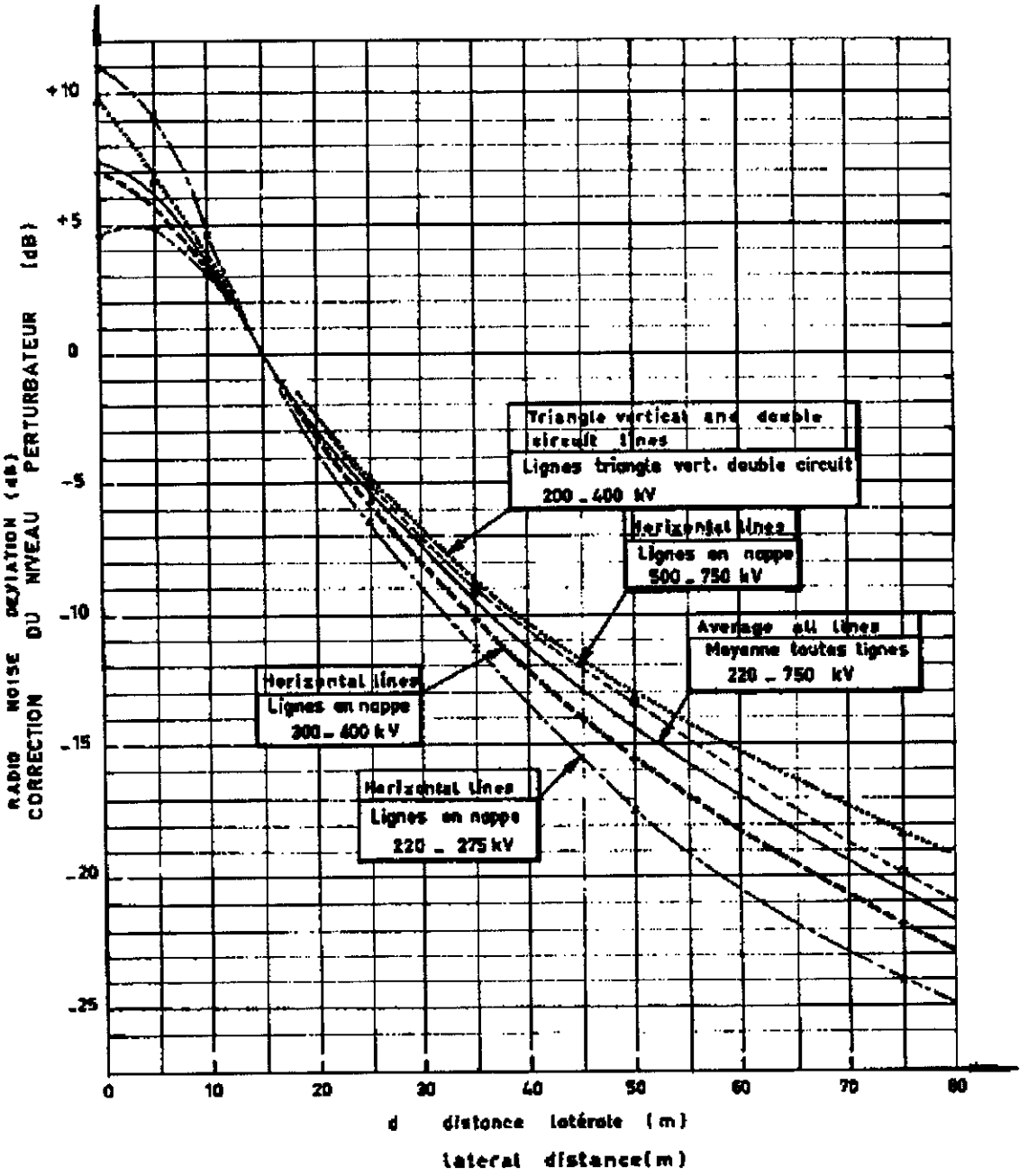

Figure 3.2

Typical lateral attenuation profiles for high voltage lines of the radio noise level at 0.5 MHz expressed relative to the value at 15 m lateral distance from the outer phase conductor, [1.1]

It has to be mentioned that the pattern of the lateral attenuation changes at about one sixth of the wavelength from the power line (100 m at 0.5 MHz). This problem is of interest especially in areas of low population density when weak reception signals of AM radio broadcasting is concerned. Only few measurements are available for the lateral profile at large distances from the line. It becomes even more critical when particularly sensitive equipment, such as radio telescopes or military communications systems, need to be located in the vicinity of a line and also when TV interference is concerned. For these reasons, new analytical methods have been developed [3.1] to allow a prediction of the lateral attenuation in far field. They reject the quasi-stationary field simplifications on which the semi-empirical methods used to predict corona radio interference fields at frequencies

below 30 MHz, are based. These methods assume the noise currents injected by corona or microgap discharges into the line conductors radiate electromagnetic fields, much like travelling wave antennae [3.2]. However, actual measurements at large distances to verify these new analytical methods are for the most part non-existent.

No actual measurements are published concerning the vertical attenuation above transmission lines. Theoretical investigations indicate a decay inversely proportional to the distance.

As already mentioned, the radio interference field strongly depends on surface conditions of conductors and in particular on the presence of water drops. For this reason, it is appropriate to represent the radio interference level in statistical terms, for example, in the form of cumulative distribution curves as the ones indicated in Figure 3.3, which refer to a one-year observation period.

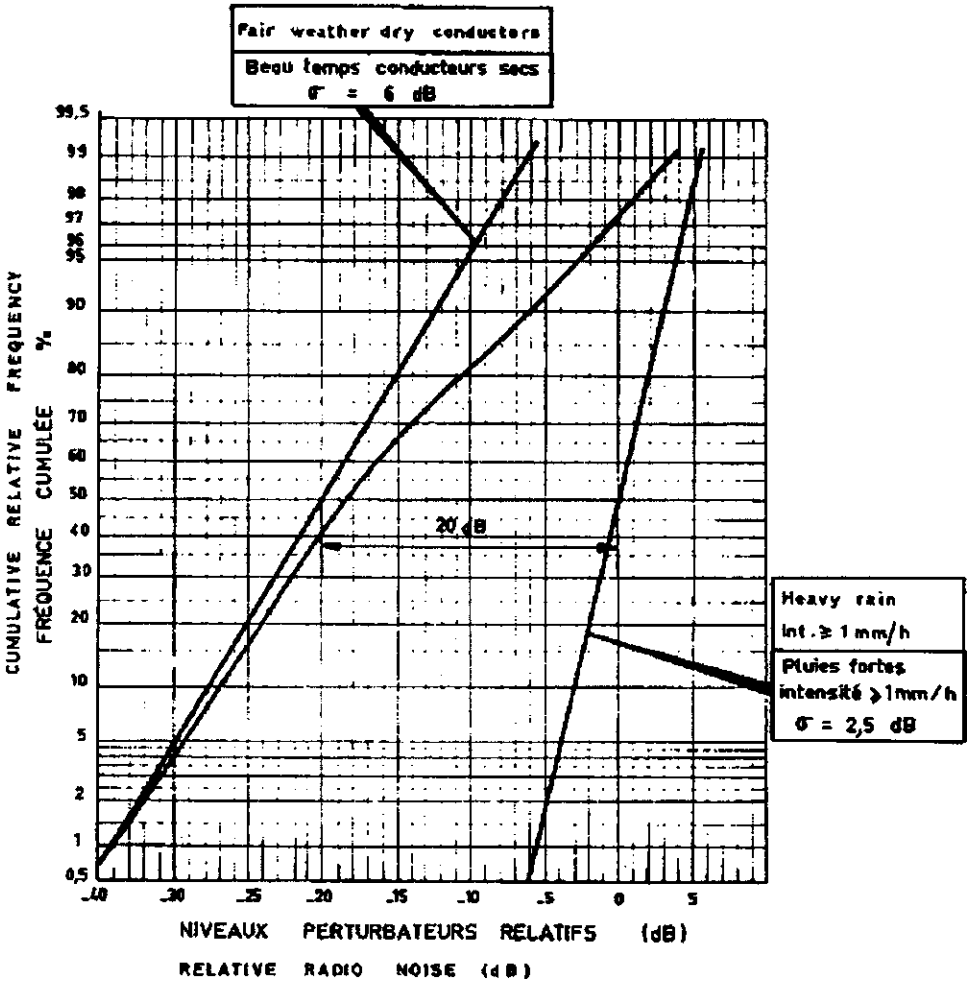

Figure 3.3

Typical radio noise distribution curves, referred to a one-year observation period, for different weather conditions [1.1]

These curves are generally identified by some characteristic values of the "all weather" curve, such as the value exceeded for the 50% of the time (L50 level) and the value exceeded for the 5% of the time (L5 level). Different factors, such as the electric field on the conductor, the climate of the site, the surface conditions of the conductors (new, aged, greased, etc.), influence the ranges of variation of the disturbance level. However, for lines of more usual design and for average climates, the differences between L5 and L50 are in the range 15-22 dB.

3.2.2 Discharges on Insulators

As regards discharges on insulators two main conditions can be identified:

- *Clean insulators under dry or wet conditions and polluted insulators in dry conditions.* In these cases, the frequency ranges involved and the propagation characteristics are very similar to those for corona of conductors. Nevertheless, the overall distribution of the disturbance due to insulator strings does not usually contribute to the total disturbance from the line. This is because it is generally not expensive to design the insulator strings to have a disturbance in dry conditions lower than that produced by the conductors and because the increase of corona on insulators under wet conditions is lower than that on conductors.

- *Polluted insulators under wet conditions.* The pulses due to sparking across dry bands are characterized by higher steepnesses than for corona and other types of discharges already considered. As a consequence, the corresponding frequency spectra extend to higher values, up to some tens of MHz, therefore affecting the lower bands of television broadcasting. For these higher frequencies, the propagation of the disturbance is mainly by radiation and has a local effect within a radius of a few hundred meters around the insulator as the source of the disturbance. The lateral attenuation is lower than for corona disturbance. The amplitude of the disturbances may be quite high, and it may be uneconomical to control them down to that of the corona of conductors.

3.2.3 Interferences due to Microgap Discharges

Bad contacts between metal parts at different potentials are the main source of interferences from microgap discharges. More often those effects are found with MV lines or LV installations, but punctured or broken insulator units on HV lines show similar phenomena. Predominantly these discharges occur under dry weather conditions, diminishing in humid atmosphere, when the gaps are short circuited by moisture.

The spectrum of this noise is almost flat in the frequency range from 0.1 to 100 MHz and is inversely proportional to the square of the frequency between 100 and 1000 MHz. Laboratory characterization of the statistical behaviour of these gaps have been performed [3.3]. Extensive measurements on transmission and distribution lines in Canada have shown that the problem of TV interference can be of great concern in the vicinity of distribution lines. Measurement in the vicinity of double circuit 400 kV lines with local gap discharge, see Figure 3.4, revealed a quite high TVI level between 80 and 500 MHz, with a reduction of the spectrum around 10 dB for doubling the distance from the line and an attenuation along the line of about 17-20 dB/km [3.23].

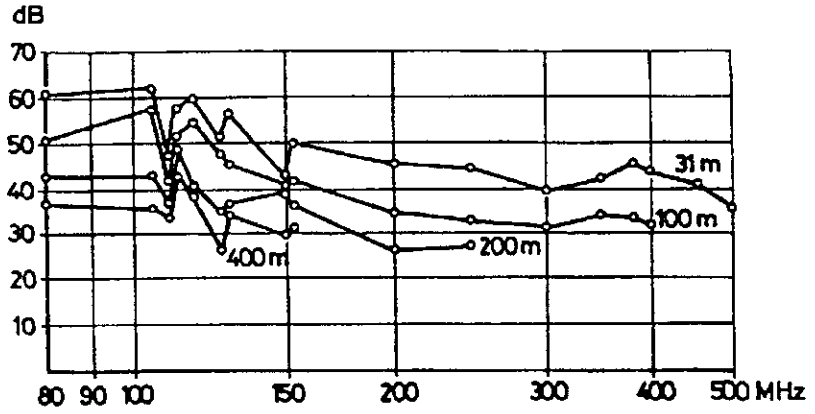

Figure 3.4

Example of the frequency spectrum generated by local microgap discharges on a 400 kV transmission line at various distances from such line.

Generally those disturbances are not present on HV lines, their occurrence indicate a faulty condition, which can be avoided by good installation and maintenance practices or eliminated by bridging the bad contacts with metal strips or conductive materials.

3.3 Quality of Radio and TV Receptions

The degree of annoyance is determined by the signal-to-noise ratio at the receiving installation. When establishing limits for the emission of radio interference and TV interference from power lines, the minimum signal strength to be protected has to be determined. This is left to the relevant national authorities and the international standards give only a guidance on how to establish limits [3.4].

For corona disturbances and discharges on clean insulators in dry or wet conditions or polluted insulators in dry conditions, and referring to AM radio broadcasting, different scales of the degradation of the reception as a function of the signal-to-noise ratio are given in the literature. The scale set up by CIGRE [1.1] is given in Table 3.1. It indicates that for a good reception, a ratio of 30 dB is adequate.

Quality of reception (AM Radio Broadcast)	signal-to-noise ratio (dB)
Interference not audible	30
Interference just perceptible	24
Interference audible, but speech perfectly received	18
Unacceptable for music, but speech intelligible	12
Speech understandable with severe concentration	6
Spoken word unintelligible; noise swamps speech totally	0

Table 3.1

Modulated signal measured with average or rms detector, noise with quasi-peak detector (QP) as dB (1 μV/m)

Based on the signal-to-noise ratio, the minimum signal strength to be protected, and the lateral profiles of disturbance, it is possible to define a corridor width outside of which the reception is acceptable for a certain percentage of time. The extent of this corridor depends on the minimum protected signal strength and on the line design. The choice of width results from both technical and economical considerations where the costs of an improved line design and of an increase in the broadcasted signal strength have to be compared [3.4].

For disturbances generated by sparking on bad contacts or by discharges across dry bands of polluted insulators, which interfere with the amplitude modulated TV video signals, it is more difficult to determine a scale of the degradation of the quality of reception.

Two comprehensive studies performed in North America by EPRI [3.5] and CEA [3.6, 3.7] have compared responses of different instruments to these disturbances and have shown, that a 40 dB signal-to-noise ratio, established as the CISPR Quasi-Peak measurement in a 120 kHz bandwidth, may be used as an indication for an acceptable performance.

Publication CISPR 18-2 [3.4] also states, that a signal-to-noise ratio of 40 dB could be adequate for a satisfactory reception with an average black and white detector. The more recent technical literature supports this ratio for colour television too.

3.4 Calculation of Electromagnetic Interference

The calculation of electromagnetic interference has to be considered separately for the two different ranges of frequency . The lower frequencies, up to 30 MHz are referred to in this guide as Radio Interference (RI) and are dealt with in section 3.4.1. The higher frequencies, above 30 MHz are referred to as Television Interference (TVI) and are dealt with in section 3.4.2.

3.4.1 Radio Interference

Chapter 4 of the previous Guide [1.1] reports empirical formulae, established by various organizations, which give the radio interference field directly at the reference frequency of 0.5 MHz or 1 MHz, at a given distance from a three-phase line, for three basic weather categories (50% fair weather, mean foul weather and mean heavy rain), as a function of the main influencing parameters

(voltage gradient, diameter of the subconductors, number of subconductors in the bundle, frequency, etc.). These formulae were based on the results of direct measurements of radio interference field performed on operating and experimental lines, with system voltages of up to 800 kV and bundles of up to four subconductors.

In the same Guide, another method is presented which calculates the radio interference field at a given distance from the line, using analytical procedures based on the modal propagation. It introduces a "radio interference excitation function" (Γ) in terms of the above-mentioned influencing parameters:

$$\boxed{\Gamma = k + f_1(g) + f_2(d) + f_3(n)} \qquad (3.1)$$

where Γ = RI excitation function

k = a constant

g = the effective value of the average of the maximum gradients of the individual subconductors (kV/cm (rms))

d = the diameter of the subconductor (cm)

n = the number of the subconductors in the bundle.

The excitation function approach utilizes the fact that the corona currents injected into a multiphase line depend not only on the intrinsic characteristics of the phase conductor under corona, usually constructed as a symmetrical bundle, but also on the self and mutual capacitances of the multiphase system [3.8, 3.9, 3.10]. Thus the radio interference currents are related to the intrinsic corona characteristics of the conductor through a relationship of the type:

$$\boxed{[I] = \frac{1}{2\pi\varepsilon_0} \cdot [C] \cdot [\Gamma]} \qquad (3.2)$$

where [I] and [Γ] are matrices of the phase currents and excitation functions of the conductors and [C] is the phase capacitance matrix.

The measurement of the RI current in a test configuration of known capacitance (a cage or an experimental span) allows the experimental determination of the excitation function and computation of the RI field for line configurations other than those tested.

Another important advantage of this approach is that the radio interference current measurements in a cage allows the determination of the excitation function under controlled ambient conditions (artificial rain corresponding to heavy rain) and for different conductor gradients. This is also a useful initiative possibility for comparison of different conductor configurations.

Under artificial rain, stable and reproducible results are achieved for a given cage, but the reproducibility is not consistent when results from cage to cage are compared [3.11]. Because of localized appearances of heavy rain conditions on lines, comparison of actual measurements with cage results is difficult.

Furthermore, attempts to determine fair weather excitation functions experimentally in cages, were even less successful in predicting fair weather performance of actual lines.

In a first approximation therefore correction factors are usually applied to results of heavy rain tests in order to evaluate the RI levels in other weather conditions (see Appendix 3.1).

It should be emphasized, that values of conductor gradients, used for the evaluation of measurements for the derivation of the excitation functions are usually calculated for smooth conductors of a symmetrical bundle in a coaxial configuration. Thus those idealized conditions are to be assumed for the actual line configurations also.

The formulae given in the Appendix 3.2 give satisfactory results for lines when ratio of the subconductor spacing s to the subconductor diameter d is higher than 10 to 15. At smaller s/d values, the real excitation function may prove to be much higher than that calculated, especially when there are ten or more subconductors in a bundle.

It should also be kept in mind, that all methods of radio interference calculation are matched to measurements close to the lines. Standard measurements are made at 20 m, radial distance (D)

between the next conductor and the field sensor, usually 2 m above ground, or 15 m lateral distance away from the outermost conductor.

Lateral profiles are confirmed by measurements up to approximately 100 m at 0.50 MHz, radio interference being proportional to $D^{-1.65}$ on an average.

The predetermination methods based on the concept of excitation function follow in general the procedure presented in Appendix 3.3 and compute the electric RI field. Following the concept of generation functions, however, primarily the magnetic component of the interference field is calculated. Though for RI frequencies not valid close to the lines, the conversion to the electric field is assumed to be

$$\boxed{E = Z_0 \cdot H} \qquad (3.3)$$

with Z_0 the impedance of free space

The same conversion is also used, when measurements are performed with a better directional, but not so sensitive magnetic loop antenna. Thus some discrepancy may be observed, when the true electric field is measured in the „near field", which includes the normal measurement range from 0 to approximately 100 m from the line.

Nevertheless methods presented in Appendix 3.2 are not restricted to those utilizing cages or single phase test spans for the determination of the excitation function. Several investigators have used statistically collected RI levels to not only propose formulae for the electric field, but also by applying the reversed process to derive from measured fields suitable expressions for the excitation function.

To make a rapid "on desk" evaluation of the radio interference field profile shape, instead of the analytical methods, the method given in [3.22] can be used with an acceptable approximation.

3.4.2 Television Interference (Frequencies above 30 MHz)

Investigations on conductor corona TVI available were not as extensive as in the case of RI from corona in the frequency range up to 30 MHz. In effect, the interferences to television reception are more often influenced by microgap discharges on power line hardware or by polluted insulators than by conductor corona.

Because of the higher frequency range, attenuation along a power line as well as that away from it, is considerably increased. Consequently, local effects of noise sources are much more pronounced when TVI is established.

Also, at these frequencies, the transition from the near field takes place within normal measurement distances, i.e. 100 meters approximately. This fact may be observed as a change in the decay of the lateral profile of the electromagnetic field at TV frequencies.

To evaluate the interference due to conductor corona in the frequency range above 30 MHz for television reception (TVI : television interference), some formulae were proposed for foul weather (see Appendix 3.4).

3.5 Corona Interference in the Case of Crossing of Lines

Radio Interference on a line, of low voltage, crossing another line having a higher voltage level may depend on two main factors:

- an increase in the electric field intensity on the wire surface of the lower voltage line (LV line in the following) at the point of the crossing with the higher voltage line (HV line in the following);
- the currents induced into the LV line, at the crossing point, from the corona on the HV line.

The enhancement of the electric field intensity on the conductor surface of the LV line due to the presence of the HV line can be calculated [3.12; 3.13; 3.14]. Figure 3.5 shows, as an example, the results of the electric field calculation on the conductor surface of a 10 kV line crossing a 750 kV line.

The crossing angle is 45°, the height of the 10 kV line is about 10 m and that of the 750 kV line is about 23.5 m at the crossing point. The length of the LV line which presents a substantial increase of the electric field is very short (it does not exceed 20 to 30 m on both sides from the external phases

of the HV line). For this reason, the gradient increase on the LV line conductor could hardly give a significant contribution to the radio interference level from the LV line itself. The high frequency electromagnetic coupling between the HV and LV line seems thus the most important factor.

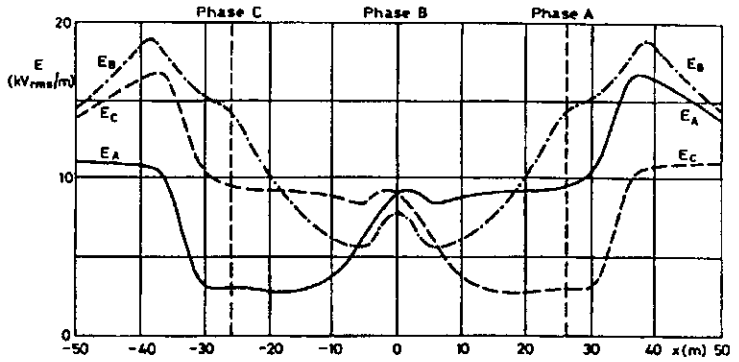

Figure 3.5

Calculated electric fields on the phase conductors, g_A, g_B, g_C, of a 10 kV line crossing a 750 kV line. Positions of phases A, B, C, of the 750 kV line are indicated by vertical dashed lines.

The calculation of the currents and voltages induced on the LV line from the corona currents on the HV line should take into account the fact that the mutual impedances and admittances of the two lines are not constant. With the simplified assumption that the propagation patterns along each line is not influenced by the presence of the other one, disregarding possible reflections due to discontinuity on both lines and disregarding the effect of the sag of the conductors on the mutual electric parameters, the following fundamental remarks can be made:

- The coupling between the LV and HV line is purely capacitive at 90° crossing angle and the resulting radio interference level on the LV line is minimum. The coupling becomes predominantly inductive at angles smaller than 60° to 70° and the difference between the radio interference levels at crossing angles of 90° and 45° reaches 6 dB.
- The main components of the currents and voltages induced in the LV line are of the conductor-to-ground mode which present a substantial damping with the travelling distance. Therefore, the radio interference level decreases rapidly with distance from the crossing point.
- The spectrum of the radio interference of the LV line is different from that of the HV line and changes at different distances from the crossing point. This is due to the fact that the electromagnetic coupling is higher for higher frequencies and that the damping along the LV line is higher for the higher frequency components. As a consequence, the 1 MHz radio interference levels may be higher than the 0.5 MHz component, equal, at the crossing point, at about 1-2 km and lower at higher distances.

Although few measurements have been performed in the field, the main results of the theoretical calculations were confirmed. Actual problems with radio interference produced from corona on HV lines in the AM broadcast band and drawn out by LV lines have been reported up to some kilometres away from the HV line corridor.

3.6 Passive Interference

The mechanisms of radio and television disturbances produced by power lines that have been indicated above can be classified as mechanisms of active interference because the line itself acts as a primary source of the disturbances. The power line can, however, be the subject of so called "passive interference". Typical cases of passive interferences are the reflection and reradiation of radio signals. These phenomena are simply related to the dimensions of the structure and are thus similarly present in other structures (buildings, poles, etc.) and not related solely to power transmission installation [3.24].

Reflections occur when the line intercepts a signal and reflects it. In the case of TV reception, this gives rise to ghost images due to the time delays of the main and of the reflected signal. Reradiation is a phenomenon that occurs when the tower of the line is in the vicinity of a broadcasting antenna array. The tower, depending on its dimensions, may act as an antenna tuned on some frequency emitted and thus change the emission patterns of the broadcasting station. Re-radiation from structures located near the receiving antenna can equally affect the reception, and the broadcast pattern is only locally modified [1.1].

Appendix 3.1 Calculation of the Radio Interference Field at a Given Distance from the Line for UHV Lines with Symmetrical Bundles and Aged Conductors

The calculation of the radio interference field at a given distance from the line for UHV lines with symmetrical bundles and aged conductors:

a) calculation of the excitation function of each conductor in heavy rain by means of a formula from Appendix 3.2

b) application of the correction factors given in Figure A3.1.1 to obtain the excitation function in other weather categories;

c) determination of the radio interference field profile for each conductor by means of analytical methods based on modal propagation, as indicated in Appendix 3.3, or a formula from Appendix 3.2 giving directly the RI field.

d) addition of the fields from the individual conductors according to [1.1]:

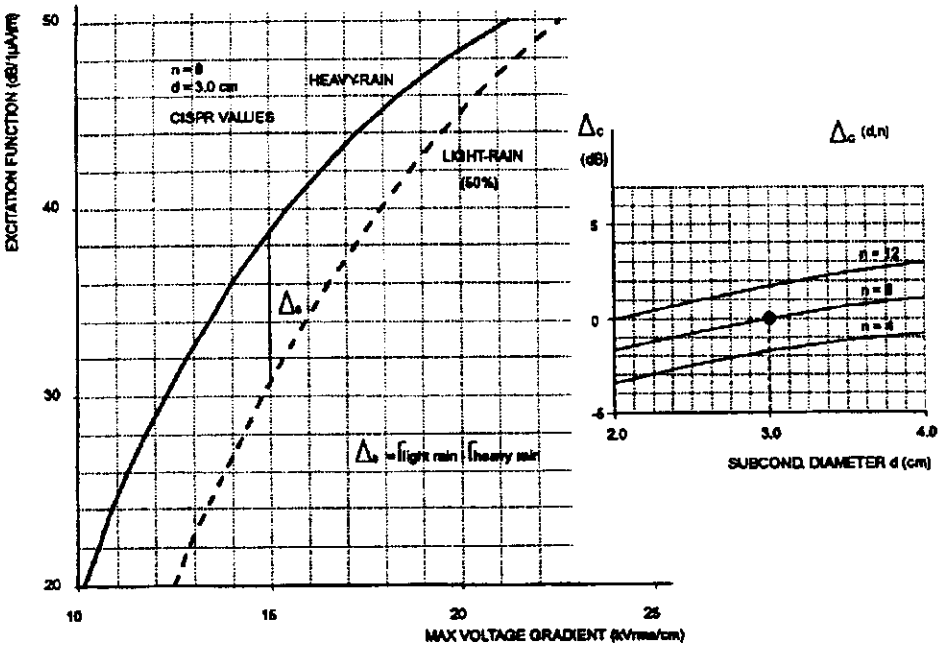

Figure A3.1.1

Correction factors to be applied to the heavy rain excitation function to obtain the light rain one as a function of maximum voltage gradient and number of subconductors, [3.22].

$$\Gamma_{\text{light-rain}} = \Gamma_{\text{heavy-rain}} + \Delta_O + \Delta_C$$

The fair weather excitation function is obtained by subtracting 17 dB from the light rain excitation function.

$$\Gamma_{\text{fair-weather}} = \Gamma_{\text{light-rain}} - 17$$

Note 1. fields from conductors of equal phase are added quadratically:

Define E as the EMI field

$$E_a = \left(\Sigma \ (E_i)^2 \right)$$

E_a : total of fields of phase a (dB (1 μV/m))

E_i : field of individual bundle conductor (i) of phase a

Note 2. ranking of the phase-fields:

$E_a \geq E_b \geq E_c$ (dB (1 μV/m))

if $E_a - E_b \geq 3$ dB: $E_t = E_a$

if $E_a - E_b < 3$ dB: $E_t = \frac{E_a + E_b}{2} + 1.5$

E_t : total radio interference field, (dB (1 μV/m))

Appendix 3.2 Overview of the Formulae Developed in Different Countries for the Evaluation of Radio Interference due to Corona

This Appendix reports the formulae developed by various experimenters for the predetermination of radio interference levels of individual conductors of AC lines.

The majority of the formulae give the excitation function Γ; some of them, however, give directly the electric field at a given distance from the line.

Specifications of measurements for QP-values [1.1]:

	Receiver		Measuring Frequency
	Pass band	Charge/discharge constant	
CISPR	9 kHz	1 ms / 160 ms	0.5 MHz
ANSI	5 kHz	1 ms / 600 ms	1.0 MHz

The result of these definitions [3.11] :

Comparison of receivers: Value (CISPR) = Value (ANSI) – 2 dB

Correction of measuring frequency:

Value (CISPR) = Value (ANSI) + 5.1 dB.

A3.2.1 BPA [3.11] (CISPR specification: QP - 9 kHz - 0.5 MHz)

Average fair weather

Add 17 dB to get mean foul weather, add 20.5 dB to get mean stable rain, add 24 dB to get heavy rain

$$RI = 46 + 120 \log\left(\frac{g}{17.56}\right) + 40 \log\left(\frac{d}{3.51}\right) + 10\left[1 - (\log(10 f))^2\right] + \frac{q}{300} - C_1 + C_2 \quad dB(1\mu V / m) \qquad (A3.2.1)$$

where: RI is the disturbance field strength, dB(μV/m) for one phase

g is the average maximum conductor surface gradient, kV_{rms}/cm

d is the conductor diameter, cm

f is the frequency, MHz

q is the altitude, m

C_1 is the value of lateral attenuation function C_a for a reference phase conductor at 13.7 m height, at 21.0 m radial distance from the antenna, ground conductivity : 4 mS/m.

C_2 is the value of lateral attenuation function C_a for the type of line the formula is being applied.

The lateral attenuation function C_a is derived from the following equations:

$$C_a = 10 \log (DW^2 + ESU^2 + EIND^2)$$

where: DW is the direct wave component

$$DW = \frac{h_c}{K D} \quad \text{when } D \leq \frac{12\, h_c\, h_a}{\lambda}$$

$$DW = \frac{h_c}{K\,D} \quad \frac{12\,h_c\,h_a}{\lambda\,D} \quad \text{when } D > \frac{12\,h_c\,h_a}{\lambda}$$

ESU is the surface wave component

$$ESU = \frac{f(\rho)\,h_c}{K\,D}$$

EIND is the induction field component

$$EIND = \frac{h_c}{(K\,D)^2}$$

where: h_a is the height of the antenna, m

h_c is the height of the conductor, m

D is the radial distance between conductors and antenna, m

f is the frequency, MHz

λ is the wavelength, m

$$K = \frac{2\,\pi}{\lambda}$$

$$f(\rho) = \frac{2 + 0.3\,\rho}{2 + \rho + 0.6\,\rho^2}$$

$$\rho = \frac{52.5\,D}{\delta\,\lambda^2}$$

δ is the ground conductivity in mS/m

The reference parameters for calculating C_1 are :

$$D_1 = 21.04 \qquad DW_1 = \frac{31.1}{f}$$

$$EIND_1 = \frac{70.55}{f^2} \qquad \rho_1 = \frac{276.16}{\lambda^2}$$

$$f(\rho_1) = \frac{2 + 0.3\,\rho_1}{2 + \rho_1 + 0.6\,\rho_1^2} \qquad ESU_1 = \frac{31.1\,f(\rho_1)}{f}$$

The RI for each phase is calculated using this formula. The highest value is the final RI. However, the total RI from all phase conductors of a power line can also be determined by the method in CISPR 18-3, Appendix A [3.22]. The maximum difference between the two approaches is 3 dB.

Generation function for "average stable foul weather" derived from long time measurements on real lines

$$\Gamma_{hr} = 37.02 + 120 \cdot \log\left(\frac{g}{15}\right) + 40 \cdot \log\left(\frac{d}{4}\right) \quad \text{dB } (1\mu A/\sqrt{m}) \qquad \text{(A3.2.2)}$$

Optimized generation function for "average stable foul weather" according to [3.11]

$$\Gamma_{hr} = 40.42 + 120 \cdot \log\left(\frac{g}{15}\right) + 40 \cdot \log\left(\frac{d}{4}\right) \quad \text{dB } (1\mu A/\sqrt{m}) \qquad \text{(A3.2.3)}$$

A3.2.2 CIGRE (derived from [1.1]), [3.11] (CISPR specification: QP - 9 kHz - 0.5 MHz)

Heavy rain:

$$E_{hr} = -10 + 3.5 \cdot g + 6 \cdot d - 33 \cdot \log\left(\frac{D}{20}\right) \quad \text{dB (1 } \mu\text{V/m)} \quad \text{(A3.2.4)}$$

$10\ m < D < 60\ m$ the term 6d is valid for $1\ cm < d < 2.5\ cm$ only

$$\boxed{\Gamma_{hr} = -40.69 + 3.5 \cdot g + 6 \cdot d \quad \text{dB (1 } \mu A/\sqrt{m})} \quad \text{(A3.2.5)}$$

Optimized according [3.11]

$$\boxed{\Gamma_{hr} = -40.39 + 3.5 \cdot g + 6 \cdot d \quad \text{dB (1 } \mu A/\sqrt{m})} \quad \text{(A3.2.6)}$$

A3.2.3 CRIEPI [3.15, 3.16] (CISPR specification: QP - 9 kHz - 0.5 MHz)

Fair weather

$$\boxed{E_{fw} = 4 + \left[(3.7\ g - 12.2)\right] + 40\log d + 20\log\left(\frac{h}{D^2}\right) - 12\left(\log(f)\right)^2 - 17\log(f) \quad \text{dB (1 } \mu V / m)} \quad \text{(A3.2.7)}$$

(standard deviation ± 3 dB)

Rainy weather

$$E_r = \frac{(E_m - E_0)}{\dfrac{\alpha\left(\dfrac{2.53}{d}\right)^2}{I+1}} + E_0$$

I	=	rate of rain (mm/hour)
α	=	$-0.16\ g^2/g' + 3.72$
g'	=	bottom surface gradient (kV/cm), rms value
E_m	=	electric field under maximum rate of rain
E_0	=	electric field under 0 rate of rain, wet conductor

E_m and E_0 are calculated by replacing the part in square brackets of the equation given for fair weather, by one of the following expressions respectively:

- To obtain E_m:

  $[10.5g' - (g'/2)^2 - 31]$ for g' ≤17 kV/cm

  $[4.38g' - (g'/4)^2 + 19.5]$ for g' > 17 kV/cm

- To obtain E_0:

  $[9.5\ g' - 0.16\ g'^2 + 50.5]$

A3.2.4 ENEL - 1000 kV Project [3.17] (CISPR specification: QP - 9 kHz - 0.5 MHz)

Heavy rain (95% of rain distribution)

rain intensity: 1.5 – 2 mm/min

$$\Gamma_{hr} = 69 - \frac{586}{g} - 10 \cdot \log n + 30 \cdot \log d \quad dB\ (1\ \mu A/\sqrt{m}) \qquad (A3.2.8)$$

rain intensity: 0.01 – 0.03 mm/min

$$\Gamma_{hr} = 73 - \frac{948}{g} - 12 \cdot \log n + 60 \cdot \log d \quad dB\ (1\ \mu A/\sqrt{m}) \qquad (A3.2.9)$$

A3.2.5 EPRI [3.10, 3.11] (CISPR specification: QP - 9 kHz - 0.5 MHz)

Heavy rain (99% of the distribution under rain, cage values, artificial rain corresponding to 8 - 12 mm/hr natural rain)

$$\Gamma_{hr} = 81.1 - \frac{580}{g} + 38 \cdot \log\left(\frac{d}{3.8}\right) + K_n \quad dB\ (1\ \mu A/\sqrt{m}) \qquad (A3.2.10)$$

Optimized according to [3.11]

$$\Gamma_{hr} = 76.62 - \frac{580}{g} + 38 \cdot \log\left(\frac{d}{3.8}\right) + K_n \quad dB\ (1\ \mu A/\sqrt{m}) \qquad (A3.2.11)$$

where : $K_n = 0$ for $n \leq 8$

$K_n = 5$ for $n > 8$

The formula is valid for conventional bundles with a ratio s/d in the range of 10 to 20. For other bundle geometries where the ratio k between the maximum gradient and the average gradient becomes greater than 1.2 ($k = 1 + (n-1)\ (d/s)\ \sin(\pi/n)$ approximately) a few dB should be added to the values calculated with the formula.

Wet conductor (comparable to "average heavy rain")

$$\Gamma_W = 10.87 + \Gamma_{hr} + F(g, d, n)$$

where:

$$F(g,d,n) = -14.2\ \frac{g^0}{g} \quad \text{and:} \quad g^0 = \frac{24.4}{d^{0.24}} \quad \text{for } n \leq 4$$

$$g^0 = \frac{24.4}{d^{0.24}} - \frac{n-4}{2} \quad \text{for } n > 4$$

Fair weather (50% of the distribution in fair weather)

$$\Gamma_{FW} = \Gamma_W - 17$$

A3.2.6 IREQ [3.18, 3.19, 3.11] (CISPR specification: QP - 9 kHz - 0.5 MHz)

Heavy rain values (18 mm/hr)

$$\Gamma = \left(\frac{C_s}{C_b}\right)\left\{\sum_{1}^{n}\frac{1}{2\pi}\int_{0}^{2\pi}\Gamma_s^2(g,d)dp\right\}^{\frac{1}{2}} \quad dB\ (1\ \mu A/\sqrt{m}) \qquad (A3.2.12)$$

where:

C_S = single conductor capacitance per length (F/m)

C_b = bundle conductor capacitance per length (F/m)

Γ_S = single conductor excitation function:

$$\Gamma_s = -90.35 + 92.42 \cdot \log g + 43.03 \cdot \log d \qquad (A3.2.13)$$

optimized according to [3.11]

$$\Gamma_s = -88.85 + 92.42 \cdot \log g + 43.03 \cdot \log d \qquad (A3.2.14)$$

For a bundle configuration, according to [3.11], the excitation function can be approximated by :

$$\Gamma = \Gamma_s - B(n,s) \quad dB\ (1\ \mu A/\sqrt{m}) \qquad (A3.2.15)$$

where : $B(n,s) = 0$ for $n = 1$

$B(n,s) = 3.7$ dB for $n = 2$

$B(n,s) = 6$ dB for $n \geq 3$

Remark: This formula is a least squares approximation to the experimental results [3.18]. A more accurate version of the generation function may be obtained by using those curves directly.

A3.2.8 Russia 1200 kV Project [3.20]

$$\Gamma = G - 20 \cdot \log\left(\frac{C_{kk}}{2\pi\varepsilon_0}\right) \quad dB\ (1\ \mu A/\sqrt{m}) \qquad (A3.2.16)$$

where : G = interference generation function

C_{kk} = diagonal element of the capacitance matrix of the line considered (F/m)

Heavy rain

$$G_{hr} = -51.6 + 3.25 \cdot g + 40 \log d$$

Fair weather

$$G_{hr} = -64.6 + 3.25 \cdot g + 40 \log d$$

It has to be noted that in the USSR, a direct use of the interference generating function G is performed to calculate analytically the radio interference field.

A3.2.9 EDF [3.9, 3.11]

Heavy rain, single conductor,

$$\Gamma_{shr} = 155 \cdot \log\left(\frac{g}{11.1}\right) + 11.5 \cdot r \qquad \text{dB (1 } \mu A/\sqrt{m})$$

r = conductor radius, cm
g < 17 kV/cm

Heavy rain, bundle conductors,

10 kV/ cm < g < 25 kV/cm average rain values > 1 mm/hr

$$\Gamma = \Gamma'(g, r) + A \cdot r - B(n) \qquad \text{dB (1 } \mu A/\sqrt{m}) \qquad \text{(A3.2.17)}$$

$\Gamma'(g, r) = 155 \cdot \log\left(\frac{g}{11.1}\right)$, $A = 11.5 + \log(n^2)$ and B in the following table.

n		1	2	3	4	6	8
B (n)	dB	0	5	7	8	9	9.5

Optimized according to [3.11]

$$\Gamma = -3.03 + \Gamma'(g, r) + A \cdot r - B(n) \qquad \text{dB (1 } \mu A/\sqrt{m}) \qquad \text{(A3.2.18)}$$

A3.2.10 ROMANIA - UPB [3.21]

Heavy rain:

$$\Gamma = 50 - \frac{540}{g} + 74 \cdot \log d - 10 \cdot \log n \qquad \text{dB (1 } \mu A/\sqrt{m}) \qquad \text{(A3.2.19)}$$

$n \geq 3$, $g \geq 17$ kV/cm

A3.2.11 CISPR [3.22]

Heavy rain: large bundle conductors, s/d ≥ 10 to 15

$$\Gamma = 70 - \frac{585}{g} + 35 \cdot \log d - 10 \cdot \log n \qquad \text{dB (1 } \mu A/\sqrt{m}) \qquad \text{(A3.2.20)}$$

Remark: This formula should only be used for pre-design purposes or comparison between different line configurations. It gives approximately the upper envelope of results from the other formulae, and therefore a conservative evaluation of the generation function.

Heavy rain: tubular conductors:

$$\Gamma = -121 + 120 \cdot \log g + 40 \cdot \log d \qquad \text{dB (1 } \mu A/\sqrt{m})$$

Compilation of the Different Formulae for the Evaluation of the Excitation Function and RI at a lateral distance of 15 m from the outer conductor.

Using the example of paragraph 2.5, the excitation function Γ (dB (1 $\mu A/\sqrt{m}$)) with the different formulae for the central phase and the RI (dB (1μV/m)) at a lateral distance of 30 m of the central phase can be calculated.

The effective value of the maximum conductor surface gradient g is necessary.

The CIGRE Guide method gives (see paragraph 2.5.1) :

g = 18.2 kV/cm (rms)

Some formulae give directly RI and for the others RI = Γ + 23.12 (see Appendix 3.3).

Method (formula)	Γ (dB (1 $\mu A/\sqrt{m}$))	RI (dB (1 μV/m))
BPA (A3.2.1)	→	64.35
BPA (A3.2.2)	41.96	65.08
BPA (A3.2.3)	45.36	68.48
CIGRE (A3.2.4)	→	63.08
CIGRE (A3.2.5)	40.84	63.96
CIGRE (A3.2.6)	41.14	64.26
CRIEPI (A3.2.7)	→	65.00
ENEL (A3.2.8)	41.99	65.11
EPRI (A3.2.10)	45.24	68.36
EPRI (A3.2.11)	40.76	63.88
IREQ (A3.2.12)	41	64.12
IREQ (A3.2.15, 13)	40.62	63.74
IREQ (A3.2.15, 14)	42.02	65.14
RUSSIA (A3.2.16)	38.61	61.73
EDF (A3.2.17)	43.55	66.67
EDF (A3.2.18)	40.52	63.64
ROMANIA (A3.2.19)	46.52	69.64
CISPR (A3.2.20)	45.44	68.56

Appendix 3.3 Predetermination of the Radio Interference at a Given Distance of a Three-Phase Line Starting from the Excitation Function of Each Phase

A3.3.1 Analytical procedure, [3.9]

1) compute the capacitance matrix of the line [C] (see paragraph 2.5.1)

2) compute the effective value of the maximum conductor surface gradient g (kV/cm (rms)) for each phases :

- effective value of the average of the maximum conductor surface gradient on each individual subconductors (see paragraph 2.5.2)

OR

- simplified method as in CIGRE Guide [1.1] with the equivalent bundle radius (see paragraph 2.5.1)

3) with one of the formulae of the Appendix 3.2, calculate the excitation function

Γ_i (dB (1 µA/√m)) for each phase

According to the modal propagation [3.9], the unit phase field ($\Gamma_i = 1$) is computed as follow :

4) compute the matrix of total modal coefficient $[m_k]$

$$[m_k] = \frac{1}{2}\left[\frac{1}{\sqrt{\alpha_k}}\right] \cdot [N]^{-1} \cdot \frac{1}{2\,\pi\,\varepsilon_0} \cdot [C]$$

- in practice, we use the symmetrical matrix of the Clarke-Concordia modes [N]

$$[N] = \begin{pmatrix} 1/\sqrt{6} & 1/\sqrt{2} & 1/\sqrt{3} \\ -2/\sqrt{6} & 0 & 1/\sqrt{3} \\ 1/\sqrt{6} & -1/\sqrt{2} & 1/\sqrt{3} \end{pmatrix} \quad \Rightarrow [N]^T = [N]^{-1}$$

Remark : In fact, the matrix [N] is obtained as the eigenvectors of the matrix [B] = [Y]·[Z] or, in a more simplified analysis, as the eigenvectors of the matrix $[C]^{-1}$.

- diagonal matrix of gains $\left[\frac{1}{\sqrt{\alpha_k}}\right]$

$$\left[\frac{1}{\sqrt{\alpha_k}}\right] = \begin{pmatrix} 216 & 0 & 0 \\ 0 & 216 & 0 \\ 0 & 0 & 54 \end{pmatrix}$$ for a line with conductors in delta configuration

$$\left[\frac{1}{\sqrt{\alpha_k}}\right] = \begin{pmatrix} 300 & 0 & 0 \\ 0 & 136 & 0 \\ 0 & 0 & 54 \end{pmatrix}$$ for a line with conductors in flat configuration

5) matrix of total modal (k) current for each phase i $[I_i]$

$$[I_i] = [N] \cdot [m_i]$$

where $[m_i]$ is the diagonal matrix which the elements are the elements of the i^{th} columns of the matrix $[m_k]$:

$$[m_i] = \begin{pmatrix} m_1 & 0 & 0 \\ 0 & m_2 & 0 \\ 0 & 0 & m_3 \end{pmatrix} \quad \text{and } m_1 = [m_k]_{i1},\ m_2 = [m_k]_{i2},\ m_3 = [m_k]_{i3}$$

6) modal field E_{ki} (μV/m)) (mode k, phase i)

$$E = Z_0 \cdot H \qquad Z_0 = \sqrt{\frac{\mu_0}{\varepsilon_0}} = \sqrt{\frac{4\pi 10^{-7}}{\frac{1}{36\pi} 10^{-9}}} = 120\pi \qquad H = \frac{I}{2\pi r}$$

$$\Rightarrow \qquad E = 120\pi \frac{1}{2\pi} \frac{I}{r} = 60 \frac{I}{r}$$

Using the notations of figure A3.3.1, and p as the depth of penetration ($p = \sqrt{\frac{2\rho}{\mu_0 \omega}}$), [3.9] :

$$E_{ki}(x) = 60 \left\{ [I_i]_{1k} \left[\frac{h_1 - h_a}{(h_1 - h_a)^2 + (x - d_1)^2} + \frac{h_1 + h_a + 2p}{(h_1 + h_a + 2p)^2 + (x - d_1)^2} \right] \right.$$
$$+ [I_i]_{2k} \left[\frac{h_2 - h_a}{(h_2 - h_a)^2 + (x - d_2)^2} + \frac{h_2 + h_a + 2p}{(h_2 + h_a + 2p)^2 + (x - d_2)^2} \right]$$
$$\left. + [I_i]_{3k} \left[\frac{h_3 - h_a}{(h_3 - h_a)^2 + (x - d_3)^2} + \frac{h_3 + h_a + 2p}{(h_3 + h_a + 2p)^2 + (x - d_3)^2} \right] \right\}$$

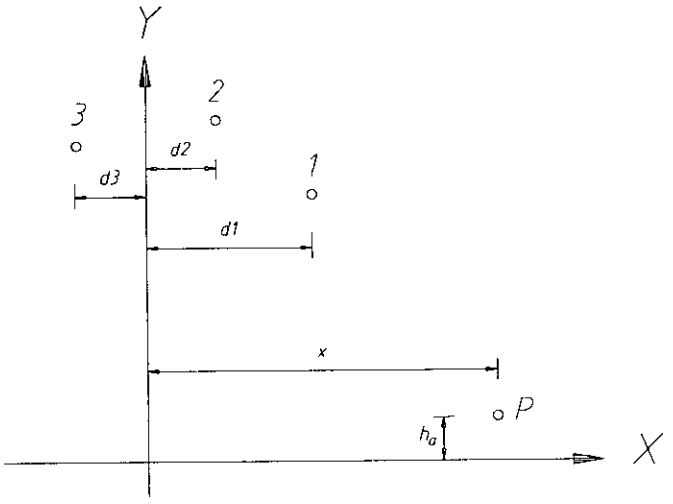

Figure A3.3.1

Each distance d_1, d_2, d_3 must be taken with their signs
h_a = height of antenna

7) phase field E_i (dB (1 μV/m)) (phase i)

$$E_i = 20 \cdot \log\left(\sqrt{\sum_{k=1}^{3} E_{ki}^2}\right)$$

8) Radio Interference RI_i (dB (1 μV/m)) of each phase

$$RI_i = E_i + \Gamma_i$$

9) Radio Interference RI (dB (1 μV/m)) of the line

ranking of the phase-fields:

$$RI_a \geq RI_b \geq RI_c \quad \text{(dB (1 μV/m))}$$

if $RI_a - RI_b \geq 3$ dB: $RI = RI_a$

if $RI_a - RI_b < 3$ dB: $RI = \frac{RI_a + RI_b}{2} + 1.5$

A3.3.2 Sample Calculation

Using the example of paragraph 2.5, the method of A3.3.2 can be followed to compute the radio interference RI.

1) capacitance matrix of the line [C], see paragraph 2.5.1.

2) effective value of the maximum conductor surface gradient g (kV/cm (rms)) for each phases by the simplified method as in CIGRE Guide [1.1], see paragraph 2.5.1.

3) with one of the formulae of the Appendix 3.2, calculate the excitation function Γ_i (dB (1 μA/√m)) for each phase

the CISPR formula (A3.2.20) gives :

for the central phase : $\Gamma_2 = 45.44$ (dB (1 μA/√m))

for the lateral phase : $\Gamma_1 = \Gamma_3 = 42.21$ (dB (1 μA/√m))

4) matrix of total modal coefficient $[m_k]$

$$\left[\frac{1}{\sqrt{\alpha_k}}\right] = \begin{pmatrix} 300 & 0 & 0 \\ 0 & 136 & 0 \\ 0 & 0 & 54 \end{pmatrix}$$ for a line with conductors in flat configuration

$$\Rightarrow \quad [m_k] = \begin{pmatrix} 20.354 & -37.361 & 20.354 \\ 12.304 & 0 & -12.304 \\ 2.683 & 2.257 & 2.683 \end{pmatrix}$$

5) matrix of total modal (k) current for each phase i $[I_i]$

$$[I_i] = [N] \cdot [m_i]$$

- $[m_1] = \begin{pmatrix} 20.354 & 0 & 0 \\ 0 & 12.304 & 0 \\ 0 & 0 & 2.683 \end{pmatrix} \Rightarrow [I_1] = \begin{pmatrix} 8.309 & 8.700 & 1.549 \\ -16.619 & 0 & 1.549 \\ 8.309 & -8.700 & 1.549 \end{pmatrix}$

- $[m_2] = \begin{pmatrix} -37.361 & 0 & 0 \\ 0 & 0 & 0 \\ 0 & 0 & 2.257 \end{pmatrix} \Rightarrow [I_2] = \begin{pmatrix} -15.251 & 0 & 1.303 \\ 30.505 & 0 & 1.303 \\ -15.251 & 0 & 1.303 \end{pmatrix}$

- $[m_3] = \begin{pmatrix} 20.354 & 0 & 0 \\ 0 & -12.304 & 0 \\ 0 & 0 & 2.683 \end{pmatrix} \Rightarrow [I_3] = \begin{pmatrix} 8.309 & -8.700 & 1.549 \\ -16.619 & 0 & 1.549 \\ 8.309 & 8.700 & 1.549 \end{pmatrix}$

6) modal field E_{ki} (µV/m)) (mode k, phase i), at 2 m above ground and 15 m of the outer phase

with : $\mu_0 = 4 \pi 10^{-7}$ H/m

$f = 500$ kHz $\Rightarrow \omega = 3.14\ 10^6$ rad/s

$$\rho = \sqrt{\frac{2\rho}{\mu_0 \omega}} = 7 \text{ m}$$

$x = 30$ m $\quad d_1 = 15$ m $\quad d_2 = 0$ m $\quad d_3 = -15$ m (see figure A3.2.1)

$\Rightarrow E_{ki}(x = 30\text{ m}) = 60 \{ [I_i]_{1k} \cdot 0.056456 + [I_i]_{2k} \cdot 0.031099 + [I_i]_{3k} \cdot 0.018503 \}$

$E_{k=1,i=1}(x) = 6.36$ µV/m $\quad E_{k=2,i=1}(x) = 19.81$ µV/m $\quad E_{k=3,i=1}(x) = 9.86$ µV/m

$E_{k=1,i=2}(x) = -11.67$ µV/m $\quad E_{k=2,i=2}(x) = 0$ µV/m $\quad E_{k=3,i=2}(x) = 8.29$ µV/m

$E_{k=1,i=3}(x) = 6.36$ µV/m $\quad E_{k=2,i=3}(x) = -19.81$ µV/m $\quad E_{k=3,i=3}(x) = 9.86$ µV/m

7) phase field E_i (dB (1 µV/m)) (phase i)

$$E_i = 20 \cdot \log\left(\sqrt{\sum_{k=1}^{3} E_{ki}^2}\right)$$

$\Rightarrow$ $E_1 = 27.24$ (dB (1 µV/m)) $\quad E_2 = 23.12$ (dB (1 µV/m)) $\quad E_3 = 27.24$ (dB (1 µV/m))

8) Radio Interference RI_i (dB (1 µV/m)) of each phase

$RI_i = E_i + \Gamma_i$

$RI_1 = 69.45$ (dB (1 µV/m)) $\quad RI_2 = 68.56$ (dB (1 µV/m)) $\quad RI_3 = 69.45$ (dB (1 µV/m))

9) Radio Interference RI (dB (1 µV/m)) of the line

ranking of the phase-fields:

$RI_1 \geq RI_3 \geq RI_2$ (dB (1 µV/m))

$RI_1 - RI_2 \leq 3$ dB $\Rightarrow$ $RI = \frac{RI_1 + RI_2}{2} + 1.5 = 70.51$ dB (1 µV / m)

Appendix 3.4 Formulae Developed for the Evaluation of Television Interference due to Corona

The **EPRI** [3.10] formula gives, for each phase, the corrections to be applied to the radio interference level of the line considered, evaluated in reference conditions (reference distance and measuring method).

$$TVI\ (f,\ x) = RI_0 + F_1(f) + F_2(x) + C \qquad \text{(A3.4.1)}$$

where:

TVI (f, x) (dB (1 μV/m))

f = frequency, (MHz)

x = lateral distance from the conductor, (m)

$F_1(f)$ = correction function for the frequency, (dB)

$F_2(x)$ = correction function for the lateral distance, (dB)

C = correction constant to take into account the different peculiarities of the measuring systems for TVI and RI (bandwidth, etc.). If the radio interference level RI_0 of the reference line is given according TVI specifications, the term C is left out, (dB)

The correction function $F_1(f)$ obtained from measurements at a three phase line under foul weather condition is given in Figure A3.4.1, [3.10].

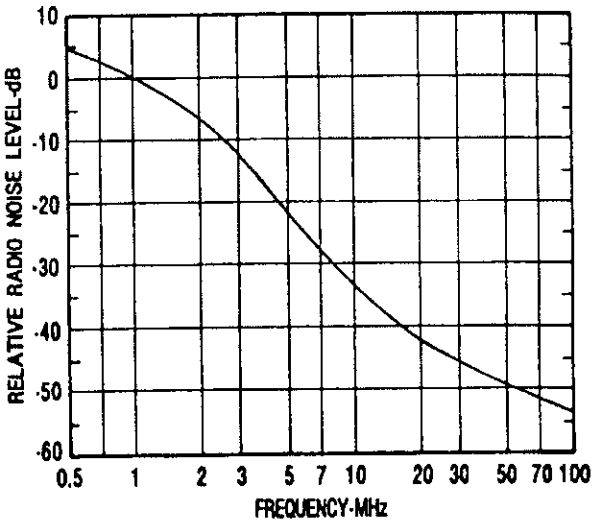

Figure A3.4.1

Correction function $F_1(f)$

For the frequency range f > 20 MHz, the correction function has a variation of 20 dB per decade and can thus be written :

$$F_1(f) = -\ 20 \log (f) \qquad \text{(A3.4.2)}$$

With the assumption that, in the frequency range of interest, radio noise attenuates by 6 dB per doubling of lateral distance, the formula proposed becomes :

$$TVI = RI_0 - 20 \log(f) - 20 \log\left(\frac{x}{x_0}\right) + C \qquad \text{(A3.4.3)}$$

Where C = 3.2 dB for a TVI reference frequency of 75 MHz, 120 kHz bandwidth and the reference RI_O given according to ANSI at the lateral distance x_0.

BPA has proposed a similar formula. The same correction function for frequencies above 20 MHz is used, but with a more sophisticated function for the distance based on the assumption that the lateral attenuation changes, at a frequency dependent "transition distance" x_c from–20 log(x) to –40 log(x).

$$TVI_{/phase} = 10 + 120 \log\left(\frac{g}{13.6}\right) + 40 \log\left(\frac{d}{3.04}\right) + 20 \log\left(\frac{75}{f}\right) + F_2(x) + K_A \qquad \text{(A3.4.4)}$$

where:

$$F_2(x) = 20 \log\left(\frac{x_0}{x}\right) \qquad \text{for } x \text{ and } x_0 \le x_c$$

$$F_2(x) = 20 \log\left(\frac{x_0}{x_c}\right) + 40 \log\left(\frac{x_c}{x}\right) \qquad \text{for } x \ge x_c \text{ and } x_0 \le x_c$$

$$F_2(x) = 20 \log\left(\frac{x_c}{x}\right) + 40 \log\left(\frac{x_0}{x_c}\right) \qquad \text{for } x \le x_c \text{ and } x_0 \ge x_c$$

$$F_2(x) = 40 \log\left(\frac{x_0}{x}\right) \qquad \text{for } x \text{ and } x_0 \ge x_c$$

x_0 = 61 m, reference lateral distance

$$x_c = \frac{12\, h_a\, h_c}{\lambda}$$

$$K_A = \frac{q}{300} \text{ (dB), altitude correction for } q < 3000 \text{ m}$$

h_a = height of antenna, (m)

h_c = height of conductor, (m)

λ = wavelength, (m)

f = frequency, (Mhz)

Note that the addition of the TVI values of the different phases in this case is not considered as the characteristic TVI of the line, but only the highest individual value.

It has to be mentioned that the investigations on conductor corona TVI were not as extensive as in the case of corona radio interferences in the frequency range up to 30 MHz. In effect, the interferences to television reception are more often influenced by microgap discharges on power line hardware than by conductor corona.

Glossary chapter 3

A	correction factor depending of n	dB/cm
B(n)	correction factor depending of n	dB
B(n,s)	correction factor depending of n	dB
C	correction constant	dB
C_a	lateral attenuation function	dB
C_b	bundle conductor capacitance per length	F/m
C_{kk}	diagonal element of the capacitance matrix of the line considered	F/m
C_s	single conductor capacitance per length	F/m
d	diameter of the subconductor	cm
D	radial distance between conductor and antenna	m
DW	direct wave component	
E	electric field	dB (1 μV/m)
E_a	total field of phase a	dB (1 μV/m)
E_b	total field of phase b	dB (1 μV/m)
E_c	total field of phase c	dB (1 μV/m)
E_i	field of individual bundle i of phase a, b or c in Appendix 3.1 OR phase field (phase i), only in Appendix 3.3	dB (1 μV/m)
EIND	induction field component	
E_{ki}	modal field (mode k, phase i)	μV/m
E_0	electric field under 0 rate of rain, wet conductor	dB (1 μV/m)
E_m	electric field under maximum rate of rain	dB (1 μV/m)
EMI	Electromagnetic Interference	dB (1 μV/m)
ESU	surface wave component	
E_t	total radio interference field	dB (1 μV/m)
f	frequency (dimension with relevant formula)	
g	effective value of the average of the maximum gradients of the individual subconductors	kV/cm (rms)
G	interference generation function	dB
g'	bottom surface gradient, rms value	kV/m (rms)
g_a	average gradient of subconductors	kV/m (rms)

h	height above ground $h_{average} = h_{minimum} + \frac{1}{3}\,sag$ $h_{average} = h_{anchoring} - \frac{2}{3}\,sag$	m
H	minimum height of conductor above the ground or only in formula (3.3) magnetic field in A/m	m
h_a	height of antenna	m
h_c	height of conductor	m
I	rate of rain	mm/hour
k	constant	dB
K	function of λ	
K_A	correction factor to take into account high altitudes (< 3000 m) (must be additionned to excitation function)	dB
K_n	empirical constant factor	dB
ln	$\ln \equiv \log_e$, e = 2.718	
log	$\log \equiv \log_{10}$	
n	number of the subconductors in the bundle	
p	depth of penetration	m
q	altitude above sea level	m
QP	quasi-peak	
r	subconductor radius	cm
R	bundle radius	cm
RI	Radio Interference	dB (1 µV/m)
s	bundle spacing	cm
S	interphase spacing	m
TVI	Television Interference	
V	voltage between phase and ground	V or kV
x	lateral distance	m
x_0	reference lateral distance (x_0 = 61 m)	m
x_c	transition distance	m
Z_0	impedance of free space	Ω
α	factor depending of g and g'	
δ	ground conductivity	mS/m
ε_0	permittivity of free space	F/m

λ	wavelength	m
μ_0	permeability of free space	H/m
ρ	earth resistivity	Ω m
Γ	excitation function	dB (1 $\mu A/\sqrt{m}$)
Γ_s	single conductor excitation function	dB (1 $\mu A/\sqrt{m}$)
[C]	capacitance matrix	F/m
[I]	matrix of phase currents	
$[I_i]$	matrix of total modal (k) current in phase i	
$[m_k]$	matrix of total modal coefficients	
[N]	symmetrical matrix of the Clarke-Concordia modes	
[q]	matrix of charges	C
[Γ]	matrix of the excitation functions of the conductors	dB (1 $\mu A/\sqrt{m}$)
$\left[\frac{1}{\sqrt{\alpha_i}}\right]$	diagonal matrix of gains	$\sqrt{\frac{m}{N_p}}$

References

[1.1] "Interferences Produced by Corona Effect of Electric Systems; Description of Phenomena, Practical Guide for Calculation", Brochure No 20, WG 36.01, CIGRE, Paris 1974.

[3.1] R.G. Olsen, S. D. Schennum "A Method for Calculating Wide Band Electromagnetic Interference from Power Line Corona", IEEE Transaction on PWRD, Vol. 10, No. 3, July 1995, pp. 1535-1540.

[3.2] W.L. Stutzmann, G.A. Thiele, "Antenna Theory and Design", Wiley, New York, 1981.

[3.3] W. Janischewskyj, A.M. Hussein, N.H.C. Santiago, "Performance and analysis of a micro-gap discharge circuit", IEEE PES Transaction paper, 1986 Summer Meeting.

[3.4] CISPR Publication 18-2, 18-3, "Radio interference characteristics of overhead power lines and high-voltage equipment", 1986.

[3.5] W. Janischewskyj, E.B. Harvey, M.G. Comber, "Power Line Interference and Assessment of Television Picture Quality", IEEE Transaction on PAS, Vol. PAS-102, No. 5, May 1983.

[3.6] G.K. Hatanaka, "Power Line TVI measurement Parameters", CEA Report No. 102 D 201, March, 1984.

[3.7] J. Reichmann, G.K. Hatanaka, "TV Interference Study on Distribution Test Line", CEA Report No. 205 D406, 1987.

[3.8] C.H. Gary, "The Theory of Excitation Function: Demonstration of its Physical Meaning", IEEE Transactions on Power Apparatus and Systems, Vol. PAS- 72, Jan./Feb. pp. 305-310.

[3.9] M.R. Moreau, C.H. Gary, "Predetermination of the Radio-Interference Level of High Voltage Transmission lines :

I - Predetermination of the Excitation Function", IEEE Transactions on Power Apparatus and Systems, Vol. PAS- 72, Jan./Feb., pp. 284-291.

II - Field Calculating Method", Transactions on Power Apparatus and Systems, Vol. PAS- 72, Jan./Feb., pp. 292-304.

[3.10] "Transmission Line Reference Book 345 kV and above", EPRI, Palo Alto Ca., 1979.

dto. second edition 1982.

dto. second edition, revised 1987.

[3.11] R.G. Olsen, S.D. Schnennum, V.L. Chartier, "Comparison of several methods for calculating power line electromagnetic interference levels and calibration with long term data", IEEE Transactions on Power Delivery, Vol. 7, No. 2, April 1992, pp. 903-913.

[3.12] Y.P. Shkarin, "Results of calculations of radio interference levels from low voltage overhead lines crossed by high voltage overhead lines exhibiting a corona discharge", Report to CIGRE WG 36.01, 1988 (referring to references of CIGRE Report 36-03, 1980).

[3.13] E.S. Kolechitsky, "Calculations of Electric Fields of High-Voltage Devices", Energoatomizdat, Moscow, 1983.

[3.14] C.D. Taylor, G.N. Elkhouri, T.E. Wade, "On the Parasitic Capacitances of Multilevel Skewed Metallization Lines", IEEE Transactions on Electron Devices, Vol. ED-33, No. 1, January 1986.

[3.15] Y. Sawada, M. Fukushima, M. Yasui, "Akagi 1000 kV Project in CRIEPI. Corona test facilities and results up to 1983", CIGRE 36-05, 1984.

[3.16] M. Fukushima, T. Sasano, Y. Sawada, "Corona performance of conductor bundles measured in corona cages and its application", CIGRE Symposium 22-81, No. 232-01, June 1981.

[3.17] B.A. Cauzillo, R. Cortina, P. Nicolini, J.C. De Medeiros, M.E. Bryant, "Design criteria of UHV overhead lines based on experience acquired in the 1000 kV Project", CIGRE 22-14, 1984.

[3.18] N. Giao Trinh, P. Sarma Maruvada, "A method of predicting the corona performance of conductor bundles based on cage test results", IEEE Transactions on Power Apparatus and Systems, Vol. PAS-96, No. 1, pp. 312-325, Jan/Feb 1977.

[3.19] R.D. Dallaire, P. Sarma Maruvada, "Analysis of radio interference from short multi-conductor lines. Part 1: Analytical and test results; Part 2: Analytical and test results", IEEE Transactions on Power Apparatus and Systems, Vol. PAS-100, No. 4, pp. 2100-2119, April 1981.

[3.20] P.Z. Rokhinson, A.S. Sokhransky, L.V. Timashova, N.N. Tykhodeev, "Corona effects of high bundle number UHV conductors: energy losses, radio and TV interference", CIGRE 36-09, 1988.

[3.21] D. Cristescu, M. Ungureanu, G Magureanu, "L´effet couronne sur les lignes compactes", CIGRE Symposium, 1991, Leningrad, paper 500 - 02.

[3.22] Amendment No 1 to IEC 18-3, "Formulae for the predetermination of radio noise level produced by large conductor bundles (more than four subconductors), and by tubular conductors".

[3.23] L. Jermendy, T. Roestel, "TV interference caused by capacitive discharges on high voltage transmission lines", ISH Braunschseig 1984, paper 83.16.

[3.24] "Measurement of re-radiation of broadcast signals by power lines", CEA Report No. 023-T-216.

Chapter 4

Audible Noise

4.1 Introduction, Generation and Propagation of Audible Noise

A person standing near an overhead line whose conductors or insulator assemblies or both are in corona - usually lines above 275 kV - can sometimes hear a special noise: frying, crackling or hissing sounds and possibly a low frequency hum. If there is rain, drizzle, fog or ice, this audible noise is more intense.

The sound is the mechanical vibration of air particles, and the easiest quantity to measure is the sound pressure, the unit of which is Newton per square metre (N/m^2) = Pascal (Pa). A single sound pressure p can be expressed as the real part of the equation

$$p = p_{max}\, e^{j2\pi ft} \tag{4.1}$$

where p_{max} is the amplitude of the pressure, t is the time in second (s) and f is the frequency in hertz (Hz).

A normal human ear can detect sound pressure varying from 20 μPa to 100 Pa. Using the sound pressure expressed in Pascal is not convenient. Instead the sound pressure level in decibels (dB) has been defined as

$$\boxed{L = 10\log\left(\frac{p^2}{p_0^2}\right) = 20\log\left(\frac{p}{p_0}\right)} \tag{4.2}$$

where p is the rms value of the sound pressure being measured and p_0 is the reference value of 20 μPa.

Corona audible noise is not purely sinusoidal vibrations. It consists of a great number of frequencies combined at random phases. All these components determine the frequency spectrum of audible noise. This frequency spectrum is often given in octave or one-third octave bands. If f_0 is the centre frequency of a band, then an octave band extends from the lower frequency $\frac{f_0}{\sqrt{2}}$ to the upper frequency $f_0\sqrt{2}$ and a one-third octave band extends from $\frac{f_0}{\sqrt[6]{2}}$ to $f_0\sqrt[6]{2}$. The octave or third-octave band sound pressure level comprises sound pressure levels of all frequencies ranging from the lower to the upper frequency of the band. An example of a third-octave frequency spectrum is given in Figure 4.1. It can be seen that the spectrum consists of two typical parts:

1. Pure tones which are at multiples of 100 Hz when the line is energized at 50 Hz or at multiples of 120 Hz for 60 Hz.
2. The broad-band part which is often described as frying, crackling or hissing. It covers a wide frequency range from hundreds of Hz to the ultrasound range. (In Figure 4.1 the broad-band part is limited to about 16 kHz because of the limited frequency response of the measuring instruments.)

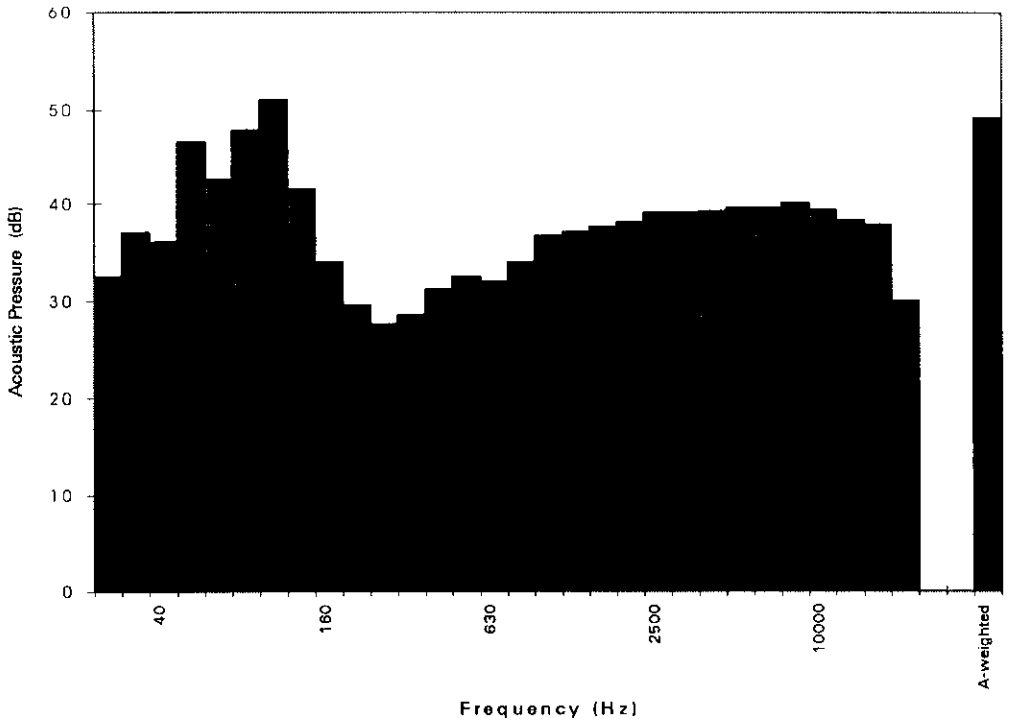

Figure 4.1

One-third octave analysis of acoustic pressure of corona audible noise

The pure tone component, called hum, is generated largely by the movement of charged ions surrounding the conductor. The hum is audible especially under heavy rain. Pulses are the sources of ionization and consequently of the hum. Hence it follows that the 100 Hz (120 Hz) hum is generated along the conductor with the same phase.

The broad-band audible noise is mainly generated by positive polarity streamers. Each such audible pulse is of limited time duration and has a broad frequency spectrum which results from the theory of the Fourier Transform. There are a lot of streamers generating audible pulses along the conductor and their frequency spectra may be distributed up to ultrasound range.

The human ear sensitivity varies according to the frequency and the loudness of pure tones. In order to express this complicated dependence and to enable the whole frequency spectrum to be expressed by one value, the standardized frequency weighting characteristics A, B, C and D have been agreed upon internationally. To a certain extent they compensate for the variation of the ears sensitivity with frequency. Generally speaking the weighting characteristics attenuate the frequency components of audible noise below 1000 Hz and above 6000 Hz. Present national and international standards for noise measurements usually recommend the use of A-weighted levels, as shown in Figure 4.2. The weighting characteristics can be applied to a noise measurement either automatically, by a weighting filter built in to the sound level meter (the readings are then in dB(A)), or, in case a frequency spectrum which has been recorded previously, it is possible to calculate the A-weighted level according to formula

$$L_A = 10 \log \sum_{i=1}^{n} 10^{\frac{L_i + K_{Ai}}{10}} \qquad (4.3)$$

where L_i (dB) is the sound pressure level of the i-th frequency band,
K_{Ai} (dB) is the correction of A-weighting characteristic of the i-th frequency band given by Figure 4.2.

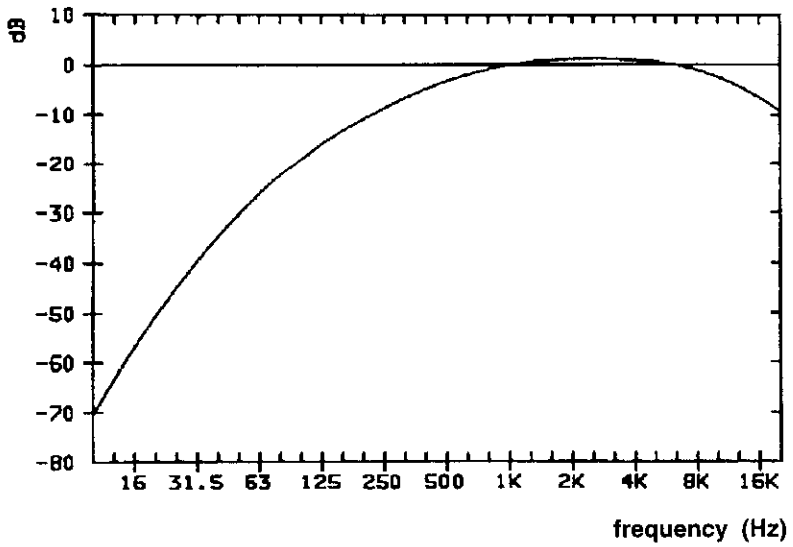

Figure 4.2

Internationally standardized weighting A curve for sound level meters

The frequency characteristic of corona audible noise consists of a hum component and a broadband component. The audible noise propagation depends on the part of the spectrum considered.

4.1.1 Hum

Since the hum is generated along the conductor with the same frequency by lots of partial acoustic sources (we can imagine them as the elements of a breathing cylinder), its sound pressure at an arbitrarily chosen point (measuring point) is given as a sum of every partial i-th (i=1 to infinite) contributions respecting their phase angle:

$$p = \frac{j\omega\sigma}{4\pi}\sum_i q_i\left[\frac{e^{-jkD_i}}{D_i} + a_r\frac{e^{-jkD_i'}}{D_i'}\right] \qquad (4.4)$$

where a_r is the reflection coefficient (for hum $a_r \equiv 1$)

$j = \sqrt{-1}$

$k = \frac{2\pi f}{c_s}$ (c_s is the sound velocity, in air c_s = 331 m/s)

q_i is the volume velocity of the i-th particle (it is a complex value), m^3/s

D_i is the distance of point, at which the sum is calculated from the i-th particle acoustic source, m

D_i' is the distance of the i-th image source, m

$\omega = 2\pi f$

f is frequency of sound (for hum it is 100 Hz or 120 Hz), Hz

σ is the air density, kg/m^3

The first part in the parentheses belongs to the direct wave, the second one to the wave reflected from the ground. Each partial acoustic source along the conductor emits the sound pressure with the same phase angle. The sound pressure at a point of its summation (e.g. at the measuring point) from these sources comes with a different phase angle. After summation in Equation (4.4) this phenomenon manifests itself as a standing wave of hum component. The level of hum can considerably vary when displacing the measuring microphone a few meters from the conductor, as shown in Figure 4.3. Fortunately, the hum decreases as the conductor ageing [4.14] and the A-weighting filter significantly suppresses hum (see Figure 4.2), so the A-weighted sound level is not usually influenced.

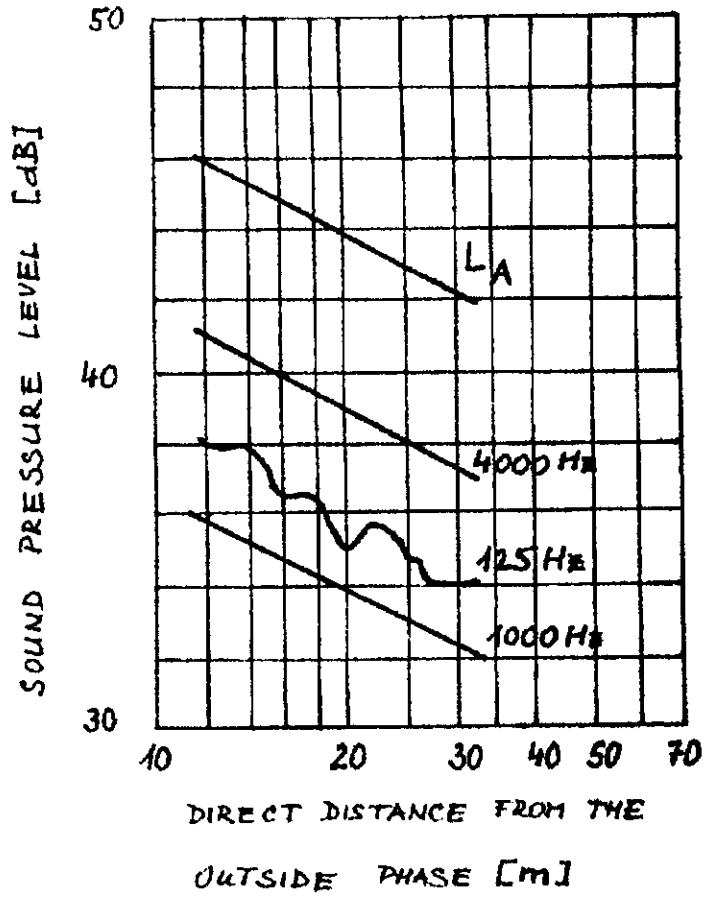

Figure 4.3

An example of octave sound pressure level and A-weighted level of corona audible noise as a function of direct distance from the outside phase

4.1.2 Broad-Band Component

The propagation of the broad-band component is simpler. Each elementary acoustic source on the conductor radiates power with the continuous frequency spectrum. If W is the acoustic power per unit of length, then the acoustic intensity I (W/m^2) at a distance D is given

$$I = \int_{-l/2}^{+l/2} \frac{W}{4\pi(D^2 + x^2)} dx \tag{4.5}$$

for a conductor of a length l. For l very large the solution of the above integral is

$$I = \frac{W}{4D} \tag{4.6}$$

Reflections from the ground may influence the intensity. Taking them into account, Equation (4.6) is modified into

$$I = W\left(\frac{1}{4D} + \frac{a_r}{4D'}\right) \tag{4.6a}$$

where a_r and D′ have similar meaning as those in Equation (4.4). The value of a_r is very low in this case ($a_r << 1$) for frequencies above 1000 Hz for current outdoor ground surfaces and can be neglected.

Similar to the sound pressure level, the sound power level in decibels (dB) can be defined as

$$L_W = 10 \log \frac{W}{W_0} \tag{4.7}$$

where W_0 is the reference value of 1 μW/m, and the sound intensity level in decibels (dB)

$$L_I = 10 \log \frac{I}{I_0} \tag{4.8}$$

where I_0 is the reference value of 1 μW/m^2

The sound pressure is given

$$p = \sqrt{\sigma \, c_s \, I} \tag{4.9}$$

where σ = 1.29 kg/m^3 is the air density and c_s = 331 m/s is the sound velocity. Then from Equation (4.6)

$$p = 10.3 \sqrt{\frac{W}{D}} \tag{4.10}$$

or in terms of sound pressure level (p_0 = 20 μPa, W acoustic power (W/m), D distance (m))

$$\boxed{L = 20 \cdot \log \frac{p}{p_0} = 114.3 + 10 \cdot \log W - 10 \cdot \log D} \tag{4.11}$$

Equation (4.11) shows that the decrease of the sound pressure level (and A-weighted sound level) of broad-band noise is "smooth" according to -10 logD (3 dB decline every doubling of the distance). This law is apparent from Figure 4.3 for A-weighted sound level or for the 1000 Hz and 4000 Hz octave bands.

If the sound pressure level or the A-weighted sound level L_1 is given at the distance D_1 from the conductor, the level L_2 at another distance D_2 from the conductor is given by

$$L_2 = L_1 - 10 \cdot \log \frac{D_2}{D_1} \tag{4.12}$$

However, the sound pressure level decreases more rapidly than it would result from Equations (4.10) or (4.11) because for longer distances the sound absorption in air must be taken into consideration, too.

This absorption may be expressed as an attenuation per distance. It depends on the frequency of sound, the temperature of air and its relative humidity. The attenuation is shown in References [3.10], [4.6]. For a typical corona noise spectrum as shown in Figure 4.1, the temperature of 15 °C and relative humidity of 70%, the attenuation is enumerated and drawn in Figure 4.4. It fits the formula [in decibels (dB)]

$$\boxed{\delta_L = -0.0094 - 0.024 \cdot D + 3.38 \cdot 10^{-5} \cdot D^2 - 2.64 \cdot 10^{-8} \cdot D^3} \tag{4.13}$$

where D (m) is a distance between the conductor and the point of calculation (D ≥ 500 metres).

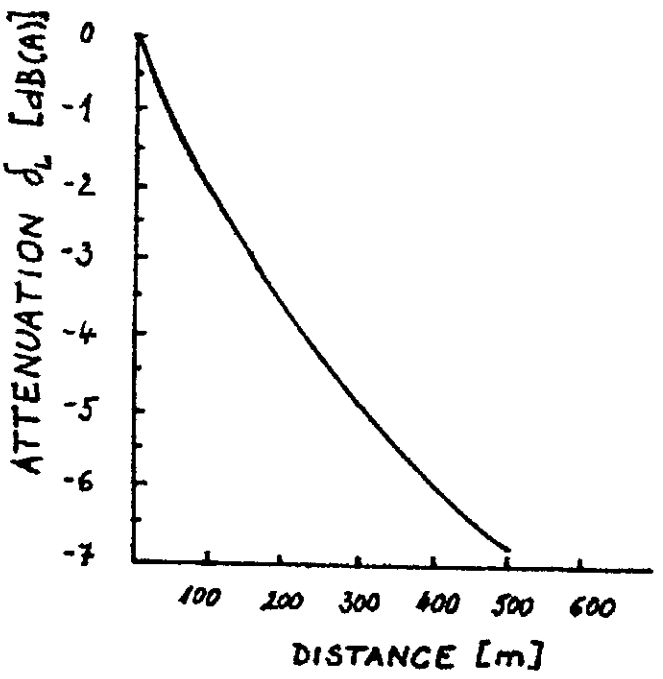

Figure 4.4

Additional attenuation of A-weighted corona audible noise which is caused by molecular absorption in air (valid for 15 °C and 70 percent of relative humidity)

This attenuation is to be added to the A-value of corona audible noise calculated at a distance D. The low frequency hum is practically not attenuated by sound absorption in air which may change the frequency spectrum of corona audible noise at larger distance from the line.

Fog, rain and snow may cause an additional attenuation of sound. There are not sufficiently reliable data of this attenuation. It is recommended that it should not be taken into account. The gradients of wind speed, temperature and the air turbulence can cause additional attenuation, too [4.8]. A more detailed discussion is out of the scope of this publication.

By analogy with the RI excitation function, the A-weighted sound power level (L_w in dB(A) (1 µW/m)) is called the acoustic generation function and symbolized by ΓA.

Derived from the equation (4.11), the determination of the A-weighted sound pressure (L_A) of each conductor/bundle at a distance D has to take into account the propagation of sound :

$$\boxed{L_A = 54.3 + \Gamma A - k_D} \qquad (4.14)$$

where $k_D = 10 \log D + \delta_L$

L_A	dB(A) (20 µPa)
ΓA	dB(A) (1 µW/m)
D	m
δ_L	dB

δ_L might be determined according to formula (4.13) or Figure 4.4, or approximated by a constant factor related to distance.

4.2 Calculation

Various research centres have developed their formulae for predicting audible noise. Some of them are listed in Appendix 4. Formulae are separately stated for heavy rain (usually as an exceedance level L_5 - the level which is exceeded 5 percent of the time period) and for average rain (L_{50}). From the reasons mentioned in chapter 4.1, the formulae are valid only for broad-band AN component.

The following structure is generally assumed for the formula giving the acoustic generation function of symmetrical bundles, aged conductors and heavy rain:

$$\boxed{\Gamma A = f_1(g) + f_2(d) + f_3(n) + C} \qquad (4.15)$$

Taking into account the different weather definitions, local situations and individual interpretation of experiments, it is difficult to derive a unique calculation method. However, for a quick survey a simple formula was derived from a comparative analysis of some methods, which are compiled in Appendix 4. It calculates the acoustic generation function for each individual phase of HV lines with symmetrical bundles and aged conductors in heavy rain.

$$\boxed{\Gamma A_5 = \Gamma A_{hr} = 25 - \frac{650}{g} + 40 \cdot \log d + 15 \cdot \log n \qquad \text{dB(A) (1µW / m)}} \qquad (4.16)$$

Approximate range of validity: $10\ \text{kV/cm} < g < 25\ \text{kV/cm}$

$$2 < n < 12$$

$$2\ \text{cm} < d < 4\ \text{cm}$$

An indication of the relevant acoustic generation function under other weather conditions might be taken from Figure 4.5.

For actual line cases however, the use of a formula from Appendix 4, which was derived from a similar conductor/line configuration under comparable climatic situations would be advisable.

The sum of the individual pressure values from all phases results in the total sound pressure at that point:

$$L_{ATot} = 10 \log \sum_{i=1}^{3} 10^{\frac{L_{Ai}}{10}} \qquad (4.17)$$

The hum component of conductor corona is low usually, but might be taken into account separately in special foul weather conditions with large corona loss [4.6].

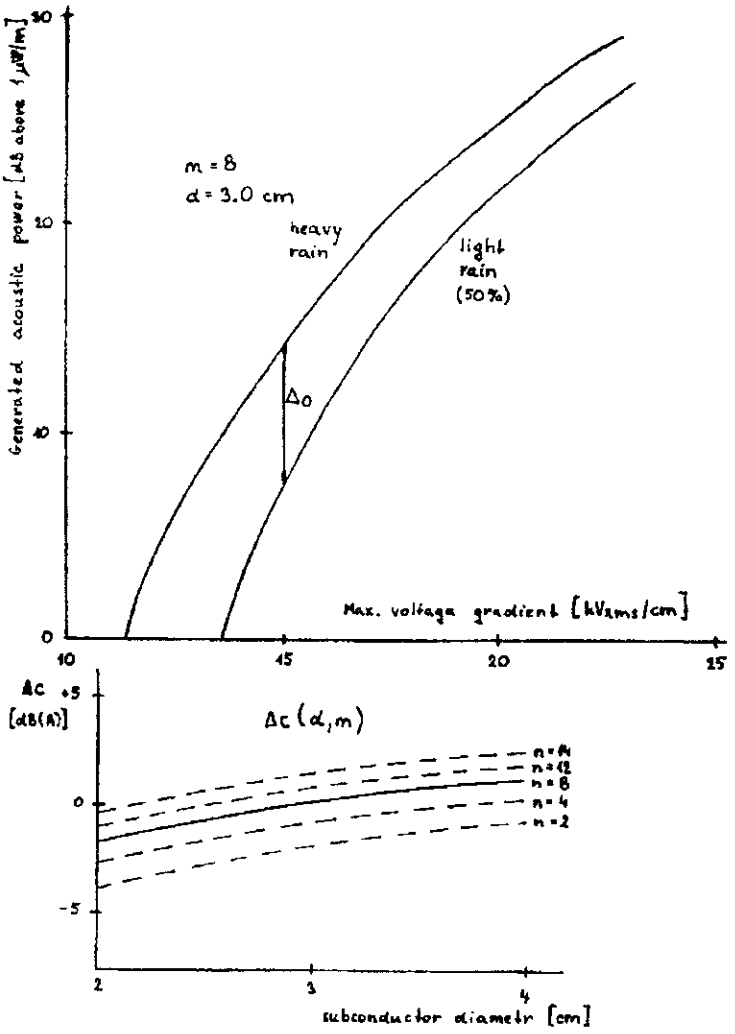

Figure 4.5

Corrections for CIGRE AN predetermination formula
Average rain (L50) : $\Gamma A_{av} = \Gamma A_{50} = \Gamma A_{hr} - \Delta_o + \Delta_c$
Fair weather : $\Gamma A_{fw} = \Gamma A_{av} - 17$

4.3 Measuring Audible Noise

4.3.1 Measuring Apparatuses

A classical basic measuring system is the sound level meter. The acoustic pressure is converted into a proportional electric signal by a measuring microphone. The electric signal is amplified, passes through a switchable network (at present usually only A-one) or through an octave (one-third-octave) band filter, and once more amplified. The RMS value of the signal is obtained by a RMS rectifier and displayed using time constants "Slow", "Fast" or "Impulse". (It is recommended to use the "Slow" or "Fast" constant for corona audible noise measurement).

There are sound level meters of various producers available. Generally, each instrument used for corona audible noise measuring should conform to current IEC standards for precision sound level meters (e.g. IEC 651 class 1).

The measuring microphone is one of the fundamental parts of the sound level meter. For corona audible noise measurement it must fulfil some basic requirements: the frequency response should be from 20 Hz to 20 kHz within ±3 dB, the dynamic range should cover low levels from 25 dB. The transmission line is a very large acoustic source. In order to be able to measure in the close vicinity of the line (e.g. at the distance of 15 m from the outer phase) without loss of sound coming from large

angles (Figure 4.3), the measuring microphone must have a good omnidirectivity. It must be able to work at high humidity and low temperature. Such requirements fulfil best up to date 1/2-inch condenser microphones. They are available as free-field, pressure and random-incidence ones. The free field ones are the best solution for audible noise measurements. Some condenser microphones for outdoor use have the diaphragm covered by a thin layer of quartz. These types of microphones are especially recommended for corona audible noise measurements.

Using a tape-recorder is very advantageous in most measurements because both the information of measured level and the information of the frequency spectrum are recorded. The tape recorder with flat frequency response within ±3 dB over the range from 100 Hz to at least 16 kHz should be used. There are a lot of other requirements on characteristics of tape-recorders: beside frequency response, the dynamic response as well, flutter, etc. To avoid problems with the choice of a recorder type and to check up its parameters the best way is to use a portable multichannel instrumentation tape-recorder. Such recorders are manufactured by companies producing sound measuring devices. They can store easily sounds of a frequency range from 25 Hz up to 20 kHz with the accuracy of ±2 dB and with dynamic range of 50 dB or even of 70 dB when using a compander. While measuring, the electronic noise level of the recorder should be at least 10 dB below the lowest audible noise level at each frequency. However, the best results are obtained by using special digital tape recorders.

A spectral analysis gives a more detailed description of corona audible noise than the A-level. The octave or one-third octave analysis using built-in filters in some types of sound level meters is the easiest way how to get sufficient information about the spectrum at field measurements. The best possibility, however, gives a real-time FFT analyzer, which determines the discrete frequency spectrum of the noise.

Generally, there are two types of frequency analyzers: the constant bandwidth analyzers, the bandwidth of which is constant over the entire frequency range (the FFT analyzer is a special case of this group) and the constant percentage bandwidth analyzers, the bandwidth of which increases proportional to the centre frequency tuned (the octave and one-third octave analyzers belong to this group). It is apparent that if the noise is examined with both types of analyzers, different curves of spectra will be obtained.

A statistical noise level analyzer is a very good tool to obtain long-term acoustic data. Such an analyzer may measure and evaluate

- equivalent sound level (L_{eq}),
- exceedance level (L_x - the level which is exceeded *x*-percent of the time period),
- mean value of sound level,

and other statistical values depending on the type of the analyzer.

However, at corona audible noise measuring, there arises the problem of how to distinguish corona noise from background noise (see next paragraphs).

4.3.2 Short-Term Measurement

Short-term measurement which, is relatively easy to carry out, shows corona audible noise in a short time interval at certain weather conditions.

In order to obtain acoustic data comparable with other measurements, it is recommended that the measuring microphone should be located 15 metres from the vertical projection of an outside phase of an AC line at the midspan and 1.5 metres above ground. The microphone should be mounted on an extension rod or better separately from the sound level meter on a tripod. In any case, the operator should not stay less than 1 metre from the microphone. The location chosen for the measurement should be flat without obstacles reflecting sound.

To obtain a lateral profile of corona audible noise, the microphone locations are at the centre of the line, between the centre and the outside phase and 0, 15, 30, 45, 60, etc. metres perpendicular from the vertical projection of the outside phase. To obtain the lateral profile of the hum component, the steps of distance of the microphone locations must be shorter, due to possible resonance patterns, probably less than 1 m.

The free-field microphone shall be directed at the nearest point of the centre phase of the AC line (positive pole of the DC line). The random microphone or the free-field one with a random incidence corrector shall be oriented vertically. The pressure microphone shall be oriented perpendicular to the line.

Before and after measurement, the sound level meter should be calibrated with an acoustic calibrator. The data from measurement should comprise the A-weighted sound level and octave or one-third octave sound pressure level analysis from 31.5 Hz to 16 kHz. If possible, a portable instrumentation tape recorder should be used and both the calibrating signal and unweighted sound pressure signal from the AC output of the sound level meter should be recorded for a later analysis in the laboratory. The background noise must be also put down or recorded (see paragraph 4.3.4 Influence of Environment). It should be measured at a distance of at least 200 metres from the line and, if possible, at the same time as the corona noise is recorded or the sound level meter readings are put down. Beside sound levels, complete meteorological and conductor surface conditions shall be put down (temperature, relative humidity, wind velocity and direction, rain, fog, snow, new/aged conductors, dry, wet, icing), microphone location and all the data concerning the measuring instrumentation (especially the type of the measuring microphone).

4.3.3 Long-Term Measurement

Since the noise varies with time, with meteorological conditions and with the voltage of the line, long-term measurement provides more detailed information.

The instrumentation in this case must be very sophisticated and must be able to record at least the A-weighted sound level (if possible, the octave sound pressure bands from 31.5 Hz to 16 kHz, too), precipitation rate, wind speed, temperature, relative humidity and the background noise levels from the microphone located 200 metres from the outside phase. It is also possible to record the 8 kHz or 16 kHz octave band sound pressure because it can help to decide if the measured noise level is caused by the line or if is to be attributed to the background noise. There is a high probability that the noise at frequencies above 8 kHz should belong only to the line and not to the background.

Special care must be paid to the choice of the microphone. It is recommended that a special microphone outdoor unit for permanent noise monitoring systems should be used. Such outdoor units are produced by specialized producers of sound measuring instruments. Before using it for corona audible noise measurement, anti-bird spikes must be removed in order to avoid undesirable electrical discharges which might influence the sound level.

The whole measuring device shall be calibrated periodically.

Data should be collected over a sufficiently long time period, at least several months.

4.3.4 Influence of Environment

Wind

To minimize the noise caused by wind blowing across the microphone, a windscreen must be used over the microphone during measurements. For the short-term measurement, it also shields the microphone from dust and especially from rain. Even if the windscreen is used the measurement should not be taken at a wind velocity exceeding 5 m/s. In order to get a minimum insertion attenuation loss of the windscreen, it is recommended that only a product of a specialized sound measuring instrument producer should be used and the data sheet should be consulted.

Humidity and Temperature

Relative humidity up to 90% does not influence the microphone. However, rapid temperature changes may cause water condensation in the microphone. At steady temperatures, current sound level meters and special outdoor microphones are able to work from about -10 to +50°C. The microphones with the diaphragm covered by a thin layer of quartz are recommended for this type of outdoor measurement.

Interference

For sound measurements near the HV lines, great care must be paid to check the sound level meter from the point of view of electromagnetic compatibility. Due to a high electric field intensity, several kinds of interference can arise in the measuring device.

Firstly, in cables and electronics of the instruments. This type of interference can be reduced relatively easily by appropriate use of shielded cables, instruments and by their proper connection.

Secondly, if a part of the microphone protection grid is not conductively connected to the body of the microphone, the electric field penetrates as far as the diaphragm. The diaphragm is then loaded by

an electrostatic force excited by electric field that consequently results in vibration of the diaphragm. Since the inside microphone system cannot distinguish whether the movement of the diaphragm is forced by an incident sound pressure or by the electric field, the sound level meter shows a considerable error. In case of the 50 Hz electric field, the acoustic spectrum displays the erroneous component of 100 Hz. (This principle of electrostatic force is currently used as a method for the determination of a pressure response of microphones carried out by a so-called Electrostatic Actuator.) The danger of such an error consists in resemblance of the incorrect frequency spectrum to the real spectrum of corona audible noise of the AC line which has a real 100 Hz hum component. In order to avoid this problem it is necessary that the diaphragm be shielded against electric field.

Background Noise

Audible corona noise levels are relatively low; the accuracy of measurements may be influenced by background noise levels. The background noise level should be measured at a distance of 200 m from the line and, if possible, at the same time as the measurement of corona noise . The A-weighted sound level and octave or one-third octave sound pressure level analysis from 31.5 Hz to 16 kHz should be put down or better, recorded on the tape recorder. After measuring, the background noise correction must be applied to the corona A-weighted sound level and octave or one-third octave band levels according to the formula $L = L_m - L_d$, where L is the corrected level of corona noise, L_m is the measured level of corona noise near the line which consists of both corona noise and the background noise, and L_d is given by Table 4.1 (L_b is the background noise level).

$L_m - L_b$	L_d
[dB]	[dB]
4	2.2
5	1.7
6	1.3
7 - 8	1
9 - 10	0.5
11 - 12	0.3
≥12	0

Table 4.1
Background noise corrections

If the difference between the noise level beneath the line and the background noise level is less than 4 dB, the measurement should not be taken in account. Generally, it is recommended that the difference $L_m - L_b$ should be larger than 6 dB.

However, the best way to avoid problems with background noise is to choose a location for measurement where there is no traffic and no other disturbing sounds. It is also recommended, that the operator should use earphones while measuring. This measure helps him to identify the background noise.

4.4 Psychoacoustic Studies

Civilization brings more and more noise. Table 4.2 gives an overview about some common noises in the environment.

Limits of noise levels set by national authorities differ in various countries (if they are set). Their values are often given in A-weighted levels. The following data can be taken as an example of maximum permissible values of outdoor noise:

- national parks, health areas at night - 30 dB(A) up to 35 dB(A)
- living estates in suburban area at night - 40 dB(A) up to 45 dB(A)
- urban areas at night - 50 dB(A).

In the case of corona audible noise, the frequency spectra differ from traffic noise or from other common noises. The corona audible noise spectrum extends up to ultrasonic range while e.g. the traffic noise does not contain so many high frequency components (figure 4.6). Knowing these facts, a principal question arises: If there are the corona noise and the traffic noise (or other common noise) of the same A-weighted level, is the annoyance or aversiveness of both kinds of sound the same ?

In order to get more information about psychoacoustic effects of the corona audible noise, various studies have been undertaken [4.8], [4.9], [4.10], [4.11], [4.12]. However, to answer the above mentioned question is very difficult. We at least quote some of the conclusions of these studies:

- For the same A-weighted sound level, the loudness of the corona noise increases with the increase of the 100 Hz component [4.8]
- The high frequency hissing and crackling components of corona noise are more aversive than the low frequency humming and buzzing components [4.8].
- A comparison between the corona noise and three other types of noise (1000 Hz noise, traffic noise and noise due to superimposed voices) has indicated that for the same A-weighted sound level the loudness of the corona noise is lower than that of the traffic noise and higher than that of 1000 Hz noise and voice noise [4.12].
- From a limited sample of comparison sounds, corona noise was found to be roughly equal in aversiveness to the noise from a room air conditioner. Corona noise is also more aversive than the sound of rainfall that often accompanies it [4.8].

Sound Level [dB(A)]	Noise Source
110 - 130	Pneumatic chipper
105 - 130	Loud automobile horn at a distance of 1 m
70 - 80	Inside bus
70 - 85	Average traffic on street
60 - 70	Conversational speech
50 - 60	Business office
40 - 50	Living room in suburban area
30 - 60	Transmission line at a distance of 30 m
30 - 40	Library
20 - 30	Bedroom at night

Table 4.2
Some common noise level [4.6], [4.8]

- All of the common frequency weighting scales underestimate the aversiveness of corona noise relative to other environmental sounds. The discrepancies were lower for the A-weighted sound level, and lowest for the D-weighted sound level [4.8].
- There are distinctly different kinds of corona noise which differ both in frequency spectrum and relative aversiveness [4.8].

However, the results of psychoacoustic studies imply a lot of problems connected with evaluation of the corona audible noise and research in this field can be hardly considered as finished, there is no other way at present than using A-weighted levels for evaluation of corona audible noise.

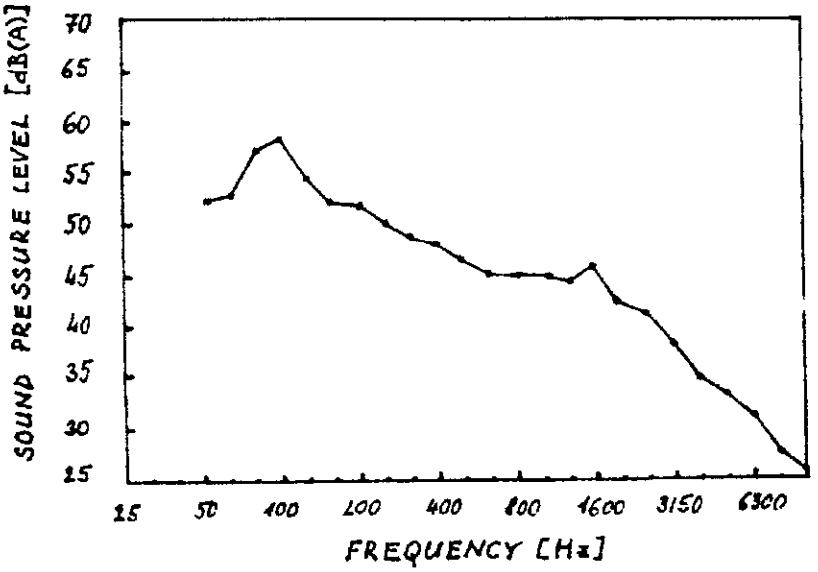

Figure 4.6

Example of the frequency spectrum of AN produced during rain by corona

4.5 Consequences for the Planning of Transmission Lines

If no limits of audible noise for HV lines are defined, at least two items should be kept in mind:

-- under fair weather conditions, when conductors are without a moister film at the surface, lines in sensible areas must be free of any visibly or audibly detectable discharges.

-- under worst ambient conditions, a maximal dB(A) value in the range of 52 dB(A) seems to be tolerated but not permanently. This corresponds to a 35 dB(A) value in a bedroom when windows are closed considering that an attenuation of 17 dB per window is achievable.

Comparing the audible noise calculation for an existing line , which has - or never has -produced complaints, to that one of a new line, might refer best to the local situation.

Appendix 4 Formulae for Determining Audible Noise

This Appendix reports formulae developed by various experimenters for the predetermination of audible noise A-weighted levels of UHV A.C. lines. For the sake of completeness, beside formulae specially developed for UHV lines other formulae previously developed for EHV lines, but considered useful also for UHV lines, are here reported. The formulae were expressed in terms of acoustic generation function. In order to calculate the A-weighted sound pressure level, the procedure according to Equation (4.14) is to be used if not otherwise specified :

$$L_A = 54.3 + \Gamma A - 10 \cdot \log D - \delta_L \qquad (4.14)$$

A4.1 EPRI [3.10]

Heavy rain

$$\Gamma A_5 = C_5 - \frac{665}{g} + 20 \cdot \log n + 44 \cdot \log d + k_n \qquad (A4.1)$$

n	k_n	C_5
1	7.5	20.9
2	2.6	20.9
≥3	22.9 (n - 1) d / (2R)	13.6

Wet conductor

$$\Gamma A_{50} = \Gamma A_5 - C_{50}(g, d, n) \qquad (A4.2)$$

n	C_{50}		n	g_{c0} for : 2 cm < d < 8 cm
<3	- 8.2 + 14.2 g_{c0}/g		≤ 8	24.4/ $d^{0.24}$
≥3	- 10.4 + 14.2 g_{c0}/g - [8 (n-1) d/2R]		> 8	24.4/ $d^{0.24}$ - 0.25 (n - 8)

Range of validity: 230 - 1500 kV, $1 \leq n \leq 16$, $2 \leq d \leq 6$

Conversion : $L_A = 54.3 + \Gamma A - 10 \cdot \log D - 0.02 \cdot D$

A4.2 ENEL, Ente Nazionale per Energia Elettrica, 1000 kV Project (Italy) [3.17]

Heavy rain

$$\Gamma A_5 = 23 - \frac{576}{g} + 10 \cdot \log n + 37 \cdot \log d \qquad (A4.3)$$

Wet conductor

$$\Gamma A_{50} = 30 - \frac{863}{g} + 7 \cdot \log n + 57 \cdot \log d \qquad (A4.4)$$

Range of validity: 400 - 1200 kV, $n \leq 10$, $2 \leq d \leq 5$

A4.3 Bonneville Power Administration (BPA) [4.19]

Wet conductor

$$\Gamma A_{50} = K_1 + 120 \cdot \log g + K_2 \cdot \log n + 55 \cdot \log d + \frac{q}{300} \qquad \text{(A4.5)}$$

	K_1	K_2
$n < 3$	- 169.7	0
$n \geq 3$	- 182.7	26.4

Range of validity : 230 - 1500 kV, $n \leq 16$, $2 \leq d \leq 6.5$

Note : Average stable rain is the median level of the upper normal distribution of the all-weather probability distribution. Measurements have shown that it is less than the ΓA_{50} level [4.22].

Conversion : $L_A = \Gamma A + 54.3 - 11.4 \cdot \log D$

$\Gamma A_5 = \Gamma A_{50} + 3.5$

A4.4 Hydro Quebec Institute of Research (IREQ) [4.21]

Heavy rain

Single conductors

$$\Gamma A_{5s} = -123.94 + 82.84 \cdot \log g + 48.28 \cdot \log d \qquad \text{(A4.6)}$$

Bundle conductors

$$\Gamma A_{5b} = \left[\sum_{i=1}^{n} \sqrt{\frac{1}{2\pi} \int_0^{2\pi} \Gamma A_{5s}(g(\phi), d) d\phi} \right]^2 \qquad \text{(A4.7)}$$

or a similar formula from another reference [4.19]

$$\Gamma A_{5b} = -111.9 + 45.8 \cdot \log d + 72 \cdot \log g + 22.7 \cdot \log n \qquad \text{(A4.8)}$$

Range of validity: 345 kV - 1500 kV, $n \geq 2$

Conversion : $L_A = 54.3 + \Gamma A - 11.4 \cdot \log D$

A4.5 FGH, Germany [4.19]

Heavy rain

$$\boxed{\Gamma A_5 = 2 \cdot g + 18 \cdot \log n + 45 \cdot \log d - 54.6} \qquad \text{(A4.9)}$$

Range of validity: $n \leq 6$, $2 \leq d \leq 6$, $14 < g < 21$ kV/cm

A4.6 Electricite de France (EDF) [4.13, 4.19]

Heavy rain

$$\boxed{\Gamma A_5 = 15 \cdot \log n + 4.5 \cdot d + A_{N0} - 54.3} \qquad \text{(A4.10)}$$

A_{N0} is given by Figure A4.1

Range of validity 400 - 1200 kV, $n \leq 6$, $2 \leq d \leq 6$

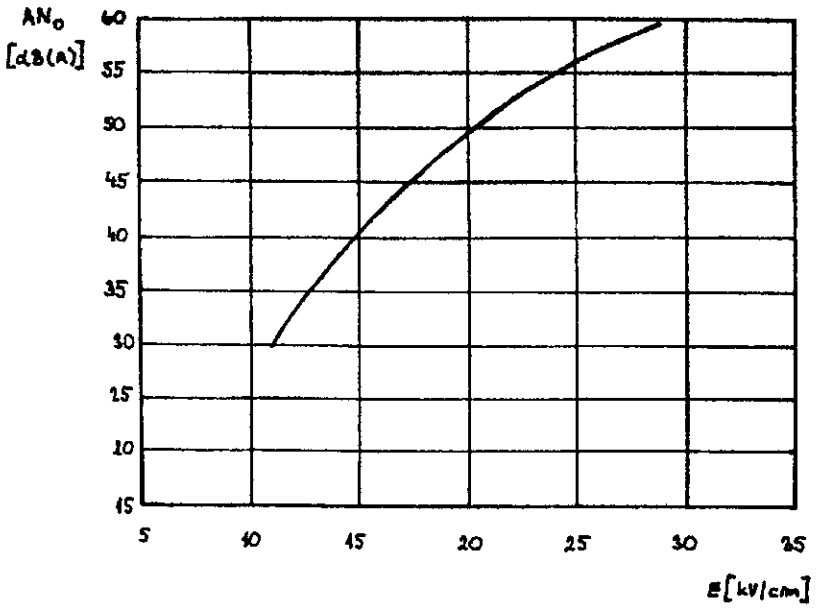

Figure A4.1

Curve for predetermination of AN with EDF formula

A4.7 Power Research Institute, Czech Republic

Heavy rain

$$\boxed{\Gamma A_5 = 106.1 \cdot \log g + 48.3 \cdot \log d + 23 \cdot \log n - 156.8} \qquad \text{(A4.11)}$$

Average rain

$$\boxed{\Gamma A_{50} = 98 \cdot \log g + 45.3 \cdot \log d + 20.2 \cdot \log n - 149.1} \qquad \text{(A4.12)}$$

Range of validity: $12 \leq g \leq 22$, $2 \leq n \leq 12$, $2.4 \leq d \leq 5.6$

A4.8 University of Liege (ULg), Belgium [1.1]

Heavy rain

$$\boxed{\Gamma A_5 = 0.00116 \cdot B^3 - 0.185 \cdot B^2 + 7.65 \cdot B - 68.7} \qquad \text{(A4.13)}$$

$$\text{where } B = g \cdot \left(\frac{n}{6}\right)^{0.3} \cdot \left(\frac{d}{2.54}\right)^{0.6}$$

Range of validity: $10 \leq g \leq 28$

A4.9 UPB Romania

Heavy rain

$$\boxed{\Gamma A_5 = \left(1.38 \cdot 10^{-4} \cdot \Gamma^{2.23} - 1\right) + 19.7} \qquad \text{(A4.14)}$$

$$\text{with : } \Gamma = 50 - \frac{540}{g} + 74 \cdot \log d - 10 \cdot \log n \quad \text{dB } (1\ \mu A/\sqrt{m}) \text{ see equation (A3.1.19)}$$

Conversion : $L_A = 54.3 + \Gamma A - 10 \log D$

A4.10 Central Research Institute of Electric Power Industry, Japan [4.20]

Heavy rain

$$\boxed{\Gamma A_5 = A^o_{hr} - \frac{665}{g}} \qquad \text{(A4.15)}$$

A^0_{hr}	n				
d	1	4	6	8	10
2.24		44			
2.53		47		50	50
2.85		49		52	
3.42	48	53			56
3.84	48	54	57	58	59
4.62				63	63
5.28				66	67

Wet conductor

The levels are given in the following table :

	ΓA_{50} dB (A)															
n	1			4			6		8					10		
d	3.42	2.24	2.53	2.85	3.42	3.84	3.84	2.53	3.84	4.62	5.28	2.53	3.42	3.84	4.62	5.28
g																
9																- 6
10																- 3
11										- 3				- 6	- 1	2
12					- 10	- 6				0	6			- 3	3	8
13					- 6	- 4			0	5	10			0	7	13
14				- 6	- 3	- 1	- 1	- 3	3	11	16	- 5	- 1	3	13	17
15				- 2	1	2	6	0	7	16	20	- 1	3	10	17	21
16	2	- 8	- 1	0	6	11	13	3	13	20	23	3	10	15	21	
17	8	- 2	2	4	12	16	17	6	18	23	26	6	15	17	24	
18	11	1	7	8	16	18	20	10	22	26		10	19	20		
19	18	3	11	12	19		22	13	26			14	20	24		
20	14	6	15	15	21		24	16	27			17	23			
21		9	15	17	22							18	26			
22		12		19	23							21				

Compilation of the Different Formulae for the Evaluation of the Acoustic Generation Function and the A-weighted Sound Pressure Level under Heavy Rain

Using the example of paragraph 2.5, the acoustic generation function ΓA (dB(A) (1 μW/m)) with the different formulae for the center phase and the A-weighted sound pressure level under heavy rain at a lateral distance D of 15 m of the center phase can be calculated.

The formula (4.14) is used for the conversion of ΓA_5 into L_A except for EPRI, BPA and UPB using their own conversion formulae.

Method	ΓA_5 (dB(A) (1 μW/m))	L_A (dB(A) (20 μPa))
EPRI (A4.1)	20.11	62.35
ENEL (A4.3)	17.95	60.85
BPA (A4.5)	21.95	62.84
IREQ (A4.8)	21.09	61.98
FGH (A4.9)	19.43	62.33
EDF (A4.10)	20.75	63.65
PRI (A4.11)	20.58	63.48
ULg (A4.13)	22.25	65.15
UPB (A4.14)	19.42	61.96
CRIEPI (A4.15)	16.27	59.17

Remark : These results for a single phase arrangement under worst weather conditions are given only to verify the calculation procedures.

Glossary chapter 4

A^0_{hr}	factor depending of n and d	dB
A_{N0}	factor depending of g	dB
a_r	reflection coefficient	
B	empirical factor depending of g, n and d	
C	constant factor	dB
C_5	factor depending of n	dB
C_{50}	factor depending of g, n and d	dB
c_s	sound velocity, in air c_s = 331 m/s	m/s
D	distance between the conductor and the point of calculation	m
d	subconductor diameter	cm
D_i	distance of point at which the sum is calculated from the i-th particle acoustic source	m
D_i'	distance of the i-th image source	m
f	frequency of sound	Hz
f_0	centre frequency of band	Hz
$f_1(g)$	empirical function of g	dB
$f_2(d)$	empirical function of d	dB
$f_3(n)$	empirical function of n	dB
g	effective value of the maximun surface conductor gradient	kV/cm (rms)
h	height of conductor above ground	m
I	acoustic intensity	W/m^2
I_0	reference value of acoustic intensity (I_0 = 1 $\mu W/m^2$)	W/m^2
k	factor depending of f and c_s	1/m
K_1	factor depending of n	dB
K_2	factor depending of n	dB
K_{Ai}	correction of A-weighting characteristic of the i-th frequency band	dB
k_D	function of D and δ_L	dB
k_n	factor depending of n, d and R	dB
L	sound pressure level	dB (20 µPa)
l	length of the conductor	m

L_A	A-weighted sound pressure level	dB(A) (20 µPa)
L_{ATot}	total sound pressure level	dB(A) (20 µPa)
L_b	background noise level	dB
L_d	correction factor	dB
L_{eq}	equivalent sound level	dB
L_i	sound pressure level of the i-th frequency band	dB (20 µPa)
L_I	sound intensity level	dB (1 µW/m^2)
L_m	measured level of corona noise	dB
ln	$\ln \equiv \log_e$, e = 2.718	
log	$\log \equiv \log_{10}$	
L_W	sound power level	dB (1 µW/m)
L_x	level which is exceeded x-percent of the time period	dB
n	number of subconductors	
p	sound pressure	N/m^2 or Pa
p_0	reference value of sound pressure (p_0 = 20 µPa)	N/m^2 or Pa
p_{max}	amplitude of the pressure	N/m^2 or Pa
q	altitude above sea level	m
q_i	volume velocity of the i-th particle (complex value)	m^3/s
t	time	s
W	acoustic power per unit of length	W/m
W_0	reference value of acoustic power per unit of length (W_0 = 1 µW/m)	W/m
ω	pulsation ($\omega = 2\pi f$)	rad/s
σ	air density	kg/m^3
Γ	RI excitation function	dB (1 µA/$\sqrt{m}$)
ΓA	acoustic generation function	dB(A) (1 µW/m)
ΓA_5	audible power level of one phase at heavy rain	dB(A) (1 µW/m)
ΓA_{50}	audible power level of one phase at average rain	dB(A) (1 µW/m)
ΓA_{5b}	audible power level of one phase at heavy rain for bundle	dB(A) (1 µW/m)
ΓA_{5s}	audible power level of one phase at heavy rain for single	dB(A) (1 µW/m)
ΓA_{av}	acoustic power level under average rain	dB(A) (1 µW/m)
ΓA_{fw}	acoustic power level under fair weather	dB(A) (1 µW/m)

ΓA_{hr}	acoustic power level under heavy rain	dB(A) (1 µW/m)
δ_L	attenuation depending of distance D	dB
Δ_c	correction factor	dB
Δ_o	correction factor	dB

References

[4.1] S. Balantine, "Journal of Acoust. Soc. ", Amer. Vol. 3 p. 319 (1932).

[4.2] J. T. Broch, "Application of Bruel-Kjaer Equipment to Acoustic Noise Measurements", Bruel-Kjaer, 1971.

[4.3] "Selected Reprints From Technical Review - Measuring Microphones", p. 97, Bruel-Kjaer, 1971.

[4.4] J.J. Clade, C.H. Gary, "Predetermination of corona losses under rain: Influence of rain intensity and utilization of a universal chart", IEEE Trans., Vol. PAS-89, No. 6, 1970, pp. 1179-1185.

[4.5] I. Kabrhel, "Contribution to Noise Measurements in Electric Plants with Strong Electric Field", The 21st Conference on Acoustic Noise and Environment, Dum techniky SVTS Bratislava, 1982 (Czechoslovakia).

[3.10] "Transmission Line Reference Book 345 kV and above", EPRI, Palo Alto Ca., 1979.

dto. second edition, 1982.

dto. second edition revised, 1987.

[1.1] "Interferences Produced by Corona Effect of Electric Systems; Description of Phenomena, Practical Guide for Calculation", Brochure No. 20, WG 36.01, CIGRE, Paris, 1974.

[4.6] L.L. Beranek, "Noise Reduction", McGraw-Hill, New York, 1960.

[4.7] Y. Sawada, M. Fulenshima, M. Yasni, "AKAGI 1000 kV project in CRIEPI Corona text facilities and results up to 1983", Paper CIGRE 36-05, Session 1984.

[4.8] J.A. Molino, G. A. Zerdyt, N.P. Lerner, D.L. Harwood, "Use of the 'Acoustic Menu' in Assessing Human Response to Auidible (Corona) Noise from Electric Transmission Lines", J. Acoust. Soc. AM, 66 (5), Nov. 1979, pp. 1435-1445.

[4.9] "IEEE Standard for the measurement of audible noise from overhead transmission lines", IEEE Std 659-1992.

[4.10] M. Fiorina, R. Piazza, F. Rosa, "Loudness annoyance of the acoustic noise produced by corona discharges in A. C. Power lines", Paper C3-5, 12th Intern congress on acoustics Toronto, July 24 - 31, 1986.

[4.11] M. Fiorina, R. Piazza, F. Rosa, "Effect of audible noise on UHV power line design", Paper C3 - 7, 12th International congress on acoustics Toronto, July 24 - 31, 1986.

[4.12] R. Cortina, F. Rosa, W. Serravalli, E. Brosio, R. Piazza, "Experimental investigation in the anechoic chamber on the loudness of acoustic noise caused by A.C. corona", IEEE Trans., Vol. PAS-100, No. 9, September 1981, pp. 4225 - 4232.

[4.13] A. Coquard, C. Gary, "Audible noise produced by electrical power transmission lines at very high voltage", CIGRE Paper 36-03, 1972.

[4.14] V. L. Chartier, R.D. Stearns, "Formulae for predicting audible noise from overhead high voltage ac and dc lines", IEEE Trans., Vol. PAS-100, No. 1, January 1981, pp. 121 - 131.

[4.15] M. Sforzini, R. Cortina, G. Sacerdote, R. Piazza, "Acoustic noise caused by A.C. corona on conductors: results of an experimental investigation in the anechoic chamber", IEEE Trans., Vol. PAS-94, No. 2, March/April 1975, pp. 591 - 601.

[4.16] J. Lundquist, "Methods for predicting A.C. transmission line audible noise by short-term single-phase tests", IEEE Trans., Vol. PAS-103, No. 2, February 1984, pp. 283 - 291.

[4.17] M.G. Comber, R. Cortina, "Audible noise generation of individual subconductors of transmission line conductor bundles", IEEE Trans., Vol. PAS-95, No. 2, March/April 1976, pp. 526 - 533.

[4.18] P. Heroux, P. Sarma Maruvada, N.G.Trinh, "High voltage A.C. transmission lines: reduction of corona under foul weather", IEEE Trans., Vol. PAS-101, No. 9, September 1982, pp. 3009 - 3017.

[3.16] M. Fukushima, T. Sasano, Y. Sawada, "Corona performance of conductor bundles measured in corona cages and its application", CIGRE Symposium 22-81, No. 232-01, June 1981.

[3.17] B.A. Cauzillo, R. Cortina, P. Nicolini, J.C. De Medeiros, M.E. Bryant, "Design criteria of UHV lines based on experience acquired, in the 1000 kV Project", CIGRE 22-14, 1984.

[3.18] N. Giao Trinh, P. Sarma Maruvada, "A method of predicting the corona performance of conductor bundles based on cage test results", IEEE Transactions on Power Apparatus and Systems, Vol. PAS-96, No. 1, Jan/Feb 1977, pp. 312-325.

[4.19] IEEE Corona and Field Effects Subcommittee, "A Comparison of Methods for Calculating Audible Noise of High Voltage Transmission Lines", IEEE Trans. on Power Apparatus and Systems, Vol. PAS-101, No. 10, Oct. 1982, pp. 4090-4099.

[4.20] M. Fukushima et al., "A Study on Audible Noise from AC and DC Transmission Lines", CRIEPI Report T - 01 (in Japanese), 1986.

[4.21] N.G. Trinh, P. Sarma Maruvada, "A semi empirical formula for evaluation of audible noise from transmission line corona", IEEE Canadian Communication and EHV Conference, Montreal, Nov. 9 - 10, 1972, pp. 166 - 167.

[4.22] V.L. Chartier, D.E. Blair, M.D. Easley, R.T. Raczkowski, "Corona Performance of a Compact 230-kV Line", IEEE Transactions on PWRD, Vol. 10, No. 1, January 1995, pp. 410-420.

Chapter 5

Corona Loss

5.1 Generation of Corona Loss

From a physical point of view, it is the movement of ions generated from corona discharges in a power-frequency electric field which results in corona loss, the energy being dissipated by the transfer of thermal energy to neutral air molecules. The movement of the ions gives rise to a current in the conductor which has a fundamental component in phase with the voltage, resulting in a power loss. It is thus seen that corona loss is drawn from the electrical source and transformed and dissipated in the form of thermal energy.

As the voltage applied to a transmission line conductor is increased, corona first occurs at a few dispersed sources along the conductor. This condition of localized corona is characterized by a few randomly distributed independent sources of discharge and results in negligible corona loss. As the voltage is further increased, or under foul weather conditions such as rain, snow or fog, the number of corona discharge sites increases drastically and results in what is known as generalized corona. This condition is characterized by a stable mechanism of almost uniformly distributed corona discharge sources and the occurrence of significant corona power loss.

A number of empirical or semi-empirical methods to calculate corona loss have been proposed in the literature, based on both experimental data and theoretical considerations. A compilation of methods is given in Appendix 5.

All formulae use conditional constants for conductor surface conditions. Loss values for aged conductors in heavy rain are well-defined and experimentally reproducible. All formulae are derived from cage tests and experimental spans of short line sections. Statistical data from actual transmission lines, if it could be obtained, cannot be used as they would be governed by the local specific climatic condition, which are unlikely to be constant along the total length of the line. Long-term corona loss data from operating lines is difficult to measure, since corona loss is much smaller than load loss.

Fair-weather loss of line configurations which have tolerable levels of radio interference and audible noise is usually low compared with the ohmic loss. Therefore interest is usually concentrated on loss under bad weather conditions.

The formulae for the corona loss P are given in Appendix 5. They are derived from experiments at low altitudes, that is with a relative air density δ of about 1. When conductors are selected for lines at high altitudes (< 3000 m) the influence of air density on corona activity has to be taken into account. From reference [2.3] a correction factor F_a is suggested (such that P_a becomes $F_a P$) given by

$$F_a = 10^{\,q/3000}$$

where q is the altitude above sea level (m).

When the corona loss is given in dB (1 W/m) (i.e. P_{dB}) then it must be increased by K_A which is given by

$$K_A = q/300.$$

5.2 Economic Consequences

Corona loss affect transmission line design in two principle ways:

- The economic impact resulting from the cost of loss due to corona
- The impact on the maximum demand requirements of generation.

The energy loss due to corona may be determined for a given line by evaluating the annual average corona loss. For this, two sets of information are required. Firstly, the corona loss should be determined for the given line configuration and operating voltage, either by calculation using one of the empirical methods described above, or by direct measurement on a test line under different weather conditions. Secondly, a weather model should be established for the actual line, comprising the percentages of time in a year during which the line is subject to different weather conditions such

as fair weather, rain, snow, etc. The annual average corona loss for the line may then be calculated using these two sets of information.

Corona loss becomes an important factor in the maximum generation demand requirements only if the maximum corona loss occurs at the same time as the maximum transmission load. Such a situation can arise, for example, if the transmission line is called upon to deliver the maximum power during heavy rain or a wet-snow storm that covers the entire length of the line. The simplest method for determining the maximum corona loss for a given line is to obtain, by calculation or measurement, the corona loss per unit length (i.e. kW/km) under heavy-rain conditions and multiplying this value by the total length of the line. For long lines under practical conditions however the weather model will not be the same for the entire length of the line. Depending on the possible spatial distribution of weather conditions along the length of the line, a reduction factor should therefore be applied to the maximum corona loss determined as described before.

5.3 Methods of Measurement

The measurement of corona loss involves the detection of a small power loss component in the presence of a very large reactive component. This is essentially the same as the problem of measuring the loss in an air-dielectric capacitor. Very stable power measuring devices of high resolution [5.1] are necessary to measure loss angles as low as 0.05°. Since it is desirable in experimental installations to measure corona loss over a range of voltages, it may be necessary to be able to measure even lower loss angles than this in the total system when measuring in the vicinity of corona onset. Most wattmeters when used directly cannot meet these requirements.

Three systems used for corona loss measurement are as follows:

- wattmeters (or watt transducers)
- bridge circuits
- bridge circuits in combination with wattmeters

A type of electronic watt transducer based on a time division multiplying system has been used in outdoor corona test installations [5.2, 5.3]. Such devices are now available as commercial instruments.

In the bridge circuits, the two high voltage arms of the bridge are composed of a loss free capacitor and the "loss capacitor" transmission line. In this method, the total line-to-ground current is compared with the current in the standard capacitor which is usually of the pressurized gas type. In principle, the large reactive component referred to above is annulled within the bridge and only the loss component needs to be balanced. In some devices, this balance is made automatically, permitting the bridge to be positioned at the high voltage terminal of the power supply.

Another bridge circuit based on the use of a special transformer-ratio arm device known as a current comparator [5.4] has also been employed. In this bridge, the currents in a standard, loss-free, capacitor and an unknown capacitor (the line) are compared in a comparator. Measurements on high-voltage standard capacitors [5.5] and on low-loss reactor [5.6] have demonstrated that this bridge has exceptional stability, high resolution and accuracy in loss measurement at low power factor. It was adapted for corona power loss measurements on transmission lines [5.7] by adding a self-balancing circuit and a thermal-converter type multiplier which forms a wattmeter. In this circuit, the bridge effectively nulls the reactive component of current, preventing it from entering the wattmeter. The in-phase component of the current is multiplied by a signal proportional to the line voltage to provide the power loss.

Since corona loss, especially those under fair-weather conditions, is normally inconsequential compared with the resistive loss, highly accurate measurements using bridge techniques are not required. Therefore simpler techniques have been used by many investigators, primarily to measure foul-weather loss.

Appendix 5 Overview of the Formulae Developed in Different Countries for the Evaluation of Corona Loss.

A5.1 Ontario Hydro Method: Nigol and Cassan [5.7] developed a semi-empirical formula for the calculation of corona loss based on extensive corona loss measurements on Ontario Hydro's Coldwater Project. The basic form of the equation is:

$$P = k \cdot f \cdot r^2 \cdot n \cdot \frac{\Delta\phi}{2\pi} \cdot G_e^2 \cdot \ln\left(\frac{G_e}{G_c}\right) \cdot \frac{1}{1.61} \qquad \text{(A5.1)}$$

For single-conductor lines, equation (A5.1) simplifies to:

$$P = k \cdot f \cdot r^2 \cdot G_e^2 \cdot \ln\left(\frac{G_e}{G_c}\right) \cdot \frac{1}{1.61} \qquad \text{(A5.2)}$$

For bundle conductor lines[1],

$$G_a = \frac{V}{n \cdot r \cdot \ln\left(\dfrac{2 \cdot h \cdot S}{r_e \cdot \sqrt{4h^2 + S^2}}\right)} \quad \text{for the central phase} \qquad \text{(A5.3)}$$

$$G_a = \frac{V}{n \cdot r \cdot \ln\left(\dfrac{2 \cdot h \cdot S}{r_e \cdot \sqrt[4]{(4h^2 + S^2)(h^2 + S^2)}}\right)} \quad \text{for the outer phase} \qquad \text{(A5.3)}$$

$$G_\phi = G_a\left[1 + 2 \cdot (n - 1) \cdot \left(\frac{r}{s}\right) \cdot \sin\left(\frac{\pi}{n}\right) \cdot \sin\phi\right] \qquad \text{(A5.4)}$$

$$\phi_1 = \arcsin\left[\frac{G_c - G_a}{G_a \cdot 2 \cdot (n - 1) \cdot \left(\dfrac{r}{s}\right) \cdot \sin\left(\dfrac{\pi}{n}\right)}\right]$$

$$\phi_2 = \pi - \phi_1 \quad ; \quad \Delta\phi = \phi_2 - \phi_1 = \pi - 2\,\phi_1$$

$$G_e = G_a\left[1 + 2 \cdot (n - 1) \cdot \left(\frac{r}{s}\right) \cdot \sin\left(\frac{\pi}{n}\right) \cdot \left|\cos\phi_1 - \cos\phi_2\right|\right] \qquad \text{(A5.5)}$$

$$r_e = r \cdot \left(\gamma \cdot \frac{s}{r}\right)^{\frac{n-1}{n}} \quad \text{with } \gamma = \qquad \text{(A5.6)}$$

1 for $n < 4$ and $\gamma = 1.12$ for $n \geq 4$

The conductor surface factor m as well as the conditional constant k depend on the actual weather conditions. Figure A5.1 shows the variation of k as a function of m, the conductor surface irregularity factor, for different rates of rain and snow fall, based on the experimental results of Coldwater Project.

---

[1] The voltage gradient computation way proposed by the authors is strictly reproduced.

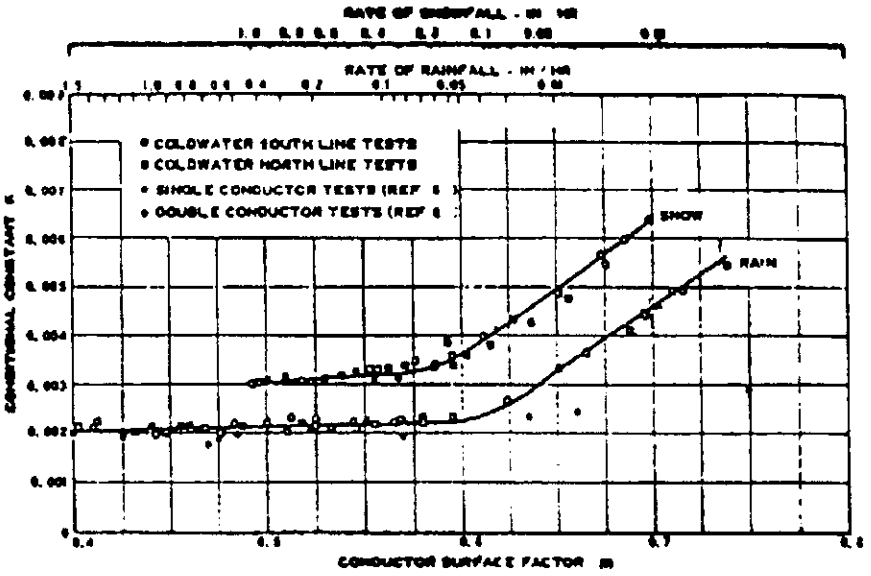

Figure A5.1

Conditional constant k as a function of conductor surface irregularity factor m and rate of precipitation

A5.2 **EDF Method:** Combining the results of an elaborate theoretical study of AC corona loss with experimental results obtained in outdoor test cages and a test line, Cladé and Gary of EDF [4.4] developed a semi-empirical method for calculating corona loss of AC transmission lines. The elements necessary for calculating corona loss are a chart of reduced loss, a reduction coefficient formula, and the correlation curves between the conductor surface factor m and the rain intensity. The corona loss is expressed as:

$$\boxed{P = K \cdot P_n} \qquad \text{(A5.7)}$$

where P = corona loss (W/m)

P_n = reduced loss, (W/m) (see Figure A5.2)

K = reduction coefficient

The reduction coefficient is given by the formula:

$$K = \frac{f}{50} \cdot (n \cdot r \cdot \beta)^2 \cdot \frac{\log \frac{R_z}{r_e} \cdot \log \frac{\rho}{r_e}}{\log \frac{R_z}{\rho}}$$

where n = number of subconductors

r = radius of subconductors, (cm)

r_e = equivalent radius of bundle, (cm) (see paragraph 2.5)

R_z = radius of equivalent zero potential cylinder, (cm) (see paragraph 2.5)

f = frequency of applied voltage, (Hz)

$\beta = 1 + \frac{0.308}{\sqrt{r}}$ (Peek coefficient)

$$\rho = 18 \cdot \sqrt{r} \quad \text{for single conductors}$$

$$18 \cdot \sqrt{n \cdot r + 4} \quad \text{for bundle conductors}$$

For each phase of the line, R_Z is determined to obtain the same capacitance in a concentric cylindrical arrangement as on the real line.

$$R_z = r_e \cdot e^{(2\pi\varepsilon_o / c_c)} \quad \text{(see paragraph 2.5.3)}$$

where $r_e = R \cdot \sqrt[n]{\frac{n \cdot r}{R}}$ (see paragraph 2.5.1)

R = radius of bundle (cm) $\quad R = \frac{s}{2 \cdot \sin\left(\frac{\pi}{n}\right)}$

C_C = total capacitance per length of the conductor within the line configuration (F/m)

Figure A5.2 shows P_n as a function g_a/g_c with m as a parameter, where g_a is the average conductor surface voltage gradient and g_c is the critical corona onset gradient with m and δ equal to 1 (Peek formula in chapter 2).

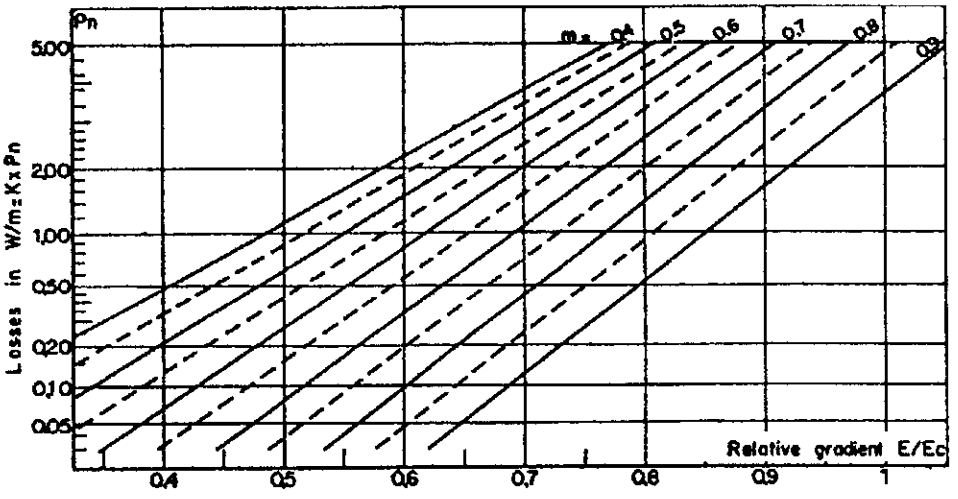

Figure A5.2

Reduced loss (P_n) for conductor surface irregularity factor (m) above the relative gradient g_a/g_c

Similarly, Figure A5.3 gives the conductor surface factor m as a function of rain intensity.

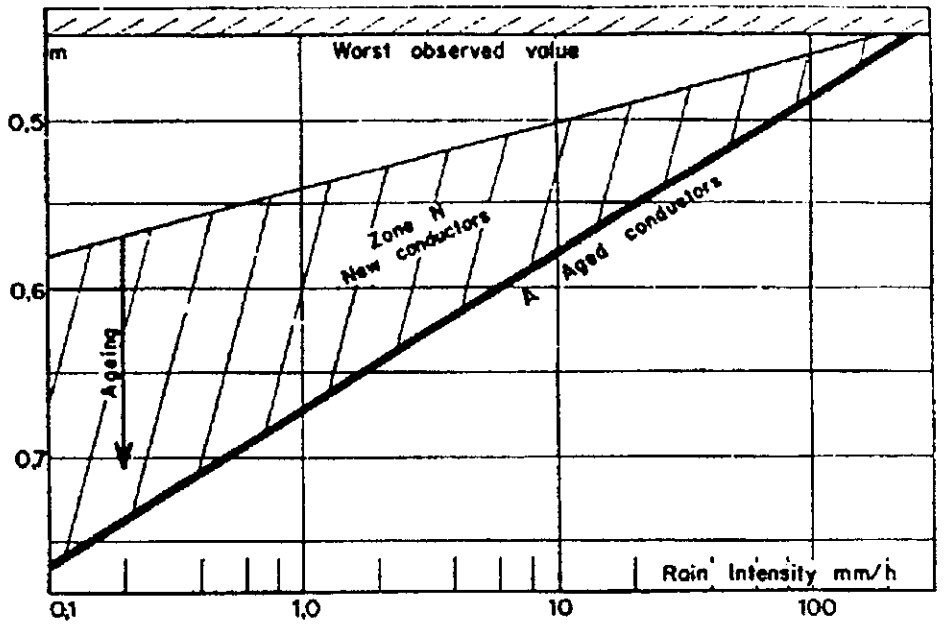

Figure A5.3

Correlation curves between conductor surface irregularity factor (m) and rain intensity

A5.3 EPRI Method: The empirical method for evaluating the corona loss developed at Project UHV [3.10] is based on the extensive corona loss measurements in test cages and on a single phase test line, and on the theoretical principles developed by EDF. A set of "Effective" corona loss curves for six-conductor bundles under heavy rain are obtained as shown in Figure A5.4.

The corona loss under heavy rain (W/m) for any other conductor bundles are then obtained as:

$$\boxed{P = K_g \cdot K_{CL} \cdot P_e} \qquad \text{(A5.8)}$$

where $K_g = \dfrac{\ln\left(\dfrac{R_z}{r_e}\right)}{\ln\left(\dfrac{R_z}{\rho'}\right)}$

R_z, r_e have the same significance as in EDF Method.

$\rho' = \sqrt{270 \cdot n \cdot r + R^2}$

K_{CL} = an empirical correction factor, given as a function of the number of subconductors as in Figure A5.5.

P_e = the effective loss (W/m) obtained from Figure A5.4.

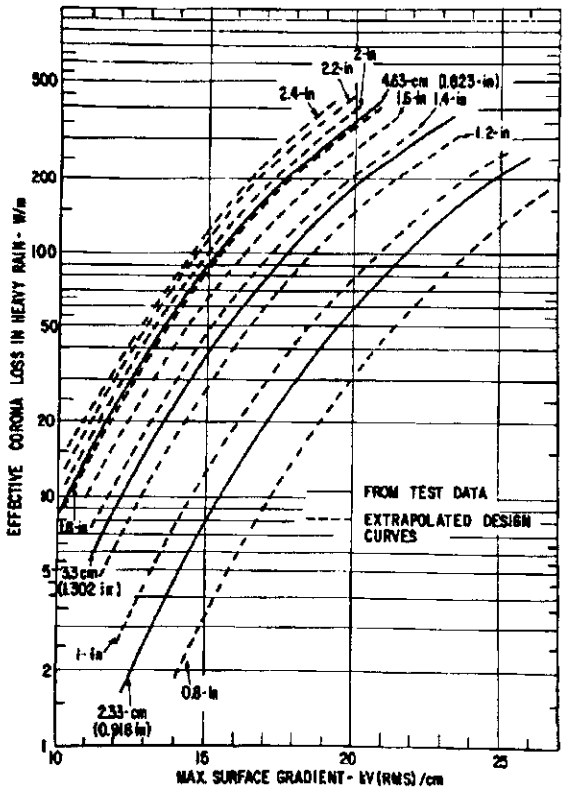

Figure A5.4

Effective corona loss (P_e) in heavy rain for six-conductor bundles with subconductors of different diameters

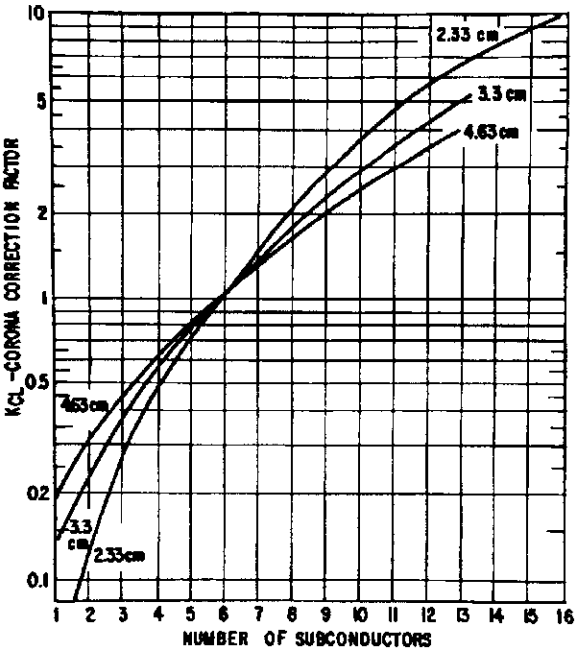

Figure A5.5

Corona loss correction factor (K_{CL}) to apply to the loss curves of figure A5.4 to obtain the loss for different numbers of subconductors

A5.4 IREQ Method: A semi-empirical method of calculation was developed by IREQ [3.18] for the calculation of corona loss of a given bundle configuration. It is based on extensive corona loss measurements under heavy rain in outdoor test cages. The method proposed takes into account the variation of generated loss as a function of electric field variation around the surface of the subconductors. A family of generated loss curves based on experimental data are obtained for single conductors under heavy rain conditions and are shown in Figure A5.6. The generated loss is shown in this figure as a function of conductor diameter, with the conductor surface electric field as a parameter.

The family of curves can be approximated by the empirical formula:

$$P_S = e^{-17.41} \cdot (g(\phi))^{5.8} \cdot d^{2.46}$$

where P_S = generated loss of a single conductor under heavy rain, (W/m)

$g(\phi)$ = effective value of the conductor surface electric field, (kV/cm (rms))

d = subconductor diameter, (cm)

This formula shows only the general trend of variation when different constructional variants are compared. Calculation of absolute values should be based on the curves of Figure A5.6.

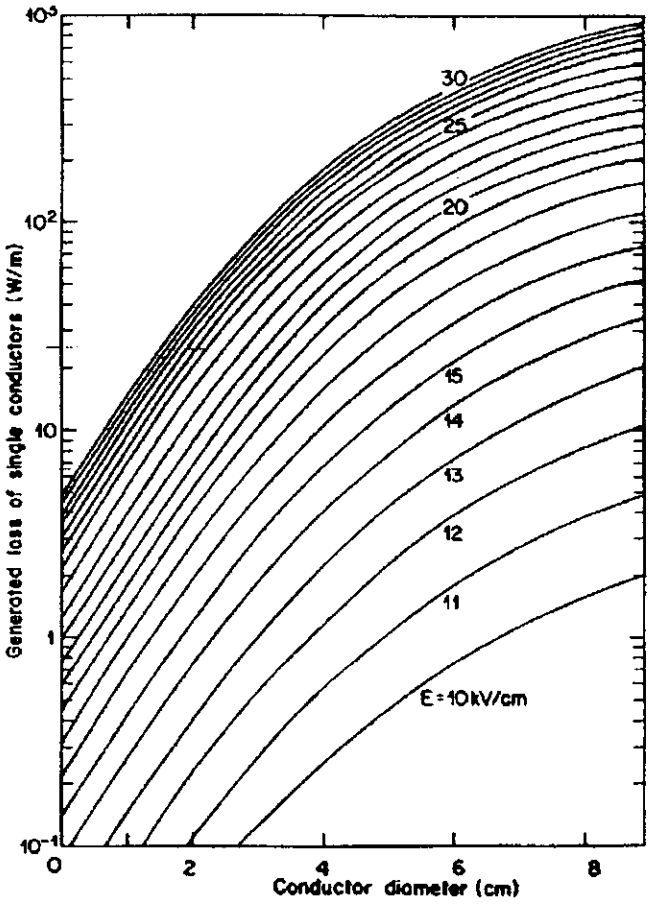

Figure A5.6

Generated loss of single conductors (P_S) based on experimental data

The generated loss of a conductor bundle is then obtained as:

$$P_b = \frac{C_b}{C_s}\left(\sum_1^n \frac{1}{2\pi}\int_0^{2\pi} P_s(g(\phi), d)d\phi\right) \qquad \text{(A5.9)}$$

where P_b = generated loss of the bundle, composed of subconductors having a diameter d, (W/m)

C_b, C_S = capacitances per length of the bundle and single conductors (F/m)

$P_S(g,d)$ = a function representing the variation of generated loss for the sub-conductor considered as a function of the surface electric field, which in turn is a function of the angle ϕ around the conductor, (W/m)

In equation (A5.9), the generated loss of the bundle is obtained by integrating on the surfaces of all the subconductors.

A5.5 BPA Method: This simple formula was derived in a manner similar to that used for the radio interference and audible noise formulae, taking into account the influence of altitude.

(personal contribution of V. L. Chartier)

$$P_{dB} = 14.2 + 65 \cdot \log\left(\frac{g}{18.8}\right) + 40 \cdot \log\left(\frac{d}{3.51}\right) + K_1 \cdot \log\left(\frac{n}{4}\right) + K_2 + \frac{q}{300} \qquad \text{(A5.10)}$$

where P_{dB} = corona loss per conductor bundle (dB above 1 W/m)

g = effective value of the maximum conductor surface gradient calculated for average height of the span (kV/cm (rms))

d = subconductor diameter (cm)

K_1 = 13 for $n \leq 4$

19 for $n > 4$

n = number of subconductors

K_2 is a term to adjust corona loss for rain intensity (I).

$$K_2 = 10 \log\left(\frac{I}{1.676}\right) \qquad \text{for } I \leq 3.6 \text{ mm/hr}$$

$$3.3 + 3.5 \log\left(\frac{I}{3.6}\right) \qquad \text{for } I > 3.6 \text{ mm/hr}$$

To calculate the loss P in W/m, the antilog of P_{dB} must be performed :

$$P = 10^{P_{dB}/10}$$

The total loss for a line (in W/m) is the summation of the loss from all the conductor bundles.

The mean loss is calculated assuming a mean rain intensity of 1.676 mm/hr, but this can vary from region to region. The mean fair-weather loss is calculated by subtracting 17 dB from the mean loss during rain. This difference of 17 dB was obtained from carefully controlled measurements during fair weather at the Apple Grove 750-kV Project.

A5.6 ENEL Method: The following formula was derived from measurements on line models and verified on the basis of measurements made in the Suvereto 1000 kV testing plant on a 1 km experimental line [3.17].

$$P = K_0 \cdot P_0 \qquad \text{(A5.11)}$$

where P = corona loss per conductor bundle at actual height above ground (W/m)

P_0 = corona loss for a conductor at infinite height above ground (W/m)

$$\log P_0 = 1.52 - \frac{30}{g} + 1.37 \cdot \log n + 2.3 \cdot \log d \quad \text{(heavy rain)}$$

$$\log P_0 = 1.04 - \frac{41}{g} + 1.13 \cdot \log n + 3.8 \cdot \log d \quad \text{(light rain)}$$

K_0 = correction coefficient (around 1.3 to 1.5 for transmission lines up to 500 kV and approximated 1 for higher voltage levels)

A5.7 Other References

Using somewhat similar theoretical considerations to the Ontario Hydro Method and their own extensive experimental results, Emiljanov and Burgsdorf [5.8, 5.9] developed an empirical method for determining the corona loss under different weather conditions: fair weather, rain, snow and frost.

Popkov and Levitov [5.10, 5.11, 5.12] have also developed a method of calculation, based on theoretical and experimental studies, somewhat similar to the EDF method.

Compilation of the Different Formulae for the Evaluation of Corona Loss.

Using the example of paragraph 2.5, the corona loss P (W/m) under heavy rain can be calculated, with the different formulae for the central phase.

The effective values of the maximum conductor surface gradient g, average surface gradient g_a, and critical corona onset gradient (visual) g_c are necessary.

The CIGRE Guide method gives (see paragraph 2.5) :

$g = 18.2$ kV/cm (rms)

$g_a = 15.4$ kV/cm (rms)

$g_c = 27.4$ kV/cm (rms)

If applicable a rain intensity of 18 mm/hour or a surface factor of 0.55 :

Method	P (W/m) for the central phase
Ontario Hydro (A5.1)	28
EDF (A5.7)	49
EPRI (A5.8)	182
IREQ (A5.9)	53.5
BPA (A5.10)	156.5
ENEL (A5.11)	161

Remark : These results for a single phase arrangement are presented mainly to illustrate the calculation procedures. Due to different approaches and definitions, the formulae cannot be compared directly.

Glossary chapter 5

C_b	capacitance per length of the bundle	F/m
C_c	total capacitance per length of the conductor within the line configuration	F/m
C_s	capacitance per length of single conductor	F/m
d	subconductor diameter	cm
f	frequency of applied voltage	Hz
F_a	correction factor to take into account high altitudes (< 3000 m) for loss in W/m (must be multiplied by loss)	
g	effective value of the maximum conductor surface gradient	kV/cm (rms)
g_a	effective value of the average conductor surface gradient	kV/cm (rms)
G_a	effective value of the average conductor surface gradient ($\phi = 0$)	kV/cm (rms)
G_c	effective value of the critical corona onset gradient (visual) for $\delta = 1$ and for given weather and conductor surface conditions	kV/cm (rms)
g_c	effective value of the critical corona onset gradient (visual)	kV/cm
G_e	effective value of the conductor surface gradient	kV/cm (rms)
G_ϕ	effective value of the conductor surface gradient at angle ϕ	kV/cm (rms)
$g(\phi)$	effective value of the conductor surface electric field	kV/cm (rms)
h	height above ground	m
I	rain intensity	mm/h
k	conditional constant for given weather and conductor surface conditions	
K	reduction coefficient	
K_0	correction coefficient	
K_1	constant factor depending of n	
K_2	term to adjust corona loss for rain intensity	dB (1 W/m)
K_A	correction factor to take into account high altitudes (< 3000 m) for loss in dB (must be additionned to loss)	dB
K_{CL}	empirical corona-loss correction factor	
K_g	geometry factor	
ln	$\ln \equiv \log_e$, e = 2.718	

log	$\log \equiv \log_{10}$	
m	conductor surface irregularity factor	
n	number of subconductors in the bundle	
P	corona loss per conductor bundle	W/m
P_0	corona loss for a conductor at infinite height above ground	W/m
P_b	generated loss of the bundle, composed of sub-conductors having a diameter d	W/m
P_{dB}	corona loss per conductor bundle	dB (1 W/m)
P_e	effective loss	W/m
P_n	reduced corona loss	W/m
P_s	generated loss of single conductor under heavy rain	W/m
$P_s(g,d)$	function representing the variation of generated loss for the subconductor considered as a function of the surface electric field, which in turn is a function of the angle ϕ around the conductor	W/m
q	altitude above sea level	m
r	radius of subconductor	cm
R	radius of bundle	cm
r_e	equivalent radius of bundle	cm
R_z	radius of the equivalent zero potential cylinder	cm
s	subconductor spacing	cm
S	interphase spacing	m
V	voltage between phase and ground	V or kV
U	voltage between phases	V or kV
δ	relative air density (RAD)	
β	Peek coefficient	
ρ	factor depending of n and r	cm
ρ'	factor depending of n and r	cm
$\Delta\phi$	angular portion of conductor surface in corona	rad

References

[2.3] V.L. Chartier, L.Y. Lee, L.D. Dickson, K.E. Martin, "Effect of High Altitude on High Voltage AC Transmission Line Corona Phenomena", IEEE Transactions, Vol. PWRD-2, No. 1, Jan. 1987, pp. 225-237.

[5.1] R.M. Morris and O. Petersons, "Measurement of Corona loss at Alternating Voltages", Bull of the Radio and Electrical Engineering Division, National Research Council of Canada, Vol. 12, No. 2, April-June, 1962.

[5.2] P.S. Maruvada and F. Denommé, "A Technique for Calibration of A.C. Corona Loss Analyzers", Proceedings of the IEEE Canadian Communication and Power Conference, Montreal, 1974, pp. 195-196.

[5.3] H. Kirkham, G.F. Nourse, H.R. Hajny, "AEP-ASEA Research Project - Instrumentation and Data Systems", IEEE Winter Power Meeting, January 29—February 3, 1978, New York, Paper A-78 164-6.

[5.4] N.L. Kisters, O. Pertersons, "A Transformer Ratio-Arm Bridge High-Voltage Capacitance Measurements", IEEE Transactions on Communications and Electronics, November, 1963.

[5.5] O. Petersons, "A Transformer Ratio Arm Bridge for Measuring Large Capacitors Above 100 Volts", IEEE Transactions, Vol. PAS-87, No. 5, May 1968, pp. 1354-1361.

[5.6] W.J.M. Moore, F.A. Raftis, "Measurement of Shunt Reactor Loss at High Voltage with an Alternating Current Comparator Bridge", IEEE Transactions, Vol. PAS-92, No. 2, March-April 1973, pp. 662-667.

[5.7] O. Nigol, J.G. Cassan, "Corona loss research at Ontario Hydro Coldwater Project", AIEE Transactions Power Apparatus and Systems, Vol. 80, Pt. III, August, 1961, pp. 304-313.

[4.4] J.J. Cladé, C.H. Gary, "Predetermination of Corona Loss Under Rain, Influence of Rain Intensity and Utilization of an Universal Chart", IEEE Transactions, Vol. PAS-89, No. 6, July/Aug 1970, pp. 1179-1185.

[3.10] "Transmission Line Reference Book 345 kV and above", EPRI, Palo Alto Ca., 1979.

dto. second edition, 1982.

dto. second edition revised, 1987.

[3.18] N. Giao Trinh, P. Sarma Maruvada, "A Method of Predicting the Corona Performance of Conductor Bundles Based on Cage Test Results", IEEE Transactions, PAS-96, No. 1, Jan/Feb. 1977, pp. 312-325.

[5.8] N.P. Emelianov, "Poteri moshchnosti pri corone na liniakh electroperedachi iz razshcheplennoi fazoi 330 V i vishche", Electricheskie stantsii, Moscow, 1967, pp. 59-65.

[5.9] V.V. Burgsdorf, N.P. Emelianov, D.V. Gimashova, "Vibor provodov i konstruktsii faz linii 750 kV", Energia, Moscow, 1974.

[5.10] V.J. Levitov, V.J. Popkov, "Metodika proschetnoi otsenki urovnia poteri moshchnosti i energii na coronu na provodakh D.E.P sverkhvisokoho napriazhenia", AN SSSR Energetika i Transport, Moscow, 1968.

[5.11] V.J. Levitov, V.J. Popkov, "Poteri na coronu na provodakh opitno-promishlennoi D.E.P. 750 kV Kontsovo Moskva", A.N. SSSR Energretika i Transport, Moscow, 1971.

[5.12] V.J. Levitov, V.J. Popkov, "Poteri moschnosti i energii na coronu na provodakh linii sverkhvisokoho napriazhenia", In the publication: Dalnie elektroperedachi 750kV, Energia, Moscow, 1974.

[3.17] B.A. Cauzillo, R. Cortina, P. Nicolini, J.C. De Medeiros, M.E. Bryant, "Design criteria of UHV overhead lines based on experience acquired in the 1000 kV Project", CIGRE 22-14, 1984.

Chapter 6

Oxidant Production of AC Transmission Lines

6.1 Introduction

By far, the majority of the excitation processes of AC corona at the surface of the overhead transmission conductor will result in the neutral recombination of the surrounding air molecules (principally oxygen (O_2) and nitrogen (N_2)). There is, however, a small probability that a free radical of oxygen, formed in the corona process, will recombine to form O_3. There is an even smaller probability that one of the disassociated nitrogen molecules will recombine with the surrounding oxygen to form an oxide of nitrogen (NO_X).

The energy necessary for the production of these oxidants by an overhead transmission line is incorporated within the overall representation of corona loss for that line. This fact enables one to develop an empirical relationship between the level of corona loss and the rate of ozone or nitric-oxides generation.

In addition to quantifying the production of the ozone (or the nitric-oxides), a more complete description of the air quality in the vicinity of the transmission line would include a model for the dispersion of these quantities into the environment. This dispersion is a function of such meteorological features of the surrounding air as atmospheric pressure, air temperature, wind speed, wind direction, and humidity.

Confirming the analytical methods developed to describe the production and dispersion of ozone (or nitric oxide) into the environment from overhead transmission is complicated by two factors:

(1) the production rates for these quantities are very low and the natural level of ozone (or the aggregation of other man-made sources of ozone and nitric oxides) is often much greater;

(2) instrumentation available to measure ozone and nitric oxides is often not sensitive enough to provide quality information on the levels of transmission line produced quantities.

Naturally occurring ozone can range, depending on locale, from 10 to over 100 parts per billion (ppb). Yet, transmission line ozone rates of 1-5 ppb are typical. This is illustrative of the measurement difficulties which need to be faced in confirming the analytical relationships of generation and dispersion of transmission line oxidants.

Because of the respiratory problems which can develop from breathing air with high quantities of either ozone or nitric oxides, national (or regional) regulatory bodies have set guidelines concerning maximum permissible O_3 or NO_X emissions. Although these regulations differ in their approach or target levels, it is reasonable to generalize in stating that transmission line production levels do not significantly contribute to impacting these regulatory objectives. In fact, as alluded to above, transmission line production of oxidants (O_3 and NO_X) are, for all practical purposes, not measurable in both rural and urban environments.

6.2 Calculation Models

Transmission line ozone and nitric-oxide production rates have been related by experimental study to the molecular weight of the species, local air temperature, pressure and humidity, as well as the conductor surface gradient and the total corona loss for the conductor arrangement [6.1]. These rates are expressed in terms of grams of O_3 (or NO_X) per kWh of corona loss within ranges of appropriate test conditions (i.e. humidity and surface gradient). Typical rates for O_3 production for test lines are 0.5 to 9.0 grammes per kWh of corona loss. Rates for NO_X production have been found to be one-fourth to one-sixth that of the corresponding O_3 rates.

The concentration of ozone (or nitrogen oxides) in the near vicinity of the overhead line is principally a function of the local wind conditions. Dispersion models have been developed [6.2] similar to dispersion of smoke, but their practical appliance is limited due to the complex assumptions necessary for calculation. Resulting in „orders of magnitude" at best, the difficulties to detect oxidants from corona discharges near HV transmission lines could be explained however.

6.3 Concluding Remarks

As to the minor importance of oxidant production over the past 10 years, an extensive summary of the literature is not justified. As with the other corona phenomena, there are methods that can be used to predict oxidant production. The following extensive list of references may help in case of more detailed investigations.

References

[6.1] J.F. Roach, V.L. Chartier and F.M. Dietrich, "Experimental Oxidant Production Rates for EHV Transmission Lines and Theoretical Estimates of Ozone Concentrations Near Operating Lines", IEEE Trans., Vol. PAS-93, March 1974, pp. 647-657.

[6.2] J.F. Roach, F.M. Dietrich, V.L. Chartier, H.T. Nowak, "Ozone Concentration Measurements on the C-Line at Apple Grove 750 kV Project and Theoretical Estimates of Ozone Concentration near 756 kV lines of Normal Design", IEEE Trans., Vol. PAS-97, July 1978, pp. 1392-1401.

[6.3] W. A. Abel, W. J. Fern, "Comparison of ozone instrumentation", IEEE Paper A 78 166-1, PES-Winter Meeting, N.Y., 1978.

[6.4] J. G. Anderson, L. E. Zaffanella, "Project UHV test line research on the corona performance of a bundle conductor at 1000 kV", IEEE Trans., Vol. PAS-91, Jan./Feb. 1972, pp. 223-232.

[6.5] U. Arndt, G. Lindner, "Zur Problematik phytotoxischer Ozonkonzentrationen im suedwestdeutschen Raum", Staub-Reinh. Luft, 41 (1981), Nr. 9, pp. 349-352.

[6.6] F. D. J. Boylett, J. S. T. Looms, "Effect of discharge products upon corona discharge and spark breakdown voltage", Proceedings IEE, Vol. 110, No. 12, 1963.

[6.7] J. G. Droppo, "Field determination of HVDC ozone production rates", IEEE Trans., Vol. PAS-100, no. 2, February 1981.

[6.8] J. P. Sponseller, "The emission of ozone from a 765-kV transmission line", M. Sc. Thesis, The Ohio State University, 1974.

[6.9] H. N. Scherer Jr., B. J. Ware, C. H. Shih, "Gaseous effluents due to EHV transmission line corona", IEEE Trans. Power Apparatus and Systems, Vol. PAS-92, May/June 1973, pp. 1043-1049.

[6.10] M. Frydman, A. Levy, S. E. Miller, " Oxidant measurements in the vicinity of energized 765 kV lines", IEEE Trans. Power Apparatus and Systems, Vol. PAS-92, May/June 1973, pp. 1141-1148.

[6.11] M. Frydman, C. H. Shih, "Effects of the environment on the oxidants production in AC corona", IEEE Trans. Power Apparatus and Systems, Vol. PAS-93, January/February 1974, pp. 436-443.

[6.12] S. A. Sebo, J. T. Heibel, M. Frydman, C. H. Shih, "Examination of ozone emanating from EHV transmission line corona discharges", IEEE Trans. Power Apparatus Systems, Vol. PAS-95, March/April 1976, pp. 693-703.

[6.13] W. J. Fern, R. L. Brabets, "Field investigations of ozone adjacent to high voltage transmission lines", IEEE Trans. Power Apparatus and Systems, Vol. PAS-93, No. 5, September/October 1974, pp. 1269-1280.

[6.14] P. E. Coffey, W. N. Stasiuk, "Evidence of atmospheric transport of ozone into urban areas", ESA-85, New York State Dept. of Environmental Conservation, Albany, NY, April 22, 1974.

[6.15] W. N. Stasiuk, P. E. Coffey, "Rural and urban ozone relationship in New York State", BTS-5, New York State Dept. of Environmental Conservation, February 1974.

[6.16] D. B. Turner, "Workbook of atmospheric dispersion estimates", Environmental Protection Agency, Research Triangle Park, N. C. 1970.

[6.17] D. F. Shankle, S. B. Griscom, E. R. Taylor Jr., R. H. Schlomann, " The Apple Grove 750 kV project equipment design and instrumentation, " IEEE Trans. Power Apparatus and System, Vol. PAS-84, July 1965, pp. 541-550.

[6.18] "Transmission Line Reference Book HVDC to ± 600 kV", Project RP 104, Electric Power Research Institute, Palo Alto, CA 94304, 1977.

[6.19] J. S. Sandberg, M. J. Basso, B. A. Okin, "Winter rain and summer ozone : a prediction relationship", Science, Vol. 200, June 1978.

[6.20] P. E. Coffey, W. M. Stasiuk Jr., "Evidence of atmospheric transport of ozone into urban areas", Environmental Science Technology, Vol. 9, 1975, pp. 59-62.

[6.21] V. H. Regener, L. Aldaz, "Turbulent transport near the ground as determined from measurements of the ozone flux and the ozone gradients", Journal of Geophysical Research, Vol. 74, 1969, pp. 6935-6942.

[6.22] L. Aldaz, "Flux measurements of atmospheric ozone near land and water", Journal of Geophysical Research, Vol. 74, 1969, pp. 6939-6946.

[6.23] I. Galbally, "Ozone profiles and ozone fluxes in the atmospheric surface layer", Quarterly Journal of the Royal Meteorological Society, Vol. 97, 1971, pp. 18-29.

[6.24] I. Galbally, "Ozone variation and destruction in the atmospheric surface layer", Nature, Vol. 218, 1968, pp. 456-457.

[6.25] O. F. T. Roberts, "The theoretical scattering of smoke in a turbulent atmosphere", Proc. Roy. Soc. A, Vol. 104, 1923, pp. 640-654.

[6.26] "Recommended guide for the prediction of the dispersion of airborne effluents, ASME Committee on Air Pollution Controls, Edited by M. Smith, May 1968.

[6.27] "Investigation of ozone precursor concentrations at nonurban locations in the Eastern United States", U. S. Environmental Protection Agency, EPA-450/3-74-034, Research Triangle Park N. C., May 1974.

Chapter 7

DC Lines

7.1 Introduction

Corona generated in the vicinity of conductors plays an important role in the design of high voltage DC transmission lines, a role that is probably even more important than that in the case of AC lines. Although the main reason for the occurrence of corona, namely the existence of high electric fields near conductor surfaces, is common to both AC and DC lines, sufficient differences exist in the corona mechanisms as well as in the corona effects between the two to make it necessary to study DC line corona effects independently and not extrapolate from experience on AC lines.

The mechanism of corona is significantly different at positive or negative direct voltages from that at the half cycles of alternating voltages having the same polarity. Although the same basic modes of corona discharge may be identified under the positive and negative polarities of both alternating and direct voltages, the mixing of space charges of opposite polarity gives the AC corona modes different physical characteristics to DC corona modes of the same polarity.

The space charges created by corona on conductors at alternating voltages oscillate and are confined to the immediate vicinity of the conductors, resulting in the mixture of positive and negative ions and in recombination of the ions. Under direct voltages, however, a conductor in corona acts as a source of ions having the same polarity as the voltage applied to the conductor itself. The space charge created by corona will therefore be not confined to the immediate vicinity of the conductors but rather fill the entire interelectrode space. The presence of such a unipolar space charge in the interelectrode region has a stabilizing effect on the corona discharge processes occurring at the conductor itself.

In the case of AC lines, the electric field and the resulting field effects produced under the line are practically unaffected by the presence or absence of corona on the conductors. For DC lines, on the other hand, corona on the conductors and the resulting space charge have a deciding effect on the electric field and particularly on the field effects produced under the line. For this reason, corona on the conductors has a much wider impact on the design of DC transmission lines since it is not limited to the usual corona effects such as power loss, RI and AN but extends also to the field and ion effects. There is in fact already a tendency to design DC lines in order to limit the electric field and ion current levels under the line to values well below those necessary for human perception. Such a design criterion requires the choice of conductor surface electric fields which may be significantly lower than those used on AC lines and which in turn result in lower levels of corona loss, radio interference and audible noise.

7.2 Corona Loss

Corona loss occurs on a DC transmission line due to the migration of the corona-generated ions from the conductor either to the ground or to the conductor of opposite polarity. In the case of a monopolar DC line, of either positive or negative polarity, the ions created near the conductor migrate toward the ground plane and thus fill the entire space between them. If the line is provided with a ground wire for lightning protection, a small fraction of the ions will also migrate from the conductor toward the ground wire.

In the case of a bipolar DC line, the ions will be of the same polarity as the conductor where they are generated. The ions from each conductor will then migrate partly towards the conductor of opposite polarity and partly to the ground plane. Two types of space charge regions may be identified in this case. The first is a monopolar space charge region existing between each conductor and the ground plane and the second is a bipolar charge region existing between the two conductors of opposite polarity. Thus a bipolar DC line will have two monopolar and one bipolar space charge regions. A small fraction of both positive and negative ions may also flow towards any ground wires present on the line.

Monopolar space charge has the effect of reducing the electric field near the conductor surface and increasing it at the ground plane. It has therefore a regulating effect on the corona processes occurring at the conductor surface. This is reflected in the relatively slower increase in corona loss with voltage compared to an AC line. The bipolar region is characterized by the mixing of both

positive and negative ions which results in a reduced net space charge as well as in the neutralization of some ions due to recombination. Both these processes lead to a reduced net space charge in the region and consequently to a reduced regulating effect on the corona processes occurring at the conductors. Bipolar corona loss therefore increases more rapidly than monopolar loss.

As in the case of AC lines, ambient weather conditions have an important influence on the generation of corona on the conductors and on the corona loss. In general, foul weather conditions such as rain, snow, fog etc., cause increased corona loss from DC lines. However, the difference between fair and foul weather loss is not as large as in the case of AC lines. Foul weather loss may be as much as two orders of magnitude higher than fair weather loss for AC lines while they may be higher by a maximum of one order of magnitude for DC lines. As a consequence of this, fair weather corona loss assumes a greater importance in the economic evaluation corona loss for DC lines.

Theoretical methods have been proposed in the literature [4.19, 6.18 and 7.1 to 7.4] for the calculation of corona loss from both monopolar and bipolar DC transmission lines. These methods involve the solution of nonlinear differential equations which define the monopolar or bipolar ionized fields associated with the monopolar or bipolar space charge regions described above. The nonlinearity arises from the mutual interaction between the electric field and space charge. The solution of these nonlinear equations becomes very difficult even for simple line configurations and requires a number of assumptions to be made.

For example, it is assumed in most of the methods that the space charge is composed of only small air ions having a constant mobility and in some methods the influence of wind is neglected. From a practical point of view, it is well known that both small air ions and charged aerosols - having order of magnitude lower mobilities - may be present, that small air ions are more appropriately characterized by a spectrum of mobilities and finally that wind has an important influence on the ionized field. These limitations reduce the applicability of the theoretical methods for calculating corona loss from DC transmission lines.

Empirical equations may be derived for corona loss if a large amount of experimental data is available from measurements on full-scale transmission lines under different weather conditions. Very few measurements are available [7.5], however, on operating DC transmission lines. Most of the available data is obtained from measurements on short full-scale test lines [7.6 to 7.9]. Empirical formulae have been developed for corona loss of DC transmission lines, some of which are summarized below:

ANNEBERG Formula [7.4, 6.18]

Based on experimental data obtained on a test line at Anneberg, Sweden, Knudsen and Iliceto proposed the formula for a monopolar line:

$$P_c = V \cdot I_c \cdot 10^{-3}$$
$$I_c = k_c \cdot n \cdot r \cdot 2^{0.25(g-g_o)} \qquad (7.1)$$

where,

P_c corona loss per circuit (kW/km)

V is the voltage of conductor (kV)

I_c is the corona current (mA/*km*)

k_C is a conductor surface coefficient

$k_c = 0.15$ for smooth conductor surface

$k_c = 0.35$ for imperfect conductor surface

$k_C = 2.5$ for all weather losses

$g_O = 22 \cdot \delta$ kV/cm where, δ is the relative air density

For a bipolar line:

$$\boxed{\begin{aligned} P_c &= 2 \cdot V \cdot I_c \cdot 10^{-3} \\ I_c &= (k + 1) \cdot k_c \cdot n \cdot r \cdot 2^{0.25(g-g_0)} \end{aligned}} \qquad (7.2)$$

where : $k = \frac{2}{\pi} \cdot \arctan\left(\frac{2H}{S}\right)$

H is the mean height of conductors (m)

S is the spacing of the poles (m)

IREQ Formula [7.1]

The corona characteristics of conductor bundles have been studied at IREQ at voltage up to 1200 kV. Based on the results of this study, an empirical formula is developed for corona loss.

$$\boxed{P_{dB} = P_0 + C_{p1} \cdot (g - 25) + 20 \cdot \log\left(\frac{d}{4.064}\right) + C_{p3} \cdot \log\left(\frac{n}{6}\right)} \qquad (7.3)$$

where, P_{dB} is the corona loss, (dB above 1 W/m)

g is the maximum bundle gradient, (kV/cm)

d is the subconductor diameter, (cm)

n is the number of subconductors

The values of P_o, C_{p1} and C_{p3} are found to vary with the seasons as well as with the weather conditions, and are summarized in Table 7.1.

Season of the year	Weather conditions	P_0 (dB)	C_{p1}	C_{p3}
Summer	Fair	13.7	0.80	28.1
	Foul	19.3	0.63	9.7
Fall/Spring	Fair	12.3	0.88	36.9
	Foul	17.9	0.72	12.8
Winter	Fair	9.6	1.00	44.3
	Foul	14.9	0.85	10.2
Overall	Fair	11.9	0.89	36.4
	Foul	16.9	0.73	8.0

Table 7.1

$$P_{dB} = 10 \log\left(\frac{P_{W/m}}{10}\right) \qquad P_{W/m} = 10^{\frac{P_{dB}}{10}}$$

7.3 Electromagnetic Interference (EMI)

Positive pulsative corona is the dominant source of EMI on DC lines because the current pulses induced by corona discharges on the positive conductor have much higher amplitudes than those on the negative polarity conductor. From the point of view of EMI, it may therefore be preferable to choose negative polarity for monopolar DC lines. In the case of bipolar DC lines, attention need be focused mainly on the positive pole as the source of EMI. Experimental studies have shown that DC lines produce very little EMI above 30 MHz. From the practical point of view of line design, one need take into account only radio interference (RI) and not television interference (TVI).

A significant difference exists between the RI performance of AC and DC lines, namely that contrary to the case of AC lines, the RI level of a bipolar DC line decreases in rain or wet snow. A satisfactory physical explanation for this observed difference does not exist, but it is believed that rain causes a decrease in the amplitudes of the corona current pulses while at the same time causing a greater increase in the pulse repetition rate. As a consequence of this, corona loss increases under rain while RI decreases.

There are no analytical approaches for calculating RI from DC lines, mainly because of the difficulty in defining the RI excitation function. The presence of space charge in the entire interelectrode space makes the electric field distribution in the vicinity of a conductor surface dependent on the actual line geometry, and thus makes it difficult to define an excitation function. If the RI excitation function is know, however, an RI propagation analysis can be carried out similar to that for an AC line. In fact the propagation analysis will be simpler for a DC line since there are only two conductors and only the positive one is the main source of RI generation.

As in the case of AC lines, the RI performance of a DC line is characterized by frequency spectrum, lateral profile and cumulative probability distribution. The RI frequency spectra of DC lines are very similar to those from AC lines. The lateral profiles are somewhat different, mainly because only the positive pole generates RI. The fact that the RI level of a DC line is decreased during foul weather conditions such as rain is reflected in the cumulative distribution curves.

Based mainly on measurements made on short test lines, several empirical formulae have been proposed for calculating the fair weather RI levels of DC lines, some of which are summarized below:

BPA [7.2] (this formula has been changed to reflect new and better data collected from ± 500 kV line)

$$RI = 51.7 + 86 \cdot \log\left(\frac{g}{25.6}\right) + 40 \cdot \log\left(\frac{d}{4.62}\right) + 10 \cdot \left[1 - (\log(10\ f))^2\right] + 40 \cdot \log\left(\frac{19.9}{D}\right) + \frac{q}{300} \qquad (7.4)$$

(CISPR QP - detector)

ANNEBERG [7.4]

$$RI = 25 + 10 \cdot \log n + 20 \cdot \log r + 1.5 \cdot (g - g_o) - 40 \cdot \log\frac{D}{30} \qquad (7.5)$$

$g_o = 22 \cdot \delta$ kV/cm where, δ is the relative air density

IREQ [7.1]

The empirical formula developed at IREQ is given in term of the excitation function as:

$$\Gamma = \Gamma_0 + K_1 \cdot (g - 25) + 40 \cdot \log\left(\frac{d}{4.064}\right) + K_3 \cdot \log\left(\frac{n}{6}\right) \qquad (7.6)$$

The excitation function is expressed in terms of dB above 1 $\mu A/\sqrt{m}$. The empirical constants Γ_0, K_1 and K_3 are given for different seasons and for different weather conditions in Table 7.2.

Season of the year	Weather Conditions	Γ_0	K_1	K_3	Maximum Error (dB)①
Summer	Fair	27.01	1.83	45.8	7.0
	Foul	20.35	1.39	48.0	-3.2
Fall/Spring	Fair	23.44	1.68	29.9	3.9
	Foul	19.84	1.68	63.5	4.9
Winter	Fair	18.74	1.63	19.65	4.9
	Foul	19.52	1.47	10.0	-6.4
Overall Fair Weather		22.94	1.71	30.8	-12.0
Overall Foul Weather		19.77	1.50	33.9	-10.4

Table 7.2

Parameters defining the IREQ empirical formula for RI excitation function
① maximum error obtained in comparison a series of data and the results obtained by the empirical formula

7.4 Audible Noise (AN)

The particularities of AN generation from DC transmission lines resemble to some extent those of RI: the positive pole is the main contributor to AN and the AN level of a DC line decreases in foul weather conditions such as rain. Another significant difference between the AN from AC and DC lines is the absence of power frequency harmonics from the AN frequency spectrum of DC lines.

Based again on measurements made on test lines, several empirical formulae have been derived for computing the AN level of DC lines. The general form of these equations is similar to that of AC lines, with the exception that the noise is considered to be generated by the positive pole of the line only. Thus, for the case of a single bipolar line there exists only noise from one set of conductors and no summation of contributions is required. If there are more bipolar lines on the same structure or in the same right-of-way, the noise from each of the positive poles should be calculated and summed according to the equation.

$$L_{AT} = 10 \cdot \log \sum_{i=1}^{n_c} 10^{L_{Ai}/10} \qquad (7.7)$$

where L_{AT} is the total A-weighted sound pressure level, n_c is the total number of conductors generating audible noise, and L_{Ai} is the noise level of the individual conductors.

In the following equations, D is the radial distance from the positive pole to the point at which the noise is to be calculated.

BPA [4.19]

Application: All line geometries

Fair weather: L_{50}

Range of validity: $4 \leq n \leq 8,\ d \leq 5$ cm

For each positive pole:

$$L_A = 86 \cdot \log g + k_n \cdot \log n + 40 \cdot \log d - 114 \cdot \log D + K_n + \frac{q}{300} \qquad (7.8)$$

where g is the average maximum bundle gradient

	k_n	K_n
$n < 3$	0	- 93.4
$n \geq 3$	25.6	- 100.6

FGH [4.19]

Application: all line geometries

Fair weather, maximum:

Range of validity: $2 \leq n \leq 4 \quad 2 \leq d \leq 4$ cm

For each positive pole:

$$L_A = 14 \cdot g + 10 \cdot \log n + 40 \cdot \log d - 10 \cdot \log D - 1 \qquad (7.9)$$

where g is the average maximum bundle gradient at the lowest point of the span.

IREQ [4.19]

Application: all line geometries

Fair weather, average:

Range of validity: $4 \leq n \leq 8,\ d \leq 5$ cm

For each positive pole:

$$L_A = k_g \cdot (g - 25) + 10 \cdot \log n + 40 \cdot \log d + K_w - 114 \cdot \log D \qquad (7.10)$$

where g is the maximum bundle gradient and k_g and K_W depend on the general fair weather climate, given on a seasonal basis in the following table:

	k_g	K_w
Summer	1.54	- 26.5
Fall/Spring	0.84	- 26.5
Winter	0.51	24.0

CRIEPI [4.19]

Application: bipolar lines geometries

Fair weather, average:

Range of validity: $1 \leq n \leq 4$, $2.24 \leq d \leq 4.94$ cm, $W \geq 8.44$ m

W is the distance between positive and negative poles

For each positive pole:

$$\boxed{L_A = AN_0 - 10 \cdot \log D} \qquad (7.11)$$

$$AN_0 = \frac{10\, g_{60} \left(1 - \frac{g_{50}}{g}\right)}{(g_{60} - g_{50})} + 50$$

g: average maximum bundle gradient

g_{50} and g_{60} represent the bundle gradients which correspond to $AN_0 = 50$ dB(A) and $AN_0 = 60$ dB(A) respectively, and are given by :

$$g_{50} = \left[\frac{\log n}{106} + \frac{\log d}{21} + \frac{1}{2W^2} + \frac{1}{113}\right]^{-1}$$

$$g_{60} = \left[\frac{\log n}{72} + \frac{\log d}{21} + \frac{1}{2W^2} - \frac{1}{2538}\right]^{-1}$$

7.5 Ozone and Ions

When discharges occur in air or oxygen, they induce the overall reaction $3\ O_2 \rightarrow 2\ O_3$. The actual reaction is much more complex since various uncharged particles are present due to the discharges, i.e. O, O+, O-, O_2, O_{-2}. Theoretically one kWh of corona loss should produce 1220 g of 0_3 . However, efficiencies as low as 0.2% reduce the amount of ozone produced by corona discharges on conductors under practical conditions. Laboratory studies have shown that negative polarity corona generally produces higher rates of ozone than those produced by positive polarity corona. However, conductor surface conditions may alter or even reverse this tendency, especially when large positive plumes occur.

The rate of ozone production from a transmission line conductor is directly related to the corona loss. Since the corona loss itselves depends very much on the ambient weather conditions, it follows that highest ozone production rates occur during steady rain conditions.

Studies on short test line have shown that the maximum probable contribution of the line to ambient ozone levels occurs during foul weather conditions. Even under the worst conditions, however, the maximum contribution is below 10 ppb on an hourly basis. Ambient ozone levels may vary between a few ppb to about 100 ppb.

Glossary chapter 7

AN	audible noise	
AN_0	empirical constant	dB
C_{p1}	constant factor	
C_{p3}	constant factor	
d	subconductor diameter	cm
D	radial distance of the measuring point from the positive pole	m
EMI	electromagnetic interference	dB (1 µV/m)
f	frequency	MHz
g	maximum bundle gradient	kV/cm
g_0	constant factor, $g_0 = 22 \cdot \delta$	kV/cm
g_{50}	function of n, d and W	
g_{60}	function of n, d and W	
H	mean height of conductors	m
I_c	corona current	mA/km or µA/m
k	constant factor depending on H and S	
K_1	empirical constant	
K_3	empirical constant	
k_c	conductor surface coefficient	
k_g	empirical constant	
k_n	empirical constant	
K_n	empirical constant	dB
K_w	empirical constant	dB
L_A	A-weighted sound pressure level	dB(A) (20 µPa)
L_{Ai}	noise level of the individual conductors	dB(A) (20 µPa)
L_{AT}	total A-weighted sound pressure level	dB(A) (20 µPa)
ln	$\ln \equiv \log_e$, e = 2.718	
log	$\log \equiv \log_{10}$	
n	number of subconductors	
n_c	total number of conductors generating audible noise	
P_0	empirical constant	dB
P_{dB}	corona loss of a bundle conductor	dB (1 W/m)
P_c	corona loss per circuit	kW/km or W/m

ppb	parts per billion	
q	altitude above sea level	m
r	subconductor radius	cm
RI	radio interference	dB (1 μV/m)
S	spacing of the poles	m
TVI	television interference	
V	voltage of conductor	kV
W	distance between positive and negative poles	m
δ	relative air density (RAD)	
Γ	excitation function	dB (1 μA/$\sqrt{m}$)
Γ_0	empirical constant	dB

References

Though not on the scope of the ADDENDUM, the influence of ions, produced from corona discharges on the electric field between the conductors and near the ground might be of interest when the compatibility of DC lines with ambient criteria are discussed. As relevant investigations had been made in parallel to corona measurements, the following references could be useful [7.10 to 7.15] :

[4.19] IEEE Corona and Field Effects Subcommittee, "A Comparison of Methods for Calculating Audible Noise of High Voltage Transmission Lines", IEEE Trans. on Power Apparatus and Systems, Vol. PAS-101, No. 10, Oct. 1982, pp.4090-4099.

[6.18] "Transmission Line Reference Book HVDC to ± 600 kV", Project RP 104, Electric Power Research Institute, Palo Alto, CA 94304, 1977.

[7.1] P. Sarma Maruvada, N. Giao Trinh, R. D. Dallaire, N. Rivest, "Corona Studies for Bipolar HVDC Transmission at Voltages Between ±600 kV and ±1200 kV - Part 1: Long Term Bipolar Studies; Part 2: Special Bipolar Line, Bipolar Cage and Bus Studies", IEEE Trans. on Power Apparatus and Systems, Vol. PAS-100, No. 3, March 1981.

[7.2] V.L.Chartier, "Empirical Expression for Calculating High Voltage Transmission Corona Phenomena", Proceedings of the First Annual Seminar Technical Career Program for Professional Engineers, Portland, Oregon, April 1983, pp.75-82.

[7.3] J.G. Droppo, "Field determination of HVDC Ozone Production Rates", IEEE Trans. on Power Apparatus and Systems, Vol. PAS-100, No. 2, Feb. 1981, pp.655-661.

[7.4] N. Knudsen, F. Iliceto, "Contribution to the electrical design of EHVDC overhead lines", IEEE Transactions on Power Apparatus and Systems, Vol. PAS-93, No. 1, Jan/Feb 1974, pp.233-239.

[7.5] T. Takuma, T. Kawamoto, "A very stable calculation method for ion flow field of HVDC transmission lines", IEEE Transactions on Power Delivery, Vol. PWRD-2, No. 1, January 1987.

[7.6] R. D. Dallaire, P. Sarma Maruvada, "Corona performance of a ± 450-kV bipolar DC transmission line configuration", IEEE Transactions on Power Delivery, Vol. PWRD-2, No. 2, April 1987.

[7.7] V. L. Chartier, L. D. Dickson, L. Y. Lee, R. D. Stearms, "Performance of a long-term unattended station for measuring DC fields and air ions from an operating HVDC line", IEEE Transactions on Power Delivery, Vol. PWRD-4, No. 2, April 1989.

[7.8] V. L. Chartier, R. D. Stearms, A. L. Burns, "Electrical environment of the uprated pacific NW/SW HVDC intertie", IEEE Transactions on Power Delivery, Vol. PWRD-4, No. 2, April 1989.

[7.9] G. B. Johnson, "Degree of corona saturation for HVDC transmission lines", IEEE Transactions on Power Delivery, Vol. PWRD-5, No. 2, April 1990.

[7.10] P. Sarma Maruvada, N. G. Trinh, D. Dallaire, N. Rivest, "Corona performance of a conductor bundle HVDC transmission at ± 750 kV", IEEE Transactions on Power Apparatus and Systems, Vol. PAS-96, No. 6, November/December 1977.

[7.11] P. S. Maruvada, R. D. Dallaire, O. C. Norris-Elye, C. V. Thio, "Environmental effects of the Nelson River HVDC transmission lines - RI, AN, electric field, induced voltage, and ion current distribution tests", IEEE Transactions on Power Apparatus and Systems, Vol. PAS-101, No. 4, April 1982.

[7.12] M. Hara, N. Hayashi, K. Shiotsuki, M. Akazaki, "Influence of wind and conductor potential on distributions of electric field and ion current density at ground level in DC high voltage line to plane geometry", IEEE Transactions on Power Apparatus and Systems, Vol. PAS-101, No. 4, April 1982.

[7.13] M. G. Comber, G. B. Johnson, "HVDC field and ion effects research at project UHV : results of electric field and ion current measurements", IEEE Transactions on Power Apparatus and Systems, Vol. PAS-101, No. 7, July 1982.

[7.14] J. G. Droppo, "Field determinations of HVDC ozone production rates", IEEE Transactions on Power Apparatus and Systems, Vol. PAS-101, No. 2, February 1981.

[7.15] P. Sarma Maruvada, R. D. Dallaire, P. Héroux, N. Rivest, "Long-term statistical study of the corona electric field and ion-current performance of a ± 900-kV bipolar HVDC transmission line configuration", IEEE Transactions on Power Apparatus and Systems, Vol. PAS-103, No. 1, January 1984.

Chapter 8

Electromagnetic Interference Generated by Substations

8.1 Introduction

The 1974 Guide [1.1], briefly reviewed the question of steady-state electromagnetic noise generated by AC substations but did not cover the topics of noise generated by HVDC converter stations and static var compensator installations. Similar comments concerning the limited treatment of noise from substations apply to the 1980 IEEE subcommittee report on limits of noise from lines and substations [8.1].

Compared with overhead lines, electromagnetic noise from conventional AC substations has received relatively little research attention; one reason has been the limited impact of such noise on nearby radio services, resulting in an approach where such problems are studied on a case-by-case basis. A major impetus to the awareness of substation noise has been created in the last few years by the need to research and control noise from HVDC converter stations and related solid state switching equipment, such as static var compensators.

In the discussions which follow, the emphasis is on the characteristic radio frequency interference radiated from substations, (conventional or converter stations), so as to serve as an aid in the general assessment of the electromagnetic impact of such stations. This could refer, for example, to the influence of such noise on a nearby radio communications site. The influence of the noise on other equipment and services within the station is outside the scope of this treatment of the subject, but will be referred to briefly.

Transient electromagnetic noise generated by isolator and breaker switching is not considered.

8.2 Sources of Noise

8.2.1 Conventional AC Substations

This review is for substations where the voltage is 132 kV or more.

Radio interference in substations is generated by two families of sources [1.1, 8.1 and 8.2]:

i) Corona discharges

ii) Gap discharges

Corona discharges occur on conductors, fittings (such as spacers and clamp), hardware on equipment (such as isolator links, circuit breakers) and isolators, and generally cause interference which is confined to the medium wave and HF frequency bands, such that beyond a few megahertz the resulting levels are much smaller. However, there is some evidence to suggest that corona discharges can lead to interference extending to the VHF bands [8.3]. This is discussed further in later paragraphs.

Gap discharges in a substation arise from dry-band sparking on polluted insulators, micro discharges across the highly stressed portions of disc insulators in dry conditions, and sparking across air gaps created by breaks in the contact between fittings. A further source of noise, which is not typically a gap type source, is the small galvanic currents generated when movement between two dissimilar metallic surfaces takes place — examples of this are the slight movement of a conductor within its clamp and the movement of a spacer-damper.

In well designed, constructed and maintained substations operating at above 132 kV, strong gap sources should not be present; discharges on insulators (either due to pollution or high stresses) are frequently present however, and are one of the major generators of noise extending from a few megahertz into the VHF and sometimes UHF bands.

It has been observed that, in substations where no obvious gap sources are present, noise spectra measured at the station boundaries may extend well into the VHF range [8.3]. It has also been observed that such noise is fairly stable with time and appears to be only minimally reduced by rain. This leads to the conjecture that corona discharges may be the source of the higher frequency interference.

Several qualitative reasons for this have been proposed: on lines, the interference, even in dry conditions, is generated mainly by corona from conductors, with corona discharges on insulators and fittings acting as secondary sources. Station noise, however, is dominated by intense corona on fittings (conductors here being a secondary source) which are in proximity to far more grounded steelwork than is the case on lines. The dimensions of the station hardware (steel lattice members and insulator strings for example) are such that the corona currents injected can set up complex antenna and re-radiation effects at VHF frequencies in particular. In this way, therefore, the basic frequency spectrum of the pulse of corona current [1.1] is amplified when radiated or re-radiated, and leads to the measurement of significant interference field strengths beyond the range usually associated with lines.

Similar mechanisms are also present on line insulator strings, but the far smaller numbers of insulators and lower concentrations of steel work per tower compared with stations lead to VHF noise levels which are generally not measurable. This point, of course, emphasizes another obvious difference between line and station noise generation, namely, that the station contains many more concentrated corona sources in a smaller area than a line does.

Substation noise is generated by a combination of corona and microdischarges, and is extremely complex in terms of the main influencing parameters, namely, the numbers of such sources, their intensities, busbar impedance and antenna properties, and atmospheric conditions.

The resulting noise is a combination of the above sources and influences, and it is not practicable or possible to attempt to separate the relative contributions. As a design approach it is important to ensure that surface gradients on conductors and fittings are kept to within levels which ensure that specified radio influenced voltage (RIV) limits are met [8.2].

Compliance with the RIV limits may require extensive laboratory testing. Operationally, it should be ensured that hardware remains well bonded, that corroded fittings are replaced where necessary and polluted insulators are regularly washed or greased.

As regards the influence of atmospheric conditions, such as rain or fog, on substation noise levels, it has been observed [by Eskom] that levels in the HF and VHF bands either do not increase significantly or may in some cases even drop slightly. This has suggested, as per the earlier hypothesis, that the radiated noise is certainly a combination of gap and corona sources; the presence of rain will generally eliminate gap sources, but at the same time intensify the corona discharges on fittings and conductors. The presence of water on the insulator strings, however, leads to modified voltage distributions along the string, washing action, and higher corona discharges in the high stress areas. More research is required to quantify insulator noise characteristics under these conditions.

Research reported in [8.3] suggests that the overall effect of reduced air density on corona generation in substations may be masked by gap-type sources and sparking from microdischarges. This phenomenon should nevertheless be taken into account in the attainment of given limits of RIV from fittings, hardware, and insulator strings.

8.2.2 HVDC Converter Stations

Steady state electromagnetic noise in HVDC systems is generated by the periodic switching of mercury-arc or thyristor valves in 6 or 12 pulse converters. This switching produces steep-fronted current pulses which are conducted from the valve-hall into the busbar configuration of the station. The conducted current causes high frequency fields to be radiated from the busbars.

Very complex radiation patterns are set up by the geometry of the busbar layout, with strong resonances usually being evident [8.5 and 8.7]. As direct radiation from the valve hall is usually prevented by effective shielding, it is generally only necessary to consider the effects of currents propagated outside the valve hall in determining the noise radiated by the converter station.

During the normal operation of a converter bridge, each of the 6 converter valves is switched on and off once per 50 Hz or 60 Hz cycle. The generation of high frequency current pulses arises from the fact that valve turn-on and turn-off times are of the order of a few microseconds. The turn-off time is slower than that of turn-on, and gives rise to low frequency disturbances, the resonances of which are determined entirely by the impedances of the converter transformers. The turn-on action is faster, and results in the injection of steep current pulses into the DC busbar system [8.5, 8.6 and 8.7]. Converter station noise is thus generated mainly during the turn-on of the thyristor valves. The modern use of thyristor valves as a replacement for the older mercury arc types has resulted in a significant reduction in interference amplitudes and the range of frequencies generated, owing mainly to the slower turn-on times of thyristor valves.

DC corona generated on the conductors and busbars is also present as a source of radio interference noise, but is far lower in level than that generated by thyristor switching. Most valuable informations are given in the amendment of CISPR Publication 18-2 which is presently under vote on FDIS-procedure [8.9].

References

[1.1] CIGRE, "Interferences Produced by Corona Effect of Electric Systems: description of phenomena and practical guide for calculation", WG 36.01, Brochure No.20, 1974.

[8.1] IEEE, "IEEE Radio Noise and Corona Subcommittee Report: Review of technical considerations on limits to interference from power lines and stations", IEEE Transactions on Power Apparatus and Systems, Vol. PAS-99, Jan/Feb 1980.

[8.2] IEEE, "Radio noise design guide for high voltage transmission lines", IEEE Trans. on Power Apparatus and Systems, Vol. PAS-90, March/April 1971.

[8.3] A.C. Britten, "Electromagnetic interference in the range 0,5 to 300 MHz generated by 400 kV distribution stations", South African Institute of Electrical Engineerings, Symposium on antennas and microwave propagation, August 1986.

[8.4] R.T. Carter et. al., "Analysis of radio interference and substation modifications for upgrading a 115 kV substation to 230 kV", IEEE Trans. on Power Delivery, Vol. PWRD-2, No. 2, April 1987.

[8.5] P.S. Maruvada, T. Gilsig, "A method for calculating the RI from HVDC converter stations", IEEE Trans., PAS-92, No. 3, May/June 1973, pp. 1009-1018.

[8.6] P.S. Maruvada, R. Malewski, P.S. Wong, "Measurement of the electromagnetic environment of HVDC converter stations", IEEE Transactions on Power Delivery, Vol. PWRD-4, No. 2, April 1989, pp. 1129-1136.

[8.7] R.D. Dallaire, P.S. Maruvada, "Evaluation of the effectiveness of shielding and filtering of HVDC converter stations", IEEE Transactions on Power Delivery, Vol. PWRD-4, No. 2, April 1989, pp. 1469-1475.

[8.8] D.G. Kasten, K.A. Roger, "Station RFI Calculations and Measurements", Proceedings of the American Power Conference, 1987, pp. 448-453.

[8.9] Amendment No. 2 to CISPR Publication 18-2, "Methods for derivation of limits for the RI noise due to HVDC converter stations", CISPR/2/85FDIS, ciculated 1996-05-31.

Chapter 9

Design Considerations in Relation with the Corona Effects on Overhead High Voltage Lines

9.1 Introduction

The design of electric power transmission systems must be based primarily on technical feasibility, service needs and safety considerations. However the actual construction of individual overhead transmission installations might also be governed by interference arising from both its existence or its regular service.

The lack of quantitative criteria for assessing the visual impact of overhead transmission lines makes it difficult to take into account the aesthetics in any more than a general way at the beginning of the planning stage.

In contrast the fundamental limits imposed by corona and field effects can exclude designs that are otherwise technically and economically feasible. Therefore the major limitations on design parameters will be outlined in this Chapter.

9.2 Consequences of Corona Effects

Corona loss, initially suspected as a limiting factor, proved not to be critical, being only a fraction of the total ohmic loss of a line. The emission of high frequency electromagnetic fields and of audible noise must be taken into account usually only in more populated areas.

Both effects show maximal values close to high voltage installations, decreasing with increase of lateral distances. The dominating parameter is the electric field at the surface of the high voltage conductors or subconductors, which in turn is mainly dependent on the operating voltage, the number of subconductors and their diameter.

For AC lines, the dry weather value is used to characterize the radio interference behaviour, though for bad weather conditions the actual value will be on an average 17 dB higher. The acceptable value is determined by signal-to-noise ratio (reception quality) that is required.

Maximum radio interference values from DC lines are produced under dry weather conditions from the positive conductor only, thus the worst case will be prevailing. For equal quality of reception, the signal-to-noise ratio for DC interference may be approximately 5 dB lower than for AC.

Due to their low attenuation along overhead lines, local radio interference values may be affected by the overhead line for up to 10 km in both directions. Axial propagation of audible noise along lines is much more limited, so local mitigation of audible noise can be achieved by improvements to several spans only.

No evidence has been found to support the supposition that ozone, NO_X or ion production from overhead electric installations have negative impact on the environment.

TV interference caused by extreme corona activity or sparking between rain drops and conductors is not a problem for conventional line configurations, though the presence of the metallic conductors and towers can reduce reception quality locally.

Limits, once fixed, can be taken into consideration for new constructions, however problems may arise when upgrading existing installations, in increasing sensitivity of the public particularly to audible noise.

9.3 AC Lines

The design of most lines that operate up to 230 kV near sea level, will be hardly influenced by corona effects. The costs of ohmic loss govern the conductor cross section needed and together with the safe clearance distances, determine the geometric and mechanical layout. These considerations usually yield field gradients at the surface of subconductors, which are below those of corona onset. However, corona effects may need consideration for lines of compact design and lines that operate at higher altitudes between 100 and 300 kV.

For operating voltages above 300 kV, the ohmic criterion often leads to conductor configurations for which the gradients are above corona onset under service conditions, thus producing corona loss, radio interference and audible noise emissions. The dominant design parameters for all corona effects are the bundle subconductor diameter and number of subconductors.

For a given line configuration and operating voltage corona loss can be derived from measurements on test lines or from calculation or both, under typical weather conditions. Maximum loss occurs during heavy rain, wet snowfall or hoarfrost, and it is restricted to relatively short sections of a lines and does not usually last very long. Dry conductors produce negligible losses compared with ohmic loss. Yearly average corona loss is determined by the relevant weather statistics.

Corona loss impacts on transmission line design in two principle ways:

1) The cost of the total energy loss due to corona. Using a proper weather model, the annual average corona loss can be estimated.

2) The impact of corona loss on the maximum demand requirements of generation. Excessive corona loss is imaginable either for rather long lines under general and persistent rain, or maximum loss emission on a shorter section of a transmission line. If these conditions can coincide with maximum transmission load, corona loss becomes an important factor for design considerations.

Considering both aspects, the optimal economical design of the line will be determined by life-time cost assessment.

Radio interference and audible noise emission is often restricted by rules and regulations or by experience based on observed levels of annoyance. Radio interference and audible noise emission can be calculated for characteristic situations: worst case or maximal values under heavy rain, fine weather average or normal rain conditions. The accuracy obtainable is sufficient to distinguish between different possible design options and to choose the most economical one with respect to lifetime costs. Audible noise characteristics can be influenced locally so that a special bundle configuration for a few spans may solve an individual problem at low costs. This approach unfortunately is not possible for the radio interference. The ease of propagation of radio interference currents along an overhead line directions prohibits effective mitigation for short sections only.

The corona loss is usually low compared with ohmic loss, and so is usually less important with respect to the line dimensions than effects that have an impact on the public, such as radio interference and audible noise. Furthermore the trend towards FM broadcasting particularly in more densely populated areas means that audible noise is becoming the crucial limitation for AC line design.

9.4 DC Lines

Though the fundamental corona discharge process are the same for DC voltages and for the AC half wave of the same polarity, the impact of DC corona on line design is determined by special DC characteristics.

The least differences are found for corona loss with maximal values occurring during bad weather conditions. During dry conductors the loss is negligible. In general there is only a weak influence of corona loss on design.

The overwhelming part of radio interference and audible noise emission is caused by the positive conductor only. In contrast to the relevant AC corona modes, these emissions decrease during bad weather. The general behaviour is determined by the dry-conductor situation.

In the same way as for AC lines, there is no significant impact of ozone or NO_X on ambient levels. The highest values produced can be hardly differentiated from natural dispersions.

Le CIGRÉ a apporté le plus grand soin à la réalisation de cette brochure thématique numérique afin de vous fournir une information complète et fiable.

Cependant, le CIGRÉ ne pourra en aucun cas être tenu responsable des préjudices ou dommages de quelque nature que ce soit pouvant résulter d'une mauvaise utilisation des informations contenues dans cette brochure.

Publié par le CIGRÉ
21, rue d'Artois
FR-75 008 PARIS
Tél. : +33 1 53 89 12 90
Fax : +33 1 53 89 12 99

The greatest care has been taken by CIGRE to produce this digital technical brochure so as to provide you with full and reliable information.

However, CIGRE could in any case be held responsible for any damage resulting from any misuse of the information contained therein.

Published by CIGRE
21, rue d'Artois
FR-75 008 PARIS
Tel : +33 1 53 89 12 90
Fax : +33 1 53 89 12 99